# REPORT DOCUMENTATION PAGE

OMB No. 0704-0188



| 1. AGENCY USE ONLY (Leave blank) | 2. REPORT DATE | 3. REPORT TYPE AND DATES COVERED |
|---|---|---|
| | 21 Jul 95 | |

**4. TITLE AND SUBTITLE**

An Integrated GPS Attitude Determination System For Small Satellites

**5. FUNDING NUMBERS**

**6. AUTHOR(S)**

Bruce Carl Chesley

**7. PERFORMING ORGANIZATION NAME(S) AND ADDRESS(ES)**

AFIT Students Attending:

Colorado University

**8. PERFORMING ORGANIZATION REPORT NUMBER**

AFIT/CI/CIA

95-049

**9. SPONSORING/MONITORING AGENCY NAME(S) AND ADDRESS(ES)**

DEPARTNEMT OF THE AIR FORCE
AFIT/CI
2950 P STREET, BDLG 125
WRIGHT-PATTERSON AFB OH 45433-7765



**10. SPONSORING/MONITORING AGENCY REPORT NUMBER**

**11. SUPPLEMENTARY NOTES**

**12a. DISTRIBUTION/AVAILABILITY STATEMENT**

Approved for Public Release IAW AFR 190-1
Distribution Unlimited
BRIAN D. GAUTHIER, MSgt, USAF
Chief Administration

**12b. DISTRIBUTION CODE**

**13. ABSTRACT** *(Maximum 200 words)*

| Accesion For | |
|---|---|
| NTIS CRA&I | ☒ |
| DTIC TAB | ☐ |
| Unannounced | ☐ |
| Justification | |
| By | |
| Distribution / | |
| Availability Codes | |
| Dist | Avail and / or Special |
| A-1 | |

**14. SUBJECT TERMS**

**15. NUMBER OF PAGES**

177

**16. PRICE CODE**

| 17. SECURITY CLASSIFICATION OF REPORT | 18. SECURITY CLASSIFICATION OF THIS PAGE | 19. SECURITY CLASSIFICATION OF ABSTRACT | 20. LIMITATION OF ABSTRACT |
|---|---|---|---|
| | | | |

# AN INTEGRATED GPS ATTITUDE DETERMINATION SYSTEM FOR SMALL SATELLITES

by

BRUCE CARL CHESLEY

B.S., University of Notre Dame, 1986

M.S., University of Texas at Austin, 1988

A thesis submitted to the

Faculty of the Graduate School of the

University of Colorado in partial fulfillment

of the requirement for the degree of

Doctor of Philosophy

Department of Aerospace Engineering Sciences

1995

This thesis for the Doctor of Philosophy degree by

Bruce Carl Chesley

has been approved for the

Department of

Aerospace Engineering Sciences

by

Penina Axelrad

Penina Axelrad

George H. Born

George H. Born

Date 7/21/95

*ABSTRACT*

Chesley, Bruce Carl (Ph.D., Aerospace Engineering Sciences)

An Integrated GPS Attitude Determination System for Small Satellites

Thesis directed by Assistant Professor Penina Axelrad

This dissertation develops attitude determination methods based on the Global Positioning System (GPS) for small satellites. A GPS attitude receiver is used in combination with other sensors planned for a small, three-axis stabilized satellite called JAWSAT. The other attitude sensors include fiber optic gyros and digital sun sensors.

The development of integrated attitude determination systems contributes to critical national technological objectives identified for small spacecraft. A recent study by the National Research Council addresses key technologies for small satellite programs. One of their principal recommendations was that, "GPS in various combinations with other guidance components can determine position and attitude very accurately, probably at significantly reduced weight and cost" [NRC, 1994, p. 4]. The report also identifies specific potential benefits of integrating GPS with other sensors on small spacecraft. "Combining GPS and an inertial measurement unit (with gyroscopes, accelerometers, or trackers) offers major advantages by bounding errors of the inertial set, providing exceptionally good long-term references and thereby

ensuring precise, on-board navigation and, with appropriate complimentary techniques, providing a higher level of redundancy and/or accuracy for position, velocity, and attitude" [NRC, 1994, p. 61]. This dissertation develops algorithms that result in improved accuracy and redundancy through the development of complimentary techniques for combining GPS measurements with gyroscopes and sun sensors.

A measurement differencing Kalman filter algorithm for spacecraft attitude determination is developed that results in improved accuracy in the presence of GPS multipath errors, the primary error source in GPS based attitude determination systems. Multipath causes time-correlated errors in the GPS attitude measurements; these time-correlated errors are mitigated using the measurement differencing approach. Improved redundancy is achieved by a decentralized state estimation method based on the federated Kalman filter. Using a similar measurement differencing technique, the decentralized filtering approach achieves improved accuracy in addition to improved redundancy for an integrated system consisting of GPS, gyros, and sun sensors. Finally, this dissertation addresses additional spacecraft applications where integrating measurements for a GPS attitude receiver with other sensors may lead to significant improvements in cost and performance.

***DEDICATION***

For Julie

*When I needed inspiration...*

*ACKNOWLEDGMENTS*

I wish to thank Dr. Penny Axelrad for supervising this thesis research and my intellectual development at the University of Colorado. Working with Penny has been a very rewarding experience, and I cannot imagine an advisor who is more supportive and accessible. I have learned many things from Penny beyond what is reflected in this dissertation, and I have enjoyed having her as a mentor and friend. I will always be proud of the fact that this is the best dissertation she has ever supervised—at least until her second student graduates. Thanks are also due to the other members of my committee, Dr. George Born, Dr. Dale Lawrence, Mr. Emery Reeves, and Dr. Renjeng Su, for the fruitful discussions and helpful feedback they provided throughout the progress of this research. I am also indebted to members of the Department of Astronautics at the U.S. Air Force Academy: Brig. Gen. (retired) Bob Giffen for offering me this opportunity and challenge, and Dr. Dave Cloud and Lt. Col. Randy Liefer for providing the initial motivation for this research when they approached me about flying a GPS attitude determination receiver on board JAWSAT.

Trimble Navigation is gratefully acknowledged for providing the Vector receiver and technical support. Mr. Emery Reeves, Lt. Col. Randy Liefer, and Capt. Dewey Parker of the USAF Academy Department of Astronautics provided many helpful insights into the design of JAWSAT. Lisa Ward kindly provided on-orbit

GPS attitude solutions from her research on the RADCAL satellite. Thanks to my colleagues and friends at the University of Colorado, especially Mark Matossian, Tim Holden, Tom Gardner, Lisa Ward, Robbie Robertson, and Chris Comp, for their help and encouragement as we struggled through this process together.

I also want to thank my family. Thanks to my parents for instilling in me the value of education, along with perseverance and commitment. My girls, Abbey and Alexandra, have made my time in Boulder (which were also my first years as a father) some of the most memorable and enjoyable times of my life. And to my wife, Julie, thank you for your enduring love, support, insight, and great friendship.

*CONTENTS*


Chapter 1. Introduction 1

1.1 Motivation and Summary of Contributions 1

1.2 JAWSAT Mission and Design 3

1.3 JAWSAT Attitude Determination System 6

1.4 Overview 7

Chapter 2. Background 9

2.1 Attitude Determination Preliminaries 9

Coordinate frames 10

Attitude representations 12

2.2 Spacecraft Attitude Determination 13

2.3 Kalman Filtering for Spacecraft Attitude Estimation 16

2.4 Attitude Estimation Simulation 19

Chapter 3. Attitude Determination Using GPS and Gyros 22

3.1 GPS Based Attitude Determination 23

Trimble Vector Receiver 24

Spacecraft Attitude Determination Using GPS 29

GPS Attitude Errors 30

GPS Attitude Test Data 30

3.2 Gyro Attitude Determination 37

Fiber Optic Gyros 37

Micromechanical Gyros 40

Gyro Measurement Model 41

Inertial Quality Gyro Simulation 43

Low Quality Gyro Simulation 45

3.3 Extended Kalman Filter Algorithm 48

3.4 Measurement Differencing Estimation Algorithm 57

3.5 Attitude Estimation Simulation 61

3.6 Simulation Results and Discussion 64

Ground Test Results 64

RADCAL Results 72

Comparison of Gyro Quality 75

3.7 Minimizing Receiver On-Time 77

3.8 Summary and Conclusions 79

Chapter 4. Attitude Determination Using Digital Sun Sensors and Gyros 81

4.1 Digital Sun Sensor Attitude Determination 82

4.2 Sun Sensor Quantization Errors 84

4.3 Attitude Estimation with Sun Sensors and Gyros 86

4.4 Digital Sun Sensor Measurement Model 89

4.5 Dead Zone Filter 95

4.6 Simulation Results and Discussion 98

4.7 Summary and Conclusions 104

Chapter 5. Integrated GPS Attitude Determination 106

5.1 Centralized Kalman Filtering 107

5.2 Decentralized Kalman Filtering 108

5.3 Federated Kalman Filter Algorithm 111

5.4 Federated Filtering with Time-Correlated Measurement Errors 117

State Propagation 124

Block Diagonal Approximation of the State Propagation 129

Measurement Update 135

5.5 Estimate Fusion for the Quaternion Filter 137

5.6 Simulation Results and Discussion 139

Ground Test Results 140

RADCAL Results 143

5.7 Summary and Conclusions 145

Chapter 6. Nonlinear Filtering Using GPS and Gyros 146

6.1 Nonlinear Filtering of Spacecraft Attitude 146

6.2 Simulation Results and Discussion 149

6.3 Summary and Conclusions 153

Chapter 7. Future Work and Summary 155

7.1 Levels of Sensor Integration 155

7.2 Augmenting the State Vector 157

Large Space Structure System Identification 158

GPS Error State Modeling 160

Antenna Baseline Estimation 160

Line Bias Calibration 161

Cross-Correlation of GPS Attitude Solutions 161

7.3 Future Work for JAWSAT 162

7.4 Summary of Research Contributions 163

7.5 Conclusion 165

References 166

*TABLES*

Table 3.1. Simulation run parameters. 62

Table 3.2. Computed error statistics for Extended Kalman Filter and Measurement Differencing Kalman Filter Algorithms using GPS Ground Test Data. 69

Table 3.3. Computed error statistics for Extended Kalman Filter and Measurement Differencing Kalman Filter Algorithms using Different Time Constants. 72

Table 3.4. Computed error statistics for Extended Kalman Filter and Measurement Differencing Kalman Filter Algorithms using RADCAL Test Data. 75

Table 6.1. Computed error statistics for Nonlinear Kalman Filter and Measurement Differencing Kalman Filter Algorithms using GPS RADCAL Data. 153

*FIGURES*


Fig. 1.1. JAWSAT Structure with Solar Panels Deployed. 4

Fig. 1.2. JAWSAT sun synchronous orbit. 7

Fig. 2.1. Inertial, Orbit Local, and Body Fixed Reference Frames 10

Fig. 2.2. Simulation Data Flow. 20

Fig. 3.1. GPS Differential Phase Geometry. 25

Fig. 3.2. GPS Antenna Test Structure. 31

Fig. 3.3. Sample GPS Attitude Output. 32

Fig. 3.4. Sample GPS Attitude Output from RADCAL. 34

Fig. 3.5. Comparison of autocorrelation functions of Markov process and measured GPS multipath. 36

Fig. 3.6. Standing Wave Interference Pattern in Fiber Optic Gyro. 39

Fig. 3.7. Simulated Bias Random Walk. 44

Fig. 3.8. Simulated Angular Rate Measurements. 45

Fig. 3.9. Simulated Bias Random Walk. 47

Fig. 3.10. Simulated Angular Rate Measurements. 48

Fig. 3.11. Extended Kalman Filter Algorithm. 50

Fig. 3.12. Simulated True Spacecraft Dynamics. 63

Fig. 3.13. True and Estimated Attitude Data. 65

Fig. 3.14. Kalman Filter Attitude Error Plot for GPS Ground Test Data. 66

Fig. 3.15. Kalman Filter Bias Error Plot for GPS Ground Test Data. 67

Fig. 3.16. Attitude Error Comparison for GPS Ground Test Data. 68

Fig. 3.17. Gyro Bias Error Comparison for GPS Ground Test Data. 69

Fig. 3.18. Attitude Estimation Errors Using Measurement Differencing Algorithm with Different Time Constants. 71

Fig. 3.19. Attitude Error Comparison for RADCAL Test Data. 73

Fig. 3.20. Gyro Bias Error Comparison for RADCAL Test Data. 74

Fig. 3.21. Attitude Error Comparison Using Low Quality Gyros. 77

Fig. 4.1. Sun sensor assembly for JAWSAT. 83

Fig. 4.2. Solar cell cut into strips for JAWSAT digital sun sensor. 84

Fig. 4.3. Quantization as a function of state. 85

Fig. 4.4. Sun sensor coordinate definition. 89

Fig. 4.5. Attitude Estimation Error: Standard EKF Algorithm. 99

Fig. 4.6. Attitude Estimation Error: Dead Zone EKF Algorithm. 100

Fig. 4.7. Attitude Estimation Error: Standard EKF Algorithm. 102

Fig. 4.8. Attitude Estimation Error; Dead Zone Algorithm. 103

Fig. 5.1. Centralized Kalman filter algorithm. 107

Fig. 5.2. Attitude Error Comparison: Centralized and Federated Kalman Filters with Measurement Differencing Using GPS Ground Test Data. 141

Fig. 5.3. Gyro Bias Error Comparison: Centralized and Federated Kalman Filters with Measurement Differencing Using GPS Ground Test Data. 142

Fig. 5.4. Attitude Error Comparison: Centralized and Federated Kalman Filters with Measurement Differencing Using GPS Data from RADCAL. 143

Fig. 5.5. Gyro Bias Error Comparison: Centralized and Federated Kalman Filters with Measurement Differencing Using GPS Data from RADCAL. 144

Fig. 6.1. Nonlinear Kalman Gain. 150

Fig. 6.2. Attitude Error Comparison for Nonlinear Filter. 151

Fig. 6.3. Gyro Bias Error Comparison for Nonlinear Filter. 152

Fig. 7.1. Loosely Coupled Attitude Estimation Algorithm. 156

Fig. 7.2. Tightly Coupled Estimation Algorithm. 157

*Chapter 1:*

# *INTRODUCTION AND OVERVIEW*

An emerging paradigm of better, faster, and cheaper space vehicles has increased the number of small satellite projects in recent years. These small, often highly capable spacecraft, have been developed by the Department of Defense (*e.g.*, Clementine [NRC, 1994]), NASA (*e.g.*, MSTI [NRC, 1994]), civilian commercial enterprises (*e.g.*, ORBCOMM) and universities (*e.g.*, SNOE [LASP, 1994], WEBERSAT [Twiggs and Reister, 1991]). In addition to the renewed interest in small satellites, a desire to exploit the full capabilities of GPS for orbit and attitude determination has also spread [*e.g.*, Gold *et al.*, 1995, Bauer *et al.*, 1994]. This dissertation ties together these two important themes in current spacecraft research and development through the design of an integrated GPS attitude determination system for small, low-cost satellites.

## 1.1 Motivation and Summary of Research Contributions

The Global Positioning System (GPS) has the capability to provide position, velocity, attitude, and timing information to a satellite in low Earth orbit. This combination of many functions in one instrument is attractive for small satellites, where size, power, and cost are constrained. The motivation for this research is to integrate GPS based attitude determination into the design of a small satellite. GPS

attitude measurements are used in conjunction with other on-board sensors to develop accurate, robust attitude estimation algorithms. A demonstration vehicle for this design is JAWSAT, the Joint Air Force Academy - Weber State University Satellite.

The basic design methodology for low cost spacecraft, particularly university sponsored satellites, is to try to extract the best possible performance from relatively low cost sensors that are commercially available. In addition to their low cost, instruments for university sponsored satellites must also typically possess attributes such as low power consumption, low weight, and low volume. Together these qualities frequently lead to poor performance as well.

The attitude sensors considered in this study are those found on JAWSAT: a GPS attitude determination receiver, fiber optic gyros, and digital sun sensors. The objective of this dissertation is to develop innovative methods for filtering the dominant error types present in the attitude sensors found on JAWSAT. In particular, minimizing the effects of GPS multipath errors, sun sensor quantization, and gyro bias errors on the attitude solution is the primary focus of this research.

The research contributions of this dissertation include Kalman filtering methods tailored to the sensors planned for a small three-axis stabilized spacecraft such as JAWSAT. A measurement differencing Kalman filtering approach is developed for gyro and GPS attitude measurements (Chapter 3). This approach

reduces attitude estimation errors due to GPS multipath. A filtering approach using digital sun sensors and gyros is developed using a "dead zone" measurement update for including quantized sun sensor measurements (Chapter 4). The first application of federated filtering to spacecraft attitude determination is presented, and a new federated filtering algorithm that uses measurement differencing to mitigate GPS multipath errors is derived and demonstrated (Chapter 5). Preliminary results of a nonlinear filtering approach for gyros and GPS are also developed (Chapter 6).

## 1.2 JAWSAT Mission and Design

JAWSAT is a combined effort to build, launch, and operate a small, three-axis stabilized satellite in low Earth orbit. The mission of JAWSAT is to demonstrate technologies for future space missions and to meet educational objectives for students at the sponsoring institutions and at various secondary schools. Technology demonstrations on the satellite include a GPS based attitude determination system, two experimental pulse plasma thrusters (PPTs) for low-thrust orbit transfer, a CCD camera, and a high energy particle detector.

JAWSAT will measure approximately 66cm $\times$ 53cm $\times$ 25cm and weigh less than 100 kg at launch (Fig. 1.1). The baseline design calls for JAWSAT to be Earth-pointing in a sun-synchronous noon-midnight orbit at an altitude of 500 km. Three-

axis stabilization will be achieved using reaction wheels and magnetic torque rods. Four GPS antennas will be mounted at the corners of the zenith face.

The attitude determination system for JAWSAT must satisfy constraints on power, size, weight, cost, and processor capabilities while meeting mission requirements. The attitude control specifications require the spacecraft to point within ± 5 degrees of nadir. In order to satisfy these pointing requirements, attitude knowledge is desired within ± 1 degrees in yaw, pitch, and roll to ensure adequate margin for the control system. Cost and size constraints limit the accuracy of the attitude determination sensors available.

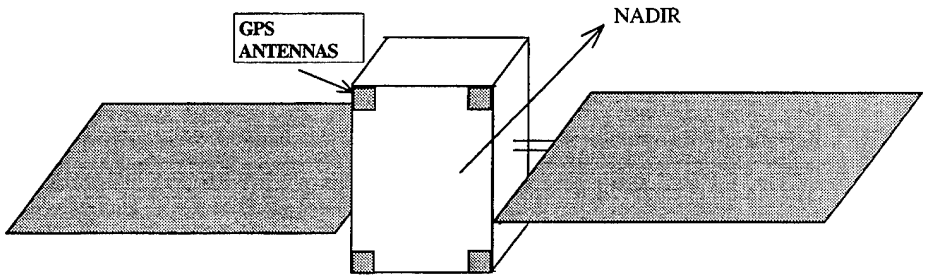


**Fig. 1.1.** JAWSAT Structure with Solar Panels Deployed.

The experience of designing, fabricating, and operating a small satellite is an important objective for undergraduate students at the Air Force Academy and Weber State University. Students at primary and secondary schools will also be involved in JAWSAT once it is on orbit by receiving synthesized voice messages and video

images directly in their classrooms. The messages and images will be received with a personal computer and a low cost receiver (less than $300).

Weber State University and the Air Force Academy each have a history of space experiments that led to their collaboration on JAWSAT. Weber State University has been designing small satellites for over ten years. Previous successful launches include NUSAT I in 1985 and WEBERSAT, a small video imaging satellite launched in January 1990 that is still operational [Hansen *et al.,* 1991; Twiggs and Reister, 1991] . Previous space experiments sponsored by the USAFA Department of Astronautics include two Get Away Special (GAS) canisters flown on the Space Shuttle. A third GAS can experiment is scheduled for launch in 1994. Participation in JAWSAT is planned to lead to a follow-on satellite built entirely at the Air Force Academy called USAFASAT I.

Out-of-pocket expenses for JAWSAT are being kept to a minimum, but the actual cost of the project is difficult to estimate since so much time and equipment is being volunteered or donated [Reeves, 1994]. USAFA and Weber State are partners in sharing equipment expenses, and USAFA is taking the lead in securing the satellite launch. USAFA will also provide some of the on-board instruments, including a GPS attitude receiver (actually being facilitated by the University of Colorado), a high-energy particle detector, and a sun sensor assembly. A ground station for control of JAWSAT will be installed at USAFA for cadets to gain practical experience as satellite operators.

## 1.3 JAWSAT Attitude Determination System

The attitude determination system for JAWSAT consists of a GPS attitude determination receiver (the Trimble TANS Vector), low cost gyroscopes, and digital sun sensors. The basic design philosophy of the attitude determination system is to use GPS and sun sensors to estimate gyro drift parameters in order to achieve the best possible overall accuracy. The idea of obtaining accurate spacecraft attitude estimates by combining measurements from less accurate sensors in a Kalman filter is not new [*e.g.,* Farrell, 1970], but the inclusion of a GPS attitude determination receiver introduces new aspects of the sensor integration related to multipath errors in the GPS measurements.

The ability of GPS and sun sensors to update the gyro drift estimates is limited by certain mission constraints. During eclipse periods the sun sensors cannot be used to correct gyro drift. GPS attitude measurement availability will be limited by the scheduling of payload operations. In particular, the GPS receiver will not be used while the PPTs are firing for two reasons. First, the PPTs generate a great deal of radio frequency noise; so in order to prevent interference with the GPS receiver, the receiver will be deactivated during PPT firings. Second, the power consumption of the PPTs is quite large, so turning off the GPS receiver will help provide enough power to perform PPT orbit maneuvering experiments. The thrust of the PPT engines is very small, so in order to effect any orbit maneuvers the engines will fire

pulses continuously for approximately half of each orbit during which maneuvers are being performed. In short, the mission constraints imposed by the PPTs and eclipse periods mean that each contributing sensor will be available to update gyro drift parameters approximately half of each orbit period. Figure 1.2 illustrates the JAWSAT orbit and mission constraints for the attitude determination system. The final orbit parameters for JAWSAT have not been established, but the design constraints represent general design considerations for the attitude determination system. The desired orbit for JAWSAT is a sun-synchronous orbit, and the availability of launch opportunities will dictate the actual orbit parameters.

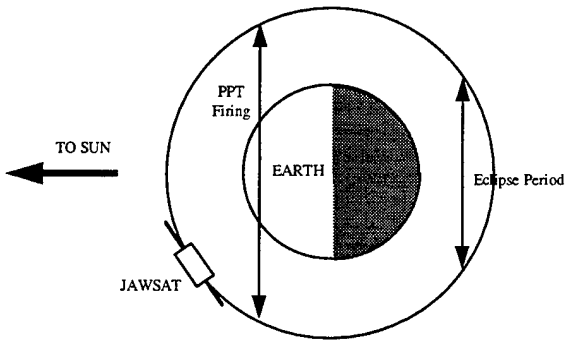


**Fig. 1.2.** JAWSAT sun synchronous orbit. *Figure shows JAWSAT in an Earth pointing attitude and a noon-midnight, sun synchronous orbit. During the eclipse period no sun sensor measurements are available. During PPT firing no GPS measurements are available.*

## 1.4 Overview

The remainder of this dissertation is organized as follows. Chapter 2 provides background on spacecraft attitude estimation and the computer simulation methodology used to evaluate attitude determination algorithms. Chapter 3 presents

Kalman filtering algorithms for GPS and gyro measurements, including a measurement differencing algorithm that reduces errors due to GPS multipath. Chapter 4 concentrates on filtering algorithms for digital sun sensors and gyros. Chapter 5 presents decentralized Kalman filtering algorithms for an integrated attitude determination system using GPS, gyros, and digital sun sensors. Chapter 6 presents a preliminary analysis of a nonlinear filter for integrated GPS attitude determination, and Chapter 7 recommends areas for future research and summarizes the key findings of this dissertation.

*Chapter 2:*

# *BACKGROUND*

Attitude determination is the problem of expressing the orientation of a spacecraft with respect to a given coordinate system, a fundamental problem of analytical dynamics [Battin, 1987, p. 79]. This chapter defines the coordinate frames of interest and summarizes the representations of the attitude used throughout the remainder of this dissertation. The fundamentals of spacecraft attitude determination are summarized for finding discrete point solutions based on attitude measurements. Integrated attitude estimation using Kalman filtering is then discussed as an extension of the point solution techniques. The Kalman filter approach, which uses gyro measurements combined with one or more other sensors, forms the foundation for the research in this dissertation. Finally, the attitude simulation methodology which provides the test bed for the attitude estimation algorithms developed in subsequent chapters is discussed.

## 2.1 Attitude Determination Preliminaries

Spacecraft attitude determination is an expression of the orientation of a body in terms of some frame of reference. The particular reference frames and the

representations used to express their relative orientations are defined for use in the remainder of this dissertation.

## Coordinate Frames

The principal coordinate frames for this study of spacecraft attitude determination are the inertial frame, the orbit local frame, and the body fixed frame. The observable attitude quantities measured by the sensors on JAWSAT are related to the coordinate transformation from inertial to body or from orbit local to body. These reference frames are depicted in Fig. 2.1.

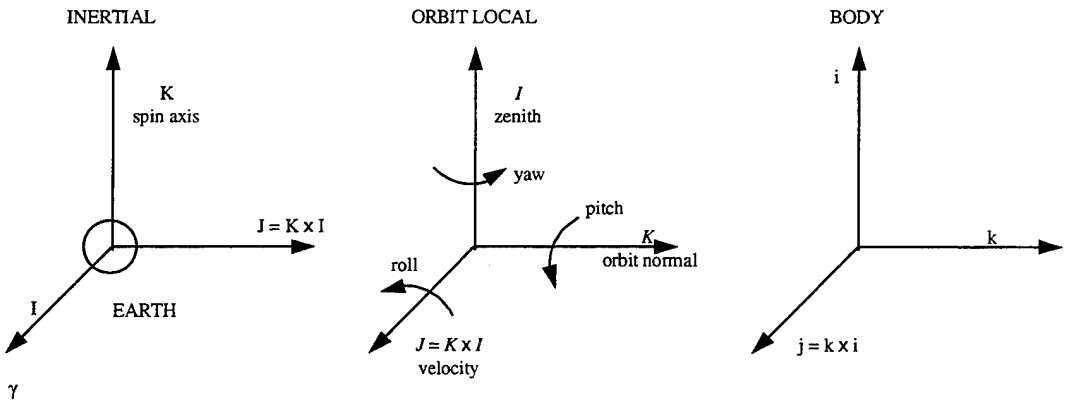


**Fig. 2.1.** Inertial, Orbit Local, and Body Fixed Reference Frames

The inertial frame (also called "Earth-centered inertial" or "geocentric inertial" coordinates) is defined in terms of the axis of rotation of the Earth [Wertz, 1978]. The center of the coordinate frame is the center of the Earth, the inertial **K** axis is aligned with the north celestial pole, and the inertial **I** axis lies in the plane of the celestial equator and is aligned with the intersection of the equatorial and ecliptic planes known as the first point of Aries. The inertial **J** axis forms a right-handed, orthonormal basis vector set. (This coordinate frame is not absolutely inertial, due to the motion of the Earth and luni-solar perturbations.)

The orbit local frame is defined in terms of the plane of the spacecraft orbit. The orbit local frame has its *I* axis aligned with the zenith (the radial from the center of the Earth to the spacecraft), the *K* axis is aligned with the orbit normal, and the *J* axis forms an orthogonal set. (For a circular orbit, *J* corresponds to the velocity direction.) The body frame axes coincide with the principal axes of the satellite, and are nominally aligned with the orbit local frames for an Earth-pointing spacecraft. The attitude Euler angles are defined as rotations of the body with respect to the orbit local frame. Yaw, roll, and pitch are defined as rotations about the *I*, *J*, and *K* axes, respectively.

**Attitude Representations**

There are no standard definitions for Euler angle representations of spacecraft attitude [Wertz, 1978]. The convention shown in Fig. 2.1, which has been used in previous work on spacecraft attitude estimation [*e.g.*, Axelrad *et al.*, 1993], will be used to define pitch, roll, and yaw rotations. This representation of the direction cosine matrix will be used primarily for ease of interpreting results. Attitude computations will be made using quaternions.

A quaternion is a four-parameter representation of the attitude that is free from singularities (unlike Euler angle representations). For a rigid body rotation about an arbitrary unit vector $\hat{\mathbf{n}}$, through an angle $\theta$, the quaternion is defined as $\bar{q} \equiv \begin{bmatrix} q_1 & q_2 & q_3 & q_4 \end{bmatrix}^T$ where $q \equiv \begin{bmatrix} q_1 & q_2 & q_3 \end{bmatrix}^T = \sin(\theta/2)\hat{\mathbf{n}}$ and $q_4 \equiv \cos(\theta/2)$ .

The four parameters of the attitude quaternion satisfy the constraint that the sum of their squares is unity. (Note that in general mathematical terms a quaternion is a four dimensional vector with arbitrary norm. The subset of quaternions that have unit norm is more precisely called a column vector of Euler-Rodrigues parameters as noted by Shuster [1993]. With this distinction in mind, the general practice in spacecraft attitude determination of referring to this quantity as the quaternion of rotation will be followed [*e.g.,* Shuster and Natanson, 1993; Wertz, 1978].)

The direction cosine rotation matrix can be expressed in terms of the quaternion components as

$$A(\bar{q})=\begin{bmatrix} q_1^2-q_2^2-q_3^2+q_4^2 & 2(q_1q_2+q_4q_3) & 2(q_1q_3-q_4q_2) \\ 2(q_2q_1-q_4q_3) & -q^2+q_2^2-q_3^2+q_4^2 & 2(q_2q_3+q_4q_1) \\ 2(q_3q_1+q_4q_2) & 2(q_3q_2-q_4q_1) & -q_1^2-q_2^2+q_3^2+q_4^2 \end{bmatrix} \tag{2.1}$$

Composition rules for combining quaternions are summarized in Shuster [1993] and Lefferts *et al.* [1982].

Attitude sensors on JAWSAT will consist of a Trimble Vector GPS receiver, gyroscopes, and a sun sensor assembly. Basic operation of these sensors is described in later chapters. The general problem of converting individual sensor measurements into attitude solutions is discussed in the next section.

## 2.2 Spacecraft Attitude Determination

Attitude determination methods based on vector observations of the attitude rely on forming solutions to Wahba's loss function [Wahba, 1965]. These methods involve finding attitude solutions based solely on measurements characterized by unit vector directions with no *a priori* knowledge of the attitude. Wahba's loss function describes a least-squares estimate of the attitude matrix and is written as

$$L(A) = \tfrac{1}{2}\sum_{i=1}^{n} a_i \left|\mathbf{b}_i - A\mathbf{r}_i\right|^2 \tag{2.2}$$

where $\mathbf{r}_i$ is the unit vector representation of the direction to a measured object in a reference frame, $\mathbf{b}_i$ is the unit vector representation of the direction in the spacecraft body frame, $a_i$ are positive weights associated with the measurements, $n$ is the number of measurements, and $A$ is the attitude matrix relating the reference and body frames.

Early approaches to minimizing Wahba's loss function focused on finding the independent elements of the $A$ matrix directly [*e.g.*, Wahba *et al.*, 1966]. The problem was later recast in terms of a cost function of the attitude quaternion, which has fewer parameters than the full attitude matrix. The attitude can be found from an eigenvalue equation for the quaternion [see Wertz, 1978]. A computationally efficient solution to this eigenvalue equation, the so-called QUEST (quaternion estimation) algorithm, was developed by Shuster and Oh [1981]. This widely used algorithm avoids computation of the eigenvectors by converting the eigenvalue equation into an algebraic equation in the attitude parameters. Despite its great speed, the QUEST algorithm suffers a singularity for attitude rotations near 180 degrees. A more complete review of attitude estimation methods beginning with the earliest solutions to Wahba's problem through the development of the QUEST algorithm can be found in Shuster [1983]. Bar-Itzhack and collaborators introduced

alternative iterative algorithms for directly estimating the direction cosine matrix [Bar-Itzhack and Reiner, 1984], the quaternion [Bar-Itzhack and Oshman, 1985], and the Euler angles [Bar-Itzhack and Idan, 1987]. These algorithms did not come into wide use due to the superior speed of the QUEST algorithm.

A computationally efficient solution to the attitude point solution based on the singular value decomposition was developed by Markley [1988]. Like the QUEST algorithm, the SVD algorithm does not require iteration, but it is not as fast as QUEST. However, the eigenvalues and eigenvectors are available for analysis. A new algorithm that computes the attitude matrix directly and rivals the QUEST algorithm in speed was discovered by Markley [1993]. This so-called fast optimal attitude matrix (FOAM) algorithm has the advantage that there is no singularity for rotations near 180 degrees. Note that the GPS attitude determination problem can be stated in terms of the Wahba loss function [Cohen, 1992; Cohen, Cobb, and Parkinson, 1992], making high output rates for GPS attitude solutions possible for high dynamic applications.

Unfortunately, attitude point solution methods do not generally allow for the combination of attitude measurements from multiple sensors or sensors characterized by bias parameters that also need to be estimated. Off-line batch estimation algorithms for simultaneously estimating attitude and sensor biases and misalignments have been developed [*e.g.,* Markley, 1991 and 1989; Shuster, 1989].

Sequential estimation techniques based on Kalman filtering are used for on-line estimation of attitude and sensor correction parameters.

## 2.3 Kalman Filtering for Spacecraft Attitude Estimation

The Kalman filter [see *e.g.*, Maybeck, 1979] provides a least squares estimate of the state and error covariance of a linear system. For nonlinear system such as quaternion attitude states, the extended Kalman filter is frequently used [*e.g.*, Lefferts *et al.*, 1982]. The extended Kalman filter linearizes state updates about the current best estimate of the state. Thus, rather than estimating the total state, only an estimate of the state correction is required. The dynamic model for the state error correction, $\Delta x$, can be described by:

$$\frac{d}{dt}\Delta x = F\Delta x + Gw \tag{2.3}$$

with observations of the state given by

$$z = \mathbf{H}x + v \tag{2.4}$$

where $x$ is the state vector, $F$ is the system dynamics matrix, $G$ is the noise distribution matrix, $z$ is the observation vector, $\mathbf{H}$ is the observation matrix, and $w$

and $v$ are zero mean Gaussian driving noise vectors with spectral density matrices $Q$ and $R$, respectively.

The Kalman filter has been developed to determine the best estimate of the state $\hat{x}$ using the measurements $z$. For a discrete-time system, the state propagation can be described by the state transition relation

$$\hat{x}_{k+1} = \Phi \hat{x}_k + \Gamma_k w_k \tag{2.5}$$

where $\Phi$ is the state transition matrix, $\Gamma$ is the discrete time noise distribution matrix, and $k$ is the time index. The superscript "-" indicates a quantity prior to a measurement update; superscript "+" indicates a quantity after a measurement update has been incorporated. The state error covariance matrix, $P$, is propagated according to

$$P_{k+1}^{-} = \Phi P_k^{+} \Phi^T + Q_d \tag{2.6}$$

where $Q_d$ is the discretized process noise covariance.

The optimal measurement update for the state error correction vector in the extended Kalman filter is given by

$$\Delta\hat{x}^{+} = K\left(z - H\hat{x}^{-}\right) \tag{2.7}$$

$$P^{+} = (I - KH)P^{-}(I - KH)^{T} + KRK^{T}. \tag{2.8}$$

where the Kalman gain, $K$, is given by

$$K = P^{-}H^{T}\left(HP^{-}H^{T} + R\right)^{-1} \tag{2.9}$$

Additional information on Kalman filtering can be found in Brown and Hwang [1992] and Maybeck [1979].

Early applications of Kalman filtering for spacecraft attitude determination used Euler angle formulations for the attitude states [Sorenson *et al.*, 1979; Farrenkopf, 1978; Farrell, 1970]. Euler angle Kalman filters for spacecraft attitude estimation are still frequently used in simulation studies where singularities can be avoided [*e.g.*, Sullivan, 1995; Kudva and Throckmorton, 1994]. A quaternion filter for spacecraft attitude estimation was developed by Lefferts *et al.* [1982]. Their approach uses gyro measurements in the state propagation step and other sensors to perform the measurement update. This use of the gyro measurements to form the dynamic model directly has become a standard practice in spacecraft attitude determination.

An extension of the measurement model introduced by Lefferts *et al.* [1982] was introduced by Shuster [1990]. In this paper the measurement model is well suited to the case of multiple non-collinear vector observations (based on the QUEST algorithm) that are available at each measurement epoch (as in the case of a CCD star camera that has several stars within its field of view). A comparison of the effects of the two different measurement models was performed by Sedlak and Chu [1993]. They used gyro and star tracker data from the Extreme Ultraviolet Explorer (EUVE) satellite and found essentially no differences in performance between the two filter types. Since no significant difference was found between the two methods, the filter algorithm of Lefferts *et al.* [1982] is used exclusively as the basis for this research. Details of the algorithm will be discussed in Chapter 3.

## 2.4 Attitude Estimation Simulation

Computer simulation has been called the third paradigm of science, joining the centuries-old paradigms of theory and experiment. The methodology for evaluating attitude estimation algorithms in this dissertation will be a computer simulation developed in MATLAB.

The simulation is composed of three primary sections as shown in Fig. 2.2: a truth model of controlled attitude dynamics, measurement models of the attitude sensors, and algorithms for spacecraft attitude determination. The truth models generate the simulated dynamics of the satellite based on the anticipated performance of the attitude control system. The spacecraft is modeled as nadir-pointing and three-axis stabilized within the performance specifications of the controller.

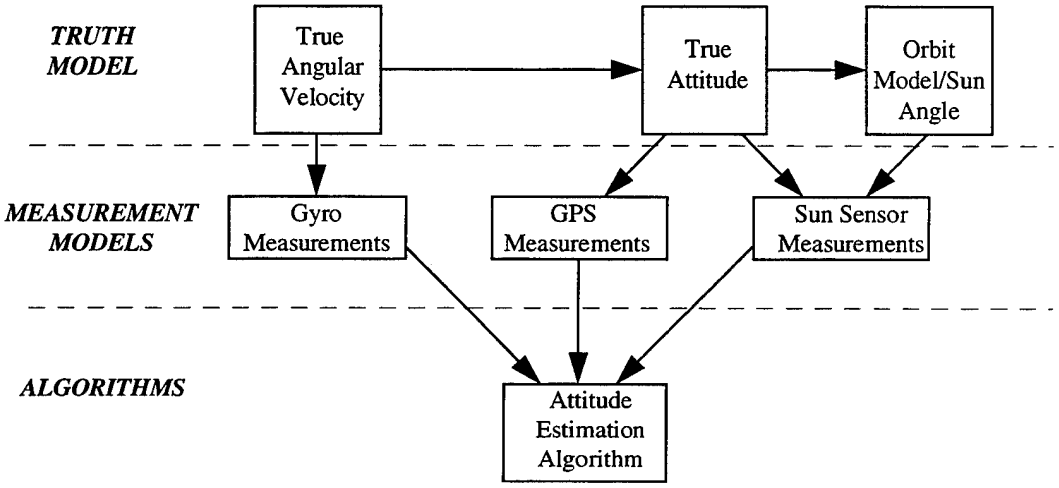


**Fig. 2.2.** Simulation Data Flow.

The measurement models for the attitude sensors have been developed so that GPS attitude data can be incorporated to make the simulations as realistic as possible. GPS attitude errors are taken from static ground tests and orbital flight data and superimposed on the dynamics generated by the truth model. This method–using actual measurement errors to contaminate the "perfect" measurements from the

truth model–has been used extensively in the development of filters for navigation systems [*e.g.*, Maybeck, 1979].

Measurement models for gyros and digital sun sensors are simulated using analytical models based on their expected performance. Details of these analytical models will be addressed in subsequent chapters. As with the GPS measurements, ground test and flight test data can be substituted for the simulated data when it becomes available.

The ultimate aim of the simulation is the evaluation of spacecraft attitude estimation algorithms. The attitude determination simulation provides the test bed for analyzing algorithms. The development and comparison of estimation algorithms for integrated GPS attitude determination systems provides the focus for the remainder of this dissertation.

*Chapter 3:*

# *ATTITUDE DETERMINATION USING GPS AND GYROS*

The Global Positioning System (GPS) has the capability to provide position, velocity, attitude, and timing information to a satellite in low Earth orbit. This combination of many functions in one instrument is attractive for small satellites, where size, power, and cost are limited. A recent report by the National Research Council advocates incorporation of GPS into small satellite designs for orbit and attitude determination [NRC, 1994]. The objective of this chapter is to develop estimation algorithms that integrate GPS based attitude with on-board gyros. A demonstration vehicle for this design is JAWSAT, the Joint Air Force Academy - Weber State University Satellite.

This chapter describes ground testing of a GPS attitude receiver using a small satellite mock-up as well as on-orbit results obtained from the U.S. Air Force RADCAL satellite. These data sets are used to test the algorithms developed later in this chapter. Error sources for gyros and simulated gyro performance are discussed. An extended Kalman filter algorithm for spacecraft attitude estimation using GPS and gyros is presented. An improved estimation algorithm that accounts for the time correlated nature of the GPS attitude estimation errors due to multipath is also

introduced. Finally, simulation results of the two algorithms are presented and compared.

## 3.1 GPS Based Attitude Determination

Attitude determination using differential carrier phase measurements from a satellite radio signal was first demonstrated more than twenty years ago using the U.S. Navy TRANSIT system to measure the heading of large ships [Albertine, 1974]. Although limited by several factors inherent in the TRANSIT system, this study touched on many of the critical issues that have been addressed in current GPS based attitude determination systems such as antenna baseline estimation, integer ambiguity resolution, accurate measurement of differential carrier phase, and multipath rejection. With the advent of GPS, accurate satellite based attitude determination is now possible for aerospace applications. Several studies helped advance the required techniques needed to extract attitude information from L-band differential phase measurements made using multiple antennas [*e.g.*, Lu, 1994; Lu *et al.*, 1993; Bass *et al.*, 1992; Brown, 1992; Schwarz *et al.*, 1992; Van Graas and Braasch, 1992; Satz *et al.*, 1991; Brown and Ward, 1990; Rath and Ward, 1989]. One successful approach has been implemented in the Trimble Vector receiver described as by Cohen [1992].

**Trimble Vector Receiver**

The Trimble Vector is a six-channel, four-antenna, C/A code receiver that is primarily used for aircraft applications, but a space version of the software has also been developed for use in low Earth orbit. The receiver measures 127 mm × 241 mm × 56 mm, weighs 1.42 kg, and draws 4 W at 9-18 Volts DC. The receiver is connected to four microstrip patch antennas with 50 Ω coaxial cable. The antennas measure 96 mm × 102 mm × 13 mm and weigh 0.19 kg each. The antennas will be mounted on the extreme corners of the zenith face of the satellite. The receiver has an RS-422 port for commands and data output at a rate of 38.4 kbaud, and attitude solutions are available at a nominal rate of 2 Hz [Trimble, 1994]. The Vector receiver observes the differential phase of L1 carrier signals received at two or more antennas.

The principal observable for GPS attitude determination is the Doppler shifted carrier phase difference between a master antenna and one or more slave antennas. Figure 3.1 shows the incident carrier wave received by a single master and slave antenna pair. The difference in the received phase, $\Delta\phi$, between the master and the slave is the quantity actually measured. The range difference between the master and slave is required to form an attitude solution. The relation between phase difference, $\Delta\phi$, and range difference, $\Delta r$, (both expressed in cycles) is as follows,

$$\Delta r = \Delta\phi + k - \beta + \upsilon \tag{3.1}$$

where $k$ is the integer number of carrier cycles in the differential phase, $\beta$ is the constant fractional cycle hardware bias between the two antennas, and $\nu$ is the measurement error due to receiver noise and multipath.

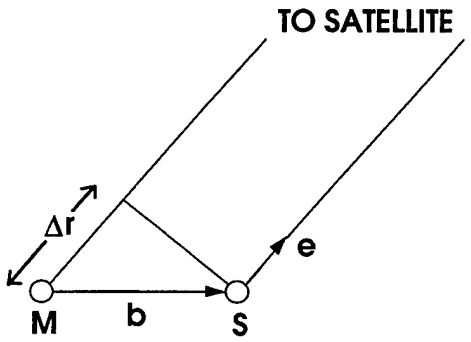


**Fig. 3.1.** GPS Differential Phase Geometry.

For multiple baselines ($i = 1,\ldots,n$) and multiple GPS satellites in view ($j = 1,\ldots,m$), the differential range measurements can be expressed as

$$\Delta r_{ij} = \Delta\phi_{ij} + k_{ij} - \beta_i + \upsilon_{ij} \tag{3.2}$$

The range differences for each baseline-satellite pair are just the projections of the baseline vectors directed from the master to each of the slaves, $\mathbf{b}_i$, onto the

user line of sight vectors to the GPS satellites, $\mathbf{e}_j$. This gives the range difference measurement model as

$$\Delta r_{ij} = \mathbf{b}_i \bullet \mathbf{e}_j \tag{3.3}$$

If the baseline vector components are known in a vehicle body fixed frame, denoted by superscript *B*, and the line of sight vector components are known in an inertial or navigation frame, denoted by superscript *N*, the range differences can be represented by,

$$\begin{aligned} \Delta r_{ij} &= \left(b_i{}^B\right)^T \left(e_j{}^B\right) \\ &= \left(b_i{}^B\right)^T \left({}^B\mathbf{C}^N e_j{}^N\right) \end{aligned} \tag{3.4}$$

where the attitude matrix, ${}^B\mathbf{C}^N$, rotates the line of sight vector from the navigation frame to the body fixed frame.

Several methods exist for computing the attitude matrix from a set of range difference measurements [*e.g.*, Shuster and Oh, 1981; Shuster, 1989; Cohen *et al.*, 1992; Markley, 1993]. The Trimble Vector receiver implements a least squares solution that minimizes the following cost function,

$$J\left({}^{B}\hat{\mathrm{C}}^{N}\right)=\sum_{i=1}^{n}\sum_{j=1}^{m}w_{ij}\left[\Delta r_{ij}-\left(b_{i}^{B}\right)^{T}\left({}^{B}\hat{\mathrm{C}}^{N}e_{j}^{N}\right)\right] \tag{3.5}$$

where $w_{ij}$ is a weighting factor for each measurement which may be based on factors such as baseline geometry or signal level. An iterative approach is used in the receiver software to solve for the best estimate of the attitude matrix in equation 3.5. A fast, non-iterative solution method is also available in the receiver software that is based on Markley's [1993] solution to Wahba's problem. However, this requires that the four antennas be noncoplanar. See Cohen [1992] for details.

When forming attitude solutions using GPS differential phase measurements, several quantities are assumed to be known. These quantities are the integer ambiguities, $k_{ij}$, the antenna baseline vectors, $\mathbf{b}_i$, and the hardware biases, $\beta_i$. In fact, these parameters are computed by the receiver prior to generating attitude solutions. The baselines and hardware biases are estimated off-line during a ground survey lasting eight hours or more. The long duration is required so that satellite motion overhead can be used to resolve integer ambiguities and estimate the constant baseline and bias values for a given hardware configuration. The integer ambiguity resolution performed during the off-line survey is not valid for later operation, so only the $\mathbf{b}_i$ and $\beta_i$ values are stored for later use. If it is not possible to perform an antenna baseline survey on the fully integrated spacecraft prior to launch, the antenna

baselines could be estimated on-orbit using the bootstrap algorithm developed by Ward and Axelrad [1995]. This method is not implemented in the receiver software.

Determining the integer ambiguities, $k_{ij}$, for attitude determination requires an initialization step. Assuming the baselines and hardware biases are known, the integer ambiguities can be resolved by moving the structure through a large angle (on the order of 90 deg), or by tracking the motion of the GPS satellites overhead for orbital applications [Cohen, 1992]. Accumulating time-differenced phase measurements and constraining the antenna baseline lengths to their known values allows for a batch estimation process to resolve the integers. This initialization batch process typically takes less than a minute to accumulate the time-differenced data and resolve the integers. Once the integers are known, they are continually updated using the incoming phase measurements.

The Vector receiver outputs attitude solutions based on the least squares algorithm described above. Raw differential phase measurements are also available as outputs from the Vector receiver, and these could be used for analysis of attitude solutions off-line. The Vector attitude solution is treated as the observation in the JAWSAT attitude determination system.

The Vector receiver hardware has not been formally space qualified, but receiver software designed for use on orbit has been developed. Small satellite

designs frequently use terrestrial hardware in the interest of keeping costs low. Certain electrical components, such as electrolytic capacitors, need to be avoided and additional shielding of terrestrial equipment may be needed to ruggedize hardware for use in space [Reeves, 1994].

**Spacecraft Attitude Determination Using GPS**

On-orbit testing of the Trimble Quadrex attitude receiver, a precursor to the Trimble Vector to be used for JAWSAT, has been described by Lightsey *et al.* [1994, 1993] and Axelrad and Ward [1994]. The Quadrex receiver was implemented on the Air Force RADCAL satellite as a separate experiment which is not integrated with the spacecraft attitude determination and control system. The output of the Trimble Quadrex receiver on RADCAL is raw differential phase measurements, not processed attitude solutions as will be the case for the Vector receiver. Thus, GPS based attitude estimation for RADCAL requires ground processing of the raw measurements to form attitude solutions.

The first known use of GPS attitude determination in a closed loop satellite attitude control system will be the NASA Spartan mission [Bauer *et al.,* 1994]. This mission is a free-flying Space Shuttle experiment that will use the Vector receiver. Launch is planned in 1995.

## GPS Attitude Errors

Frequently, the dominant error source in GPS attitude determination is multipath contamination of the differential carrier phase measurements. Mitigation of multipath errors in these measurements has been investigated by Georgiadou and Kleusberg [1988], Cohen and Parkinson [1991], and Axelrad, Comp, and MacDoran [1994]. The latter approach uses receiver reported signal to noise ratios to characterize multipath errors in the phase residuals. This research is expected to bring about significant improvements in GPS attitude receiver performance in the presence of multipath. However, the algorithms being developed will require substantial modification of receiver software that is not anticipated for the JAWSAT receiver. Later in this chapter a multipath mitigation scheme is proposed for GPS attitude solutions through integration of gyroscope measurements.

## GPS Attitude Test Data

The GPS attitude measurements used in computer simulations come from two sources: ground tests and RADCAL orbit data.

Ground based performance testing of the Vector receiver has been reported by Gomez *et al.* [1995] and Axelrad and Chesley [1993]. Further ground based testing was conducted at the University of Colorado using a JAWSAT test structure. The test structure is an aluminum box with a plate for mounting the four GPS antennas. The plate measures 66 cm × 53 cm, with the four GPS patch antennas mounted at the extreme corners. The JAWSAT mock up with GPS antennas and Vector receiver is shown in Fig. 3.2 on the roof of the Engineering Center at the University of Colorado.

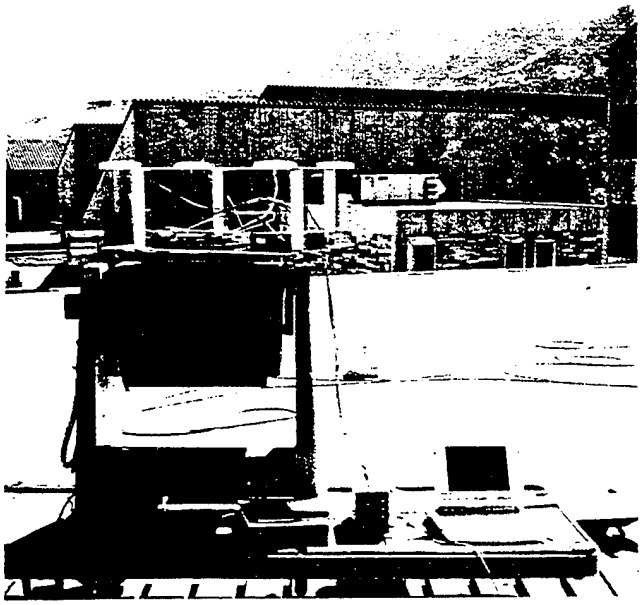

**Fig. 3.2.** GPS Antenna Test Structure.

Sample results from a static test run are shown in Fig. 3.3. No filtering of the receiver output or integration with measurements from other sensors was included in this test. Note that for the short baselines used, the attitude error is approximately

0.9 degrees, 3-σ. Also note the apparent time correlation in the attitude solutions indicative of multipath errors affecting the raw signal.

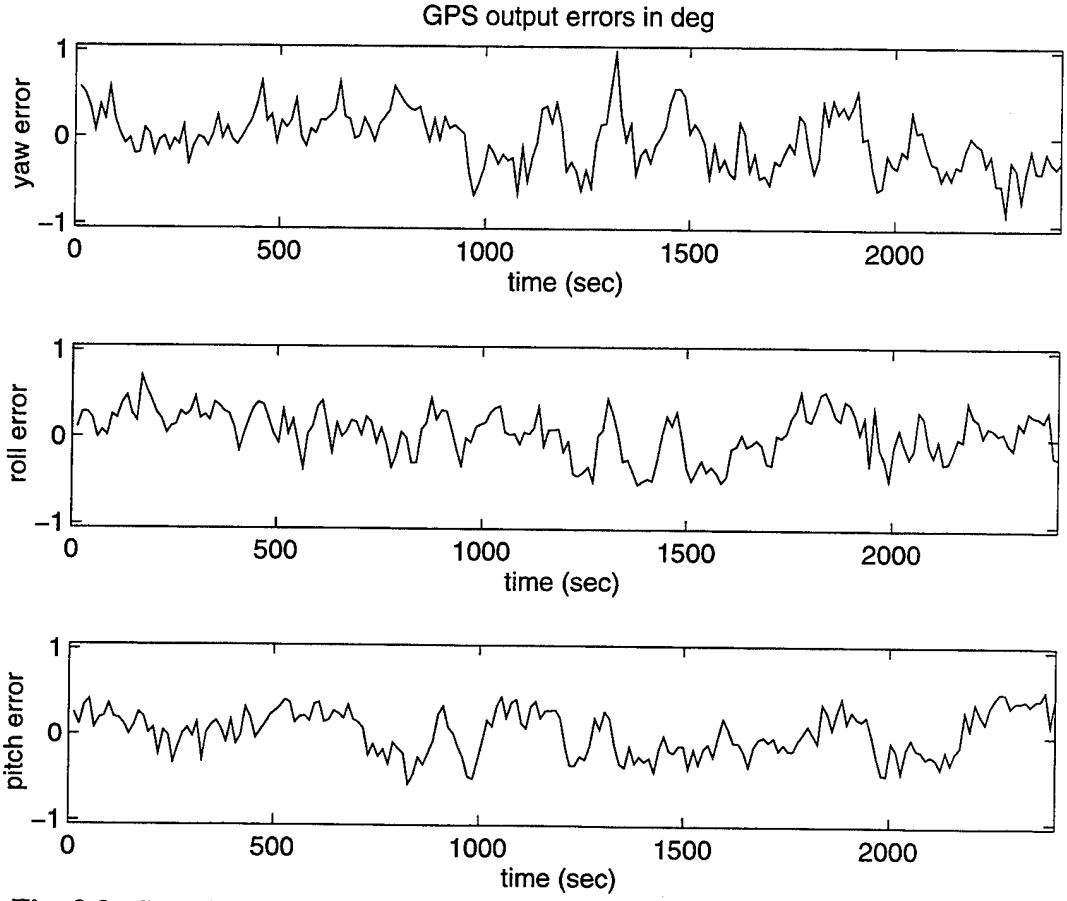


**Fig. 3.3.** Sample GPS Attitude Output. *Data was collected on October 11, 1994, using a Trimble Vector attitude receiver and the JAWSAT mock up structure.*

In this case the attitude was known to be fixed, so any variations in the results were assumed to be measurement errors. The attitude error characteristics shown in Fig. 3.3 are used in a simulation of an integrated GPS attitude determination system described later in this dissertation.

Flight test results from the Quadrex receiver aboard RADCAL were also used. The RADCAL satellite is a gravity-gradient stabilized satellite with GPS antennas arranged in a square so that the baseline lengths are 62 cm for the two shorter legs and 78 cm along the diagonal. These baseline lengths are very similar to the antenna baseline lengths that will be used on JAWSAT. A key difference between RADCAL and JAWSAT is the existence of the gravity gradient boom that extends 6 m from the zenith face of the satellite. This boom creates more severe multipath characteristics than would be expected on JAWSAT.

In order to use the on-orbit results from RADCAL, filtered attitude solutions were subtracted from GPS point solutions [Ward and Axelrad, 1995]. This was required since there is no "truth reference" sensor for the attitude of RADCAL. Therefore, the accuracy of the attitude solutions can only be characterized in comparison with filtered solutions using the same data. Unfortunately, the filtered solutions may contain errors due to any mismodeled dynamics of the spacecraft. In order to reduce the modeling errors in the differenced data, the data was high-pass filtered using an eighth-order Butterworth filter. This filter attenuated frequency contributions with periods longer than 20 minutes which are likely to be due to mismodeled dynamics. A sample of this GPS attitude error data is shown in Fig. 3.4.

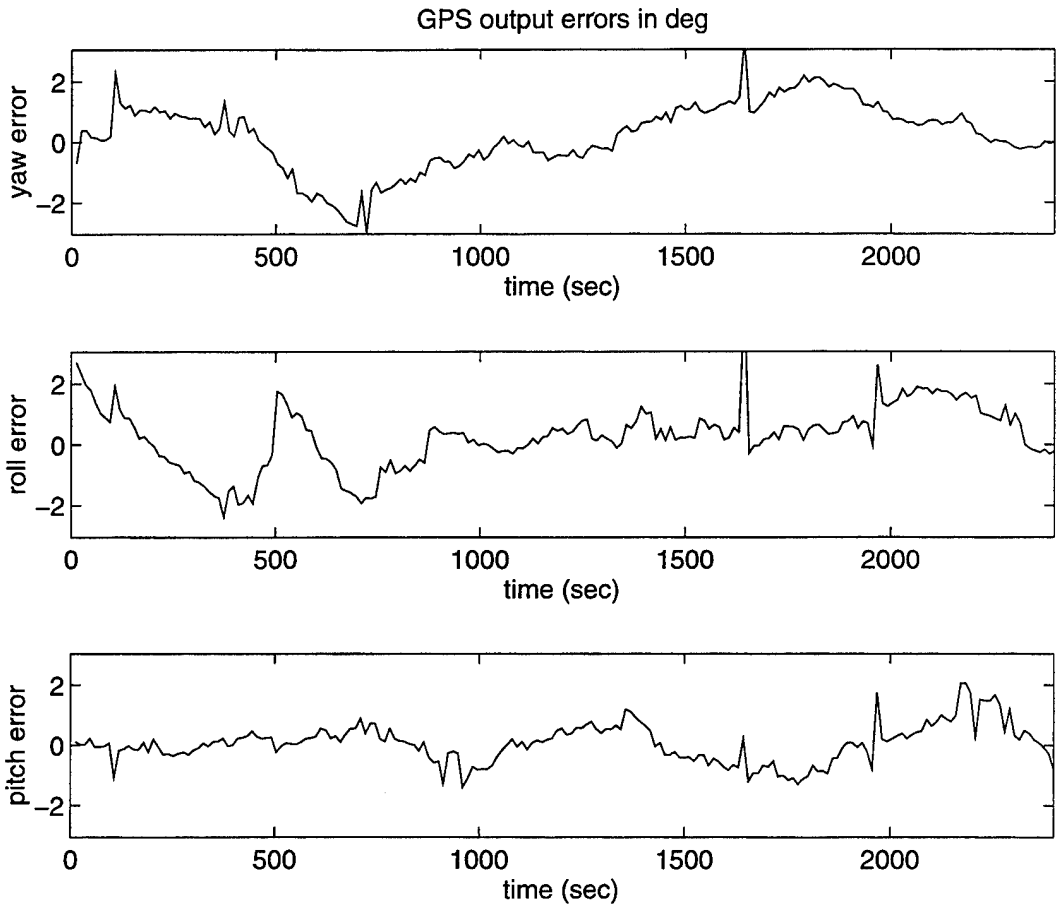


**Fig. 3.4.** Sample GPS Attitude Output from RADCAL. *Data was collected on RADCAL day 107 using a Trimble Quadrex attitude receiver. Plot shows GPS point solutions minus filtered solutions with low frequency errors removed.*

Note that the RADCAL results generally exhibit larger errors than the ground test data. There are several reasons for the poor quality of the RADCAL measurements. These include the fact that the four GPS antennas on RADCAL are canted away from zenith by 17 deg and no antenna ground planes were used. In addition, the gravity gradient boom and UHF antennas protruding from the zenith face of the spacecraft contribute to a severe multipath environment. Finally, poor satellite geometry and poor measurement quality cause large attitude errors such as the outliers at approximately 1600 sec in Fig. 3.4. Nonetheless, the RADCAL data

will be used as a baseline case in the remainder of this dissertation for two reasons: first, the poor quality of the GPS data from RADCAL is likely to represent a worst case for JAWSAT; and second, the RADCAL data is the only available on-orbit GPS attitude data, so it offers the most realistic simulation data available.

The time correlation in the multipath errors can be modeled as a first order Markov process. Figure 3.5 compares the autocorrelation functions of an ideal Markov process with multipath data from ground tests and RADCAL. The autocorrelation function for the ideal Markov model is from Gelb [1974]. The computed autocorrelation functions have been normalized to have unit magnitude.

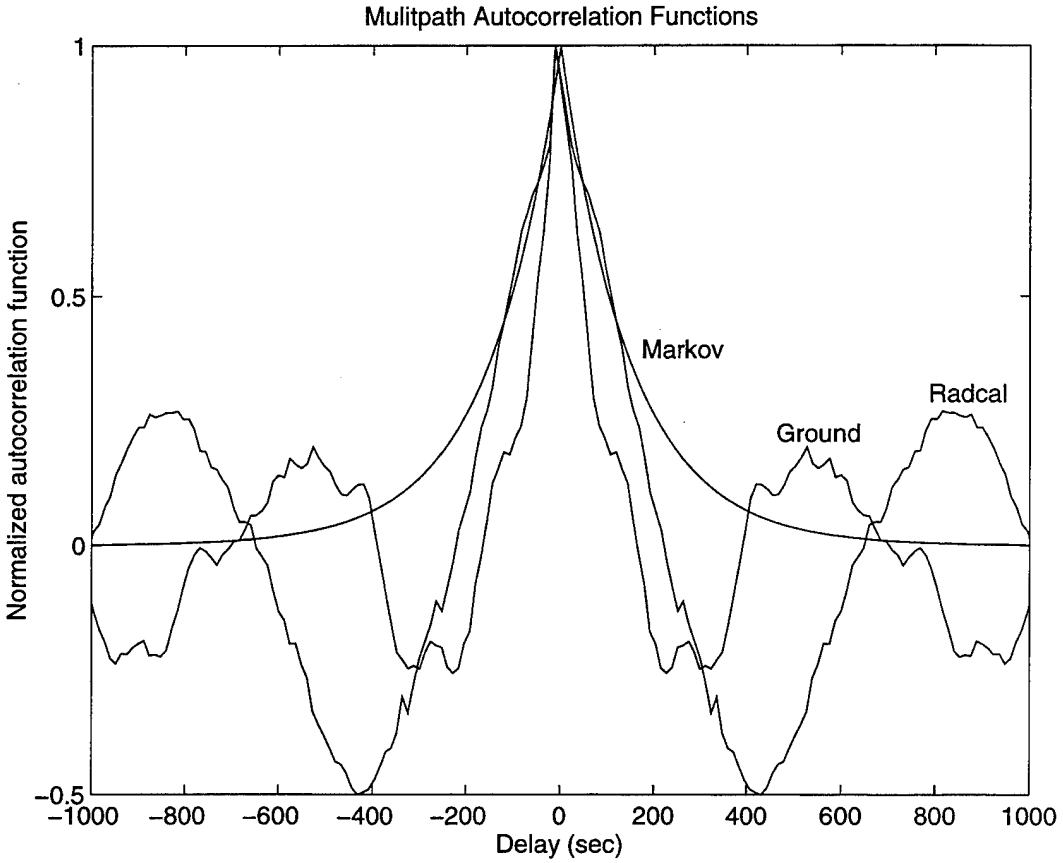


**Fig. 3.5.** Comparison of autocorrelation functions of Markov process and measured GPS multipath.

The dominant sharp peaks in the autocorrelation plots indicate that a Markov model for multipath captures most of the effect. The experimental GPS attitude data from RADCAL and ground tests exhibit side lobes which suggest the presence of smaller periodic effects of unknown frequency in addition to the time-correlation modeled by the Markov process. If the frequency components present in the multipath were known, these effects could be added to the model. The measurement differencing algorithm developed in Section 3.4 uses a Markov model for multipath effects.

## 3.2 Gyro Attitude Determination

The use of gyroscopes for spacecraft attitude determination and inertial navigation systems is well established [Wertz, 1978]. Generally, gyroscopes rely on the properties of a rotating medium (usually a spinning mass or counter-rotating beams of light) to sense angular velocity. Current navigation grade gyroscopes are very accurate, but their long term performance is limited by how well their random drift can be compensated. For a general discussion of gyroscope properties and drift limitations, see Litton [1994], Siouris [1993], Pandit and Zhang [1986], and Wertz [1978], for example.

The gyros selected for JAWSAT will be determined by the cost and performance characteristics. In this dissertation, fiber optic gyros and micromechanical gyros based on the piezoelectric effect will be considered. The basic operation and typical performance of these gyros is described in this section.

### Fiber Optic Gyros

Fiber Optic Gyros are attitude sensors that measure changes in transit times of counter rotating beams of light in a closed optical path. FOGs were developed from research on interferometry and ring laser gyros. FOG technology is considered very promising as an accurate, low-cost attitude sensor since many of the

components (such as optical fiber and superluminescent diodes) are already produced in relatively large quantities for telecommunications systems [Mark *et al.*, 1991; Nuttall, 1990]. The Clementine spacecraft launched in January 1994 included FOGs in its attitude sensor suite [NRC, 1994].

FOGs operate by splitting a light source into two beams. One rotates clockwise through a coil of optical fiber, the other beam rotates counterclockwise. When the beams are recombined after traveling the same optical path in opposite directions, the interference pattern can be used to measure the rotation rate. These sensors are sometimes called interferometric fiber optic gyros (IFOG) for this reason.

The counter rotating light beams can be used to sense rotation since the light (photons) moving in opposite directions around the ring will travel different path lengths if the ring is rotating. This effect is predicted by relativity theory and was first studied by Sagnac *circa* 1919 [Post, 1967; Arditty and Lefèvre, 1981]. The basic principle of FOG rotation sensing is shown in Fig. 3.6. The phase shift as the fiber coil rotates through the angle $\Delta\theta$ is sensed by a photodetector. Practical implementation issues for FOGs and additional theoretical details are discussed in Lefèvre [1993], Udd [1991], Lefèvre *et al.* [1984].

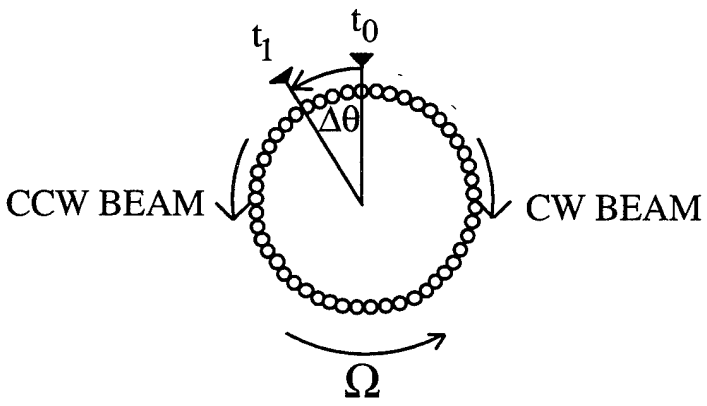


**Fig. 3.6.** Standing Wave Interference Pattern in Fiber Optic Gyro.

Measuring these path differences in a practical way and expressing these measurements in a usable form were the key challenges to using optical gyros as precision angular velocity sensors. The primary error sources for FOGs are random drifts in the angular rate bias. The angular rate bias is an offset between the FOG measurement and the true angular velocity. These bias drifts arise due to imperfections in the optical fiber that cause the clockwise and counter clockwise beams to experience slightly nonreciprocal paths. The drift in the rate bias can be characterized by random walk behavior. Environmental effects such as thermal and magnetic disturbances also contribute to the random bias drift [Siouris, 1993]. Significant improvements have been made in calibrating and compensating for these bias drifts, and high accuracy FOGs are available with drift rates on the order of $5\times10^{-8}$ rad/sec.

**Micromechanical Gyros**

Micromechanical gyros are miniature tuning fork sensors based on the piezoelectric effect. These gyros are currently being developed primarily for automotive and military applications because of their low cost, relative ease of construction, and modest performance [Weinberg *et al.*, 1994; Blanco and Geen, 1993]. However, these attributes could also be exploited by small satellite programs and result in a "breakthrough in size, weight, and cost" for spacecraft applications [NRC, 1994, p. 59].

Micromechanical gyros are being developed and tested using micromachining processes developed by the integrated circuit industry. The gyros are fabricated from thin wafers of silicon or quartz typically about 1 $mm^2$. Integrated electronics can be included so that an entire gyro sensor can be included on one chip. Several development efforts are currently being conducted [*e.g.*, Weinberg *et al.*, 1994, 1993; Blanco and Geen, 1993; Maseeh, 1993; and Sitomer *et al.*, 1993].

Tuning fork gyros operate as follows. Two well balanced micromechanical accelerometers are dithered out of phase. If the accelerometers are both mounted along one axis and the dither is excited along a second perpendicular axis, then the difference signal between the two accelerometers contains angular rate information for the third orthogonal axis [Blanco and Geen, 1993]. Signals due to linear

acceleration along the gyro axis cancel because of the out-of-phase dithering. For micromechanical gyros based on this principle, a comb of tuning-fork accelerometers is bonded to a glass substrate [Weinberg *et al.*, 1993].

Single silicon crystal gyros made by microfabrication technologies have been tested in laboratory environments [Weinberg *et al.*, 1994]. Their results indicate promising results for low cost spacecraft applications. In particular, they report quite stable gyro biases under ambient conditions and 0.8 deg/(hr)$^{1/2}$ angle random walk. These performance parameters will be used to generate simulated measurements for low quality gyros.

**Gyro Measurement Model**

Gyro model parameters have been adapted from Siouris [1993] and Lefferts *et al.* [1982] for use in the attitude estimation simulation. The gyro measurement model is described by

$$u = \omega + n_1 + b \tag{3.6}$$

where $u$ is the measured angular rate output, $\omega$ is the true angular rate, $n_1$ is the random drift rate noise, and $b$ is the drift rate bias. This gyro model has been used

extensively in spacecraft attitude determination studies [*e.g.*, Sedlak and Chu, 1993; Markley *et al.*, 1993; Fisher *et al.*, 1989]. The noise term is described by

$$\begin{aligned} &\mathrm{E}[n_1] = 0 \\ &\mathrm{E}\left[n_1 \cdot n_1^{\,T}\right] = Q_1 = \sigma_1^{\,2} I_{3\times 3} \end{aligned} \tag{3.7}$$

Note that since attitude is the integral of the angular velocity, the random errors in angular rate due to $n_1$ will result in random walk errors in the attitude. Thus, $n_1$ is often referred to as angle random walk noise.

The drift rate bias, $b$, is not constant, but varies slowly in a manner that can be characterized by a random walk model

$$\dot{b} = n_2 \tag{3.8}$$

where $n_2$ is the random walk in drift rate with noise described by

$$\begin{aligned} &\mathrm{E}[n_2] = 0 \\ &\mathrm{E}\left[n_2 \cdot n_2^{\,T}\right] = Q_2 = \sigma_2^{\,2} I_{3\times 3} \end{aligned} \tag{3.9}$$

**Inertial Quality Gyro Simulation**

The gyros modeled as the baseline design for this dissertation are medium grade inertial instruments, typical of the FOGs projected for use on JAWSAT [Page and Sugarbaker, 1995; Sullivan, 1995; Sedlak and Chu, 1993; Mathews, 1990]. The specific noise strengths used are

$$\sigma_1^{\,2} = 10^{-11}\,\frac{\text{rad}}{(\text{sec})^{1/2}}$$
$$\sigma_2^{\,2} = 10^{-11}\,\frac{\text{rad}}{(\text{sec})^{3/2}} \qquad (3.10)$$

Simulated gyro bias drift due to the $n_2$ term is shown in Fig. 3.7 for the case of no dynamics. Figure 3.7 shows about 6.5 hours of bias drift in order to show an appreciable effect. Fig. 3.8 shows the gyro output for the first 40 minutes of the same simulation run. Note that the angular rate noise due to the $n_1$ term dominates the output errors in Fig. 3.8; thus, angular rate noise is the most serious error source for time frames of interest for spacecraft attitude estimation [Markley, 1993]. However, accurate estimation of the gyro bias is also critical, since the bias drift depicted in Fig. 3.7 will accumulate over longer time periods. The general error characteristics described in this section will be modified to match the flight hardware when that data becomes available.

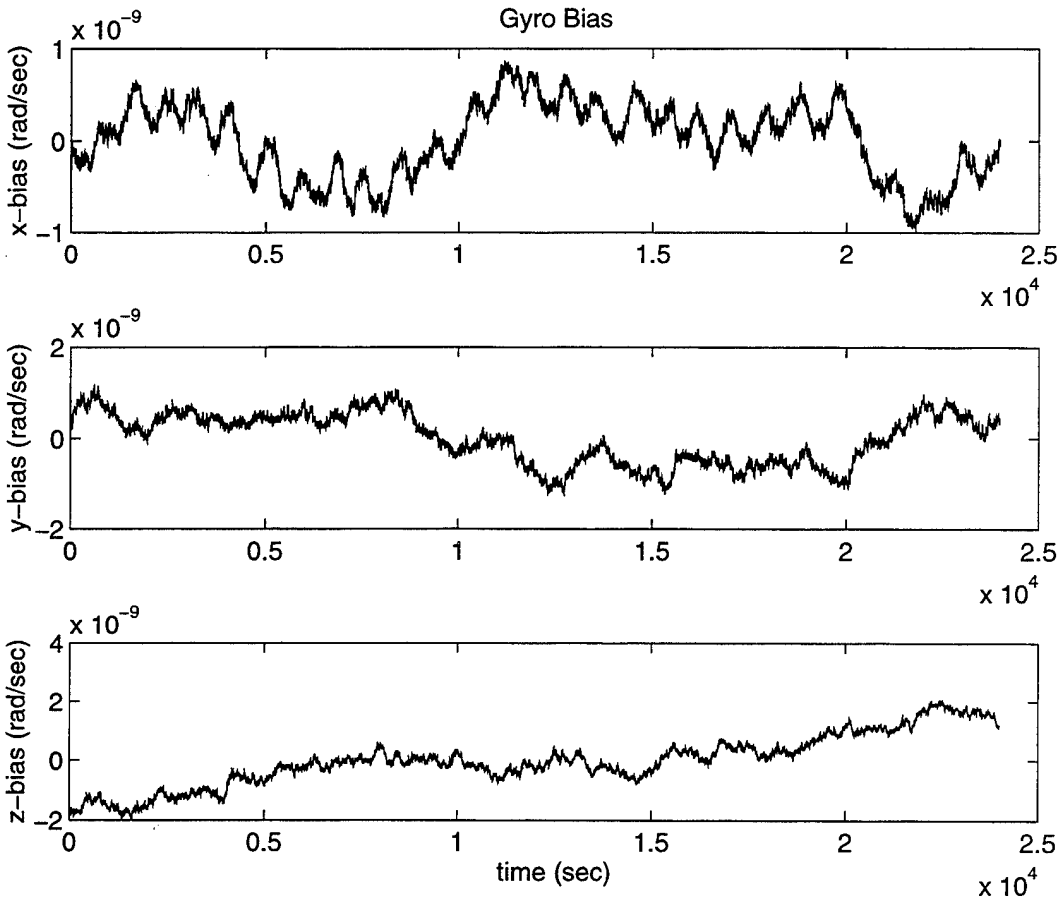


**Fig. 3.7.** Simulated Bias Random Walk. *Graphs show changes in drift rate bias for gyros aligned with each of the three body axes. Angular velocity input is zero for each axis. Mean offset, typically on the order of 10 deg/hr, has been removed from the plots.*

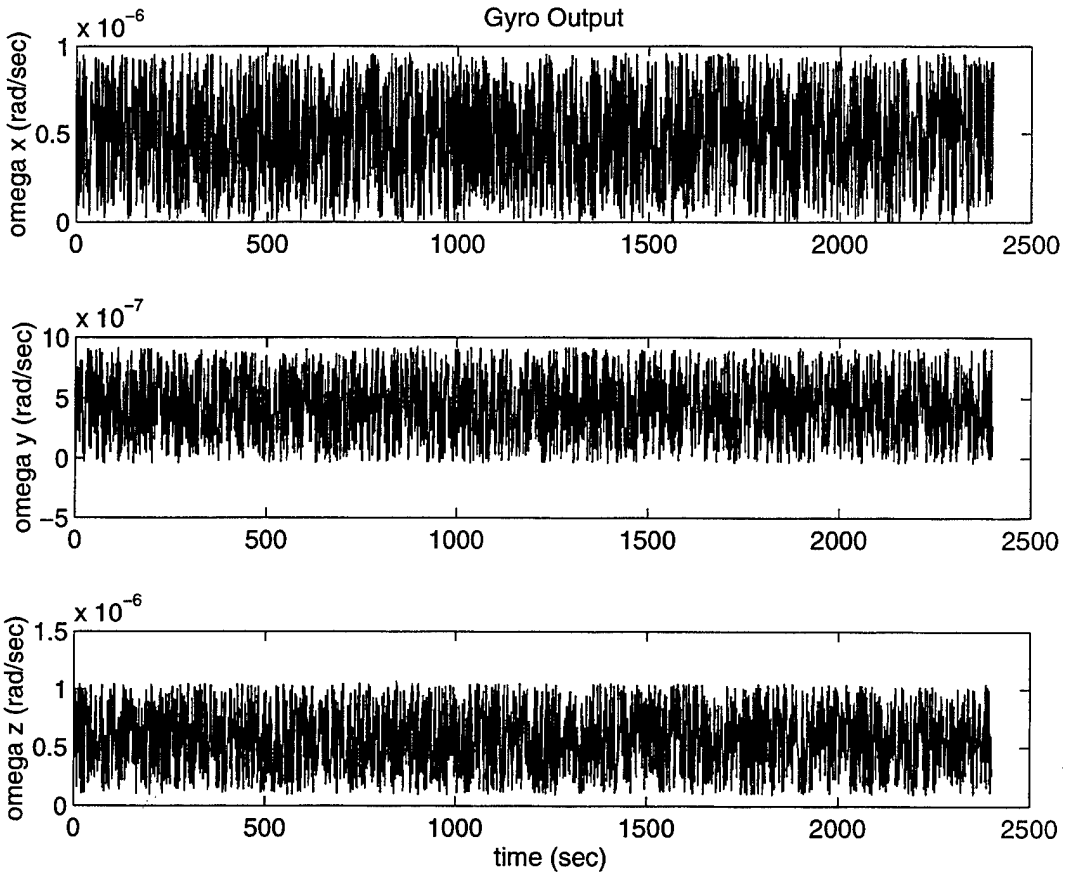


**Fig. 3.8.** Simulated Angular Rate Measurements. *Graphs show measurement noise characteristics for gyros aligned with each of the three body axes. Angular velocity input is zero for each axis.*

## Low Quality Gyro Simulation

Since the final gyro hardware for the JAWSAT design has not been established, low quality gyros are also considered as a comparison case to test the performance of the attitude estimation algorithms. These low quality gyros have performance specifications typical of low quality FOGs or micromechanical gyros

that may ultimately be used on board JAWSAT. The noise strengths used to simulate low quality gyros are [Sullivan, 1995; Weinberg, *et al.*, 1994]

$$\sigma_1^{\,2} = 5.4 \times 10^{-8} \frac{\text{rad}}{(\text{sec})^{1/2}}$$
$$\sigma_2^{\,2} = 10^{-11} \frac{\text{rad}}{(\text{sec})^{3/2}} \tag{3.11}$$

Figures 3.9 and 3.10 show the gyro bias drift and output noise for the low quality gyros. Figure 3.9 shows 6.5 hours of bias drift, and Fig. 3.10 shows 40 minutes of gyro angular rate output.

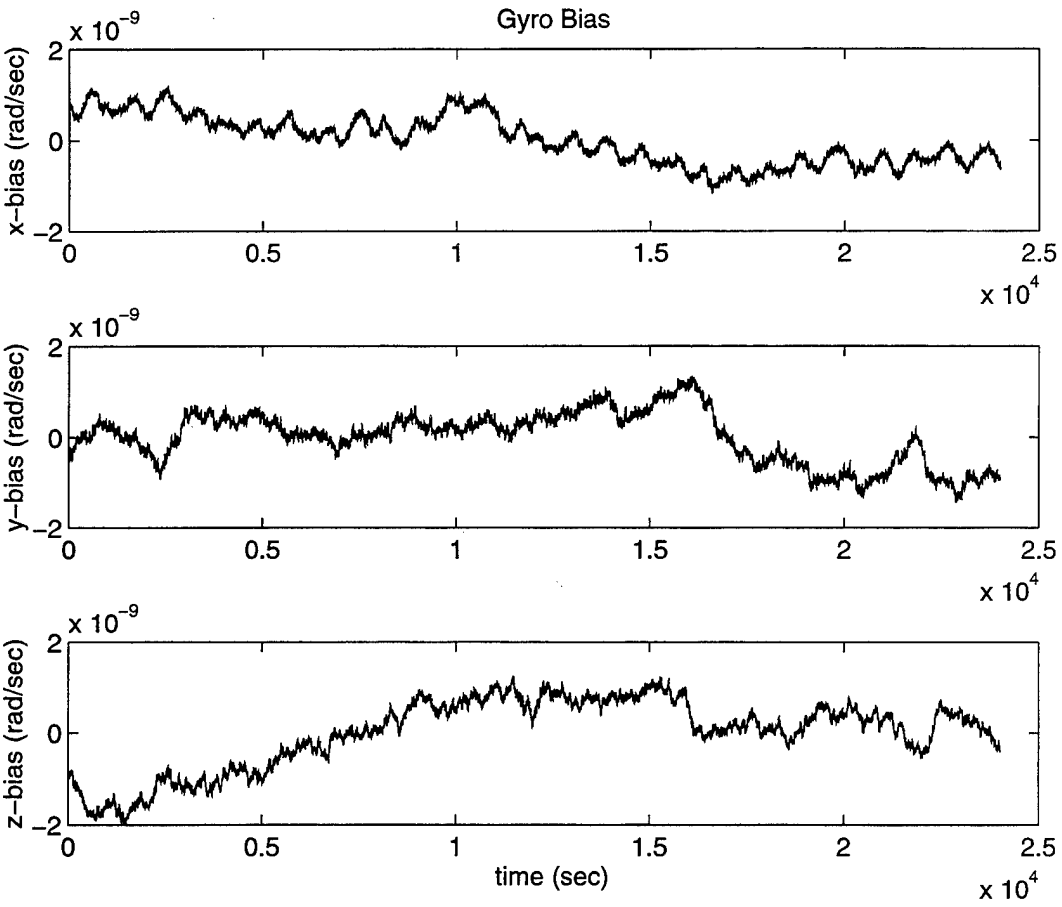


**Fig. 3.9.** Simulated Bias Random Walk. *Graphs show changes in drift rate bias for low quality gyros aligned with each of the three body axes. Angular velocity input is zero for each axis. Mean offset, typically on the order of 100 deg/hr, has been removed from the plots.*

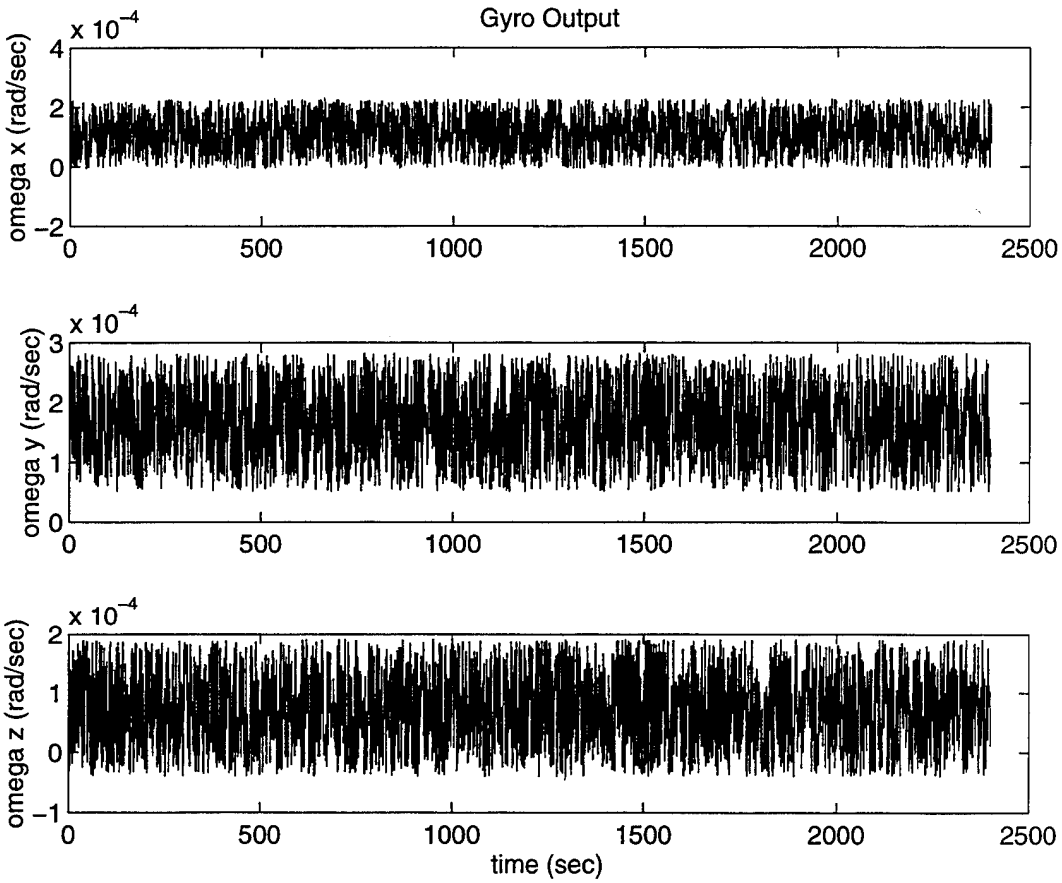


**Fig. 3.10.** Simulated Angular Rate Measurements. *Graphs show measurement noise characteristics for low quality gyros aligned with each of the three body axes. Angular velocity input is zero for each axis.*

## 3.3 Extended Kalman Filter Algorithm

An extended Kalman filter algorithm to estimate spacecraft attitude and gyro bias parameters using FOG and GPS measurements was developed. The full state vector has seven dimensions: four states for the attitude quaternion, $\bar{q} = [q_1 \quad q_2 \quad q_3 \quad q_4]^T$, and three gyro bias states, $b = [b_1 \quad b_2 \quad b_3]^T$, (one for each

axis). The Kalman filter implementation uses only three of the quaternion states since inclusion of all four gives rise to a singularity in the covariance matrix time update; therefore, a six-state formulation is used following Lefferts, Markley, and Shuster [1982]. The fourth quaternion state can be computed at any time from the other three to give the full seven dimensional state. The time propagation and measurement update processes are depicted in Fig. 3.11.

Time propagation of the quaternion state estimate and the covariance matrix is performed using FOG angular rate measurements. The GPS quaternion measurements are then compared with the propagated state vector estimate to form the measurement residual at each state update epoch. The extended Kalman filter then forms a quaternion state correction term from which a new estimate of the total quaternion of rotation can be determined by quaternion composition. The gyro bias terms are accumulated in the usual way by adding the incremental update to the reference trajectory. Details are in Lefferts *et al.* [1982], and summarized below. Additional information on general Kalman filter theory can be found in Maybeck [1979] and Gelb [1974].

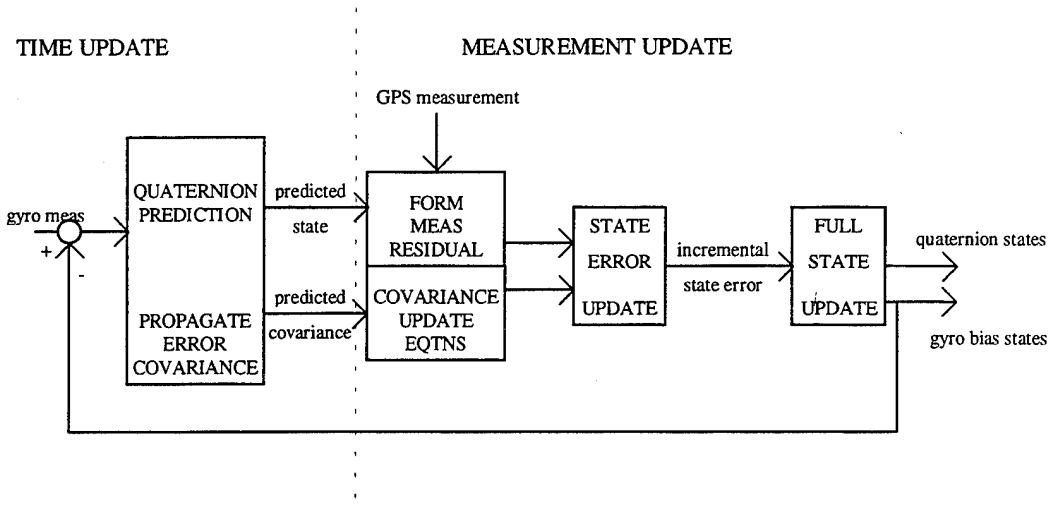


**Fig. 3.11.** Extended Kalman Filter Algorithm

The dynamic model for the full state $\hat{x}$ is given by

$$\frac{\mathrm{d}}{\mathrm{d}t}\hat{\bar{q}} = \tfrac{1}{2}\Omega^{\times}\hat{\bar{q}}$$
$$\frac{\mathrm{d}}{\mathrm{d}t}\hat{b} = 0 \qquad (3.12)$$

where

$$\hat{x} = \begin{bmatrix} \hat{\bar{q}} \\ \hat{b} \end{bmatrix} \qquad (3.13)$$

where the matrix $\Omega^{\times}$ is given by

$$\Omega^{\times} = \begin{bmatrix} 0 & \hat{\omega}_3 & -\hat{\omega}_2 & \hat{\omega}_1 \\ -\hat{\omega}_3 & 0 & \hat{\omega}_1 & \hat{\omega}_2 \\ \hat{\omega}_2 & -\hat{\omega}_1 & 0 & \hat{\omega}_3 \\ -\hat{\omega}_1 & -\hat{\omega}_2 & -\hat{\omega}_3 & 0 \end{bmatrix} \tag{3.14}$$

and the angular velocity estimate $\hat{\omega}$ is obtained from

$$\hat{\omega} = \omega_{meas} - \hat{b} \tag{3.15}$$

where $\omega_{meas}$ is the raw (biased) gyro measurement vector and $\hat{b}$ is the best estimate of the gyro bias vector. Note that the dynamic model for the controlled spacecraft motion is derived directly from the gyro measurements.

The time propagation for the total attitude quaternion $\hat{\bar{q}}$ from time *k-1* to *k* is obtained from the gyro angular velocity measurements and the attitude kinematics described by

$$\hat{\bar{q}}_k = e^{\frac{1}{2}\Omega^{\times}\Delta t}\hat{\bar{q}}_{k-1}. \tag{3.16}$$

The covariance propagation and measurement update equations are formulated in terms of a six-dimensional state vector to avoid singularities following Lefferts *et al.* [1982]. The six-dimensional state vector is defined as

$$\tilde{x} \equiv \begin{bmatrix} \delta q \\ b \end{bmatrix} \tag{3.17}$$

where $\delta q$ represents the three components of the small quaternion correction. Thus, the four dimensional quaternion $\delta\bar{q}$ represents the rotation between the true state and the estimated state, as defined by

$$\delta\bar{q} \equiv \bar{q} \otimes \hat{\bar{q}}^{-1} \tag{3.18}$$

where an overbar indicates a four-dimensional quaternion, a carat indicates an estimated quantity and $\otimes$ denotes quaternion composition.

Next the state equations are linearized about the reference trajectory provided by the angular velocity, and formulate the extended Kalman filter for the state error vector, noting that

$$\Delta\tilde{x} \equiv \begin{bmatrix} \delta q \\ \Delta b \end{bmatrix}. \tag{3.19}$$

The dynamic equations for the state error are then

$$\frac{d}{dt}\Delta\tilde{x} = F\Delta\tilde{x} + Gw \tag{3.20}$$

where

$$\mathbf{F}(t_k) = \begin{bmatrix} 0 & \hat{\omega}_3(t_k) & -\hat{\omega}_2(t_k) & -\frac{1}{2} & 0 & 0 \\ -\hat{\omega}_3(t_k) & 0 & \hat{\omega}_1(t_k) & 0 & -\frac{1}{2} & 0 \\ \hat{\omega}_2(t_k) & -\hat{\omega}_1(t_k) & 0 & 0 & 0 & -\frac{1}{2} \\ 0 & 0 & 0 & 0 & 0 & 0 \\ 0 & 0 & 0 & 0 & 0 & 0 \\ 0 & 0 & 0 & 0 & 0 & 0 \end{bmatrix} \tag{3.21}$$

$$G = \begin{bmatrix} -\frac{1}{2}I_{3\times3} & 0_{3\times3} \\ 0_{3\times3} & I_{3\times3} \end{bmatrix} \tag{3.22}$$

and $w \sim \mathrm{N}(0, Q_d)$.

The state error covariance matrix of dimension 6×6 is defined as [Fisher *et al.* 1989]

$$P \equiv \mathrm{E}\left[\Delta\tilde{x} \cdot \Delta\tilde{x}^T\right] \tag{3.23}$$

where $\Delta\tilde{x}$ is defined in equation (3.19).

To propagate the state error covariance matrix $P$, the state transition matrix, $\Phi$, is computed as

$$\Phi(k+N|k) = e^{\mathbf{F}(t_{k+N}-t_k)} \tag{3.24}$$

where $N$ is the number of time propagation steps between measurement updates. Then the time propagation for the covariance matrix is given by

$$P_{k+1}^{-} = \Phi P_k^{+} \Phi^T + Q_d \,. \tag{3.25}$$

Next a transformed measurement residual vector that relates the GPS measurement $\bar{q}_{GPS}$ to the state vector correction $\Delta\tilde{x} = \begin{bmatrix}\delta q & \Delta b\end{bmatrix}^T$ is defined. First the measurement residual is formed as

$$\Delta z = \Delta\bar{q} \equiv \bar{q}_{GPS} - \hat{\bar{q}}^{-} \,. \tag{3.26}$$

This measurement residual is not a quaternion, but it is related to the state according to equation (127) in Lefferts *et al.* [1982]

$$\bar{q}_{GPS} = \bar{q} + \Xi(\bar{q})v \tag{3.27}$$

where

$$\Xi\left(\hat{\bar{q}}\right)=\begin{bmatrix} \hat{q}_4 & -\hat{q}_3 & \hat{q}_2 \\ \hat{q}_3 & \hat{q}_4 & -\hat{q}_1 \\ -\hat{q}_2 & \hat{q}_1 & \hat{q}_4 \\ -\hat{q}_1 & -\hat{q}_2 & -\hat{q}_3 \end{bmatrix} \tag{3.28}$$

and the three independent quantities representing the small angle measurement error, $v$, are described by

$$v \sim \mathrm{N}\left(0, R_{3\times 3}\right) . \tag{3.29}$$

Then

$$\Delta z = \Delta\bar{q} = \Xi\left(\hat{\bar{q}}\right)\delta q + \Xi\left(\hat{\bar{q}}\right)v \tag{3.30}$$

where the matrix $\Xi\left(\hat{\bar{q}}\right)$ accounts for the combination of quaternion components. A filter using this form gives rise to a singularity in the gain equation. To avoid this problem, the transformed measurement residual of dimension three is defined as

$$\Delta\tilde{z} = \Xi^T\left(\hat{\bar{q}}\right)\Delta z = \delta q + v . \tag{3.31}$$

Note that the transformed measurements consists of three quantities that retain all the information contained in the original four-dimensional measurement residual. This

formulation relies on the matrix $\Xi(\hat{\bar{q}})$ . Dynamic equations utilizing the form of $\Xi(\hat{\bar{q}})$ were first introduced by Sir Arthur Cayley [1843]. The many useful properties of the matrix $\Xi(\hat{\bar{q}})$ are reviewed by Shuster [1993] and Lefferts *et al.* [1982].

The measurement observation matrix for the transformed measurement residual is just

$$H = \begin{bmatrix} I_{3\times3} & 0_{3\times3} \end{bmatrix} . \tag{3.32}$$

The optimal updated state and covariance are then given by the Kalman filter equations

$$K = P^{-}H^{T}\left(HP^{-}H^{T} + R\right)^{-1} \tag{3.33}$$

$$\Delta\hat{\tilde{x}} = K\left(\Delta\tilde{z}\right) \tag{3.34}$$

$$P^{+} = (I - KH)P^{-}(I - KH)^{T} + KRK^{T} . \tag{3.35}$$

The updated total state can be obtained as in Lefferts *et al.* [1982], using the following relations

$$\Delta\tilde{x}^{+} \equiv \begin{bmatrix} \delta\hat{q}^{+} \\ \Delta\hat{b}^{+} \end{bmatrix} \tag{3.36}$$

$$\delta\hat{\bar{q}}^{+} \equiv \begin{bmatrix} \delta\hat{q}^{+} \\ 1 \end{bmatrix} \tag{3.37}$$

$$\hat{\bar{q}}^{+} = \delta\hat{\bar{q}}^{+} \otimes \hat{\bar{q}}^{-} \tag{3.38}$$

$$\hat{b}^{+} = \hat{b}^{-} + \Delta\hat{b}^{+}. \tag{3.39}$$

## 3.4 Measurement Differencing Estimation Algorithm

GPS attitude errors are time-correlated as discussed in Section 3.1. A technique for improved Kalman filtering in the presence of time correlated measurement errors involves differencing successive measurements to "whiten" the errors. This approach was first suggested by Bryson and Henrickson [1968], and was discussed further by Bryson and Ho [1975]. Provided the time constant of the measurement error correlation is large compared to the sampling frequency, the errors in successive differenced measurements will not be correlated in time. The disadvantage of this approach is that the measurement noise at each epoch is

increased. However, measurement differencing is preferred over state vector augmentation to account for the non-white measurement errors because increasing the dimension of the state vector is inconvenient for real-time applications and, more importantly, computations of the filter gains are typically ill-conditioned [Bryson and Ho, 1975].

Measurement differencing requires a very good dynamic model or measurements with relatively little high frequency noise to successfully overcome the increased measurement noise introduced by the approach. In the present case, FOG measurements provide the dynamic model very accurately for short time spans relative to the gyro drift and angle random walk. The prediction equations for the measurement differencing case are the same as those given by equations (3.16 - 3.25). The measurement update equations are modified from Bryson and Henrickson [1968] to relate the transformed (three-dimensional) measurement residual to the total state, as in the previous section. Transformed measurement residuals are used to account for quaternion composition relations and prevent singularities in the covariance update equations. The new model for the transformed measurement residual is given as

$$\Delta\tilde{z}_k = H\begin{bmatrix}\delta q \\ b\end{bmatrix}_k + \varepsilon_k \tag{3.40}$$

where

$$\varepsilon_k = \Psi \varepsilon_{k-1} + w_k \tag{3.41}$$

$$\Psi = e^{-\beta \Delta t} I_{3\times 3}. \tag{3.42}$$

Note that $\varepsilon_k$ is a first order Markov process described by the transition matrix $\Psi$. $\beta$ is the inverse time constant of the Markov process that models the multipath errors, $\Delta t$ is the interval between GPS measurements, and $w_k$ is a Gaussian white noise parameter with covariance $Q_{df}$. The measurement observation matrix, $H$, is as defined in equation (3.32).

The pseudo measurement is defined to be the difference

$$\zeta_{k-1} = \Delta \tilde{z}_k - \Psi \Delta \tilde{z}_{k-1}. \tag{3.43}$$

The pseudo measurement error covariance matrix is given by

$$R = H \Gamma Q_d \Gamma^T H^T + Q_{df} \tag{3.44}$$

where $Q_{df}$ is the covariance of the gyro noise.

Note that the (pseudo) measurement and process noises are now correlated according to the covariance matrix

$$C \equiv \mathrm{E}\left[w\varepsilon^T\right] = Q_d \Gamma^T H^T . \tag{3.45}$$

Following Bryson and Ho [1975], a matrix $D$ is defined to be

$$D \equiv \Gamma C R^{-1} . \tag{3.46}$$

Then the Kalman filter measurement update equations become

$$K = P_k^- H_r^T \left(H_r P_k^- H_r^T + R\right)^{-1} \tag{3.47}$$

$$\begin{aligned} P_{k-1|k} = {} & (I - KH_r) P_{k-1}^- (I - KH_r)^T \\ & + KRK^T \end{aligned} \tag{3.48}$$

$$\begin{aligned} P_{k|k} = {} & (\Phi - DH_r) P_{k-1|k} (\Phi - DH_r)^T \\ & + Q_d - DRD^T \end{aligned} \tag{3.49}$$

$$\Delta\hat{\tilde{x}}_{k-1|k} = K(\zeta_{k-1}) \tag{3.50}$$

$$\Delta\hat{\tilde{x}}_{k|k} = \Phi\Delta\hat{\tilde{x}}_{k-1|k} + D\left(\zeta_{k-1} - H_r\Delta\hat{\tilde{x}}_{k-1|k}\right) \tag{3.51}$$

where

$$H_r = H\Phi - \Psi H\,. \tag{3.52}$$

The notation *k-1|k* is used to denote quantities computed at time step *k-1* given a GPS measurement at time *k*. This time lag of one update epoch is introduced by the pseudo measurement which includes measurements at time *k-1* and *k*. Equations (3.49) and (3.51) propagate the covariance and state estimates to the current measurement epoch.

### 3.5 Attitude Estimation Simulation

Three simulation configurations were performed to analyze the attitude estimation algorithms developed in this chapter. The three simulations include different combinations of GPS and gyro data. All three simulations include gyro measurements taken once per second and GPS measurements are available every 12 seconds. The simulation parameters for the three runs are summarized in Table 3.1.

**Table 3.1.** Simulation run parameters.

| | Simulation #1 | Simulation #2 | Simulation #3 |
|---|---|---|---|
| GPS Data | JAWSAT mock up | RADCAL | RADCAL |
| Gyro Quality | High | High | Low |
| Initial Covariance | $P_0 = \begin{bmatrix} 10^{-3} I_{3\times3} & 0_{3\times3} \\ 0_{3\times3} & 10^{-6} I_{3\times3} \end{bmatrix}$ | $P_0 = \begin{bmatrix} 10^{-3} I_{3\times3} & 0_{3\times3} \\ 0_{3\times3} & 10^{-6} I_{3\times3} \end{bmatrix}$ | $P_0 = \begin{bmatrix} 10^{-3} I_{3\times3} & 0_{3\times3} \\ 0_{3\times3} & 10^{-6} I_{3\times3} \end{bmatrix}$ |
| Process Noise Cov. (EKF) | $Q = 1.5 \begin{bmatrix} \sigma_1^2 \Delta t \cdot I_{3\times3} & 0_{3\times3} \\ 0_{3\times3} & \sigma_2^2 \cdot I_{3\times3} \end{bmatrix}^{\dagger}$ | $Q = 1.5 \begin{bmatrix} \sigma_1^2 \Delta t \cdot I_{3\times3} & 0_{3\times3} \\ 0_{3\times3} & \sigma_2^2 \cdot I_{3\times3} \end{bmatrix}^{\dagger}$ | $Q = 1.5 \begin{bmatrix} \sigma_1^2 \Delta t \cdot I_{3\times3} & 0_{3\times3} \\ 0_{3\times3} & \sigma_2^2 \cdot I_{3\times3} \end{bmatrix}^{\ddagger}$ |
| Process Noise Cov. (Meas. Diff.) | $Q = \begin{bmatrix} \sigma_1^2 \Delta t \cdot I_{3\times3} & 0_{3\times3} \\ 0_{3\times3} & \sigma_2^2 \cdot I_{3\times3} \end{bmatrix}^{\dagger}$ | $Q = \begin{bmatrix} \sigma_1^2 \Delta t \cdot I_{3\times3} & 0_{3\times3} \\ 0_{3\times3} & \sigma_2^2 \cdot I_{3\times3} \end{bmatrix}^{\dagger}$ | $Q = \begin{bmatrix} \sigma_1^2 \Delta t \cdot I_{3\times3} & 0_{3\times3} \\ 0_{3\times3} & \sigma_2^2 \cdot I_{3\times3} \end{bmatrix}^{\ddagger}$ |
| Meas. Noise Cov. | $R = 2.4e-5 \cdot I_{3\times3}$ rad$^2$ | $R = 2.8e-4 \cdot I_{3\times3}$ rad$^2$ | $R = 2.8e-4 \cdot I_{3\times3}$ rad$^2$ |
| Multipath Time Constant | $\beta = 1/100$ sec | $\beta = 1/100$ sec | $\beta = 1/100$ sec |

$^{\dagger}$where $\sigma_1$ and $\sigma_2$ are from eqn (3.10) and $\Delta t$ is the gyro sampling interval
$^{\ddagger}$ where $\sigma_1$ and $\sigma_2$ are from eqn (3.11) and $\Delta t$ is the gyro sampling interval

The multipath time constant was kept the same for all simulation runs for the basis of comparison. A reasonable choice for the multipath time constant in the measurement differencing algorithm yields improved performance compared to the basic Kalman filter algorithm, as will be discussed in Section 3.6.

Simulation number one includes GPS measurements taken from ground test data using the Trimble Vector receiver and the JAWSAT test structure (see Fig. 3.3). High quality gyro measurements are included in this simulation (see Figs. 3.7 and 3.8). Simulation number two uses RADCAL GPS data (see Fig. 3.4) and high quality gyros. Finally, simulation three uses RADCAL GPS data with low quality gyros.

The attitude truth model for the simulated spacecraft was the same for all three simulations. The true attitude used in the simulation runs in shown in Fig. 3.12. The spacecraft was modeled as three-axis stabilized and Earth pointing within the performance specifications of the attitude control system. Attitude control errors were included in the simulation by adding an arbitrary oscillating component to the attitude motion that is roughly at the limits of the expected controller performance. This method has been used previously in spacecraft attitude estimation simulations [*e.g.*, Fisher *et al.*, 1989].

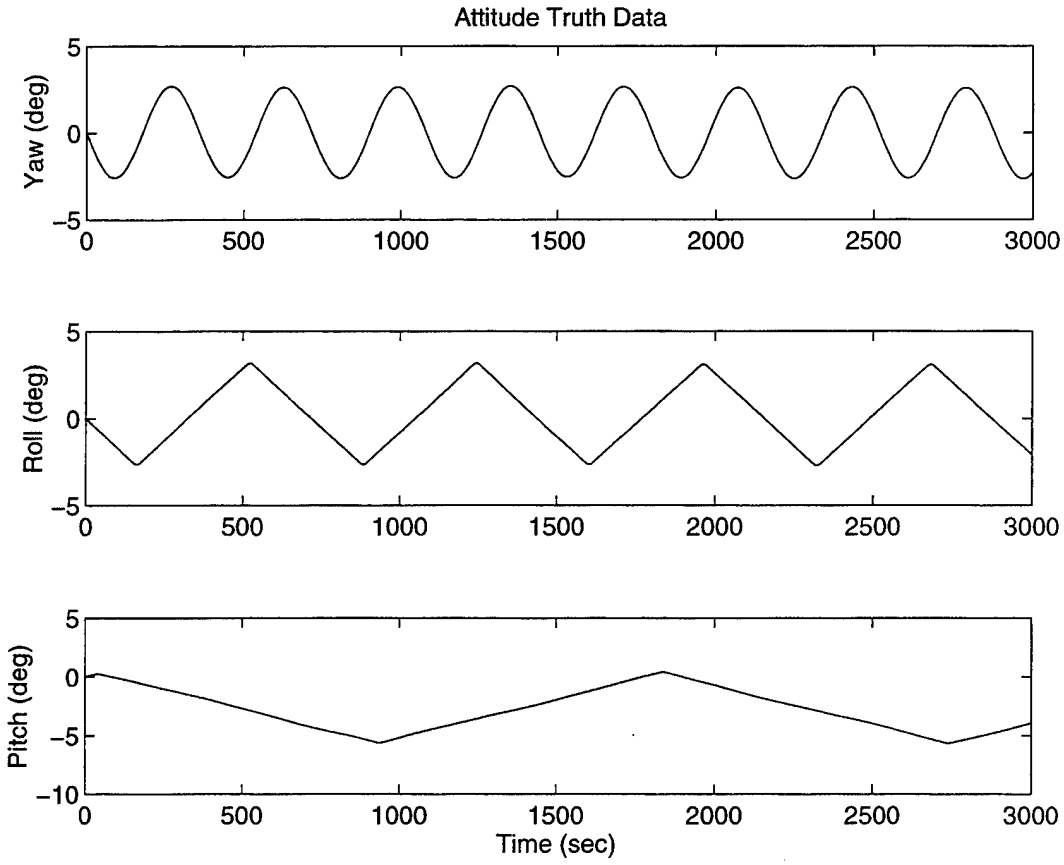


**Fig. 3.12.** Simulated True Spacecraft Dynamics.

## 3.6 Simulation Results and Discussion

In this section simulation results from the extended Kalman filter and measurement differencing algorithms discussed previously in this chapter are compared. Simulation results are based on GPS measurements obtained from ground testing with a mock up of the JAWSAT spacecraft and on-orbit results from RADCAL. The effects of high and low quality gyros on the performance of these algorithms is also considered.

### Ground Test Results

The simulation parameters for run number one in Table 3.1 were used in an attitude determination simulation with the true dynamics shown in Fig. 3.12. The attitude truth data and the attitude estimates from the extended Kalman filter algorithm are shown in Fig. 3.13. Attitude quaternion output has been converted to yaw, roll, and pitch for easier interpretation. Subsequent results show estimation errors only with true dynamics removed.

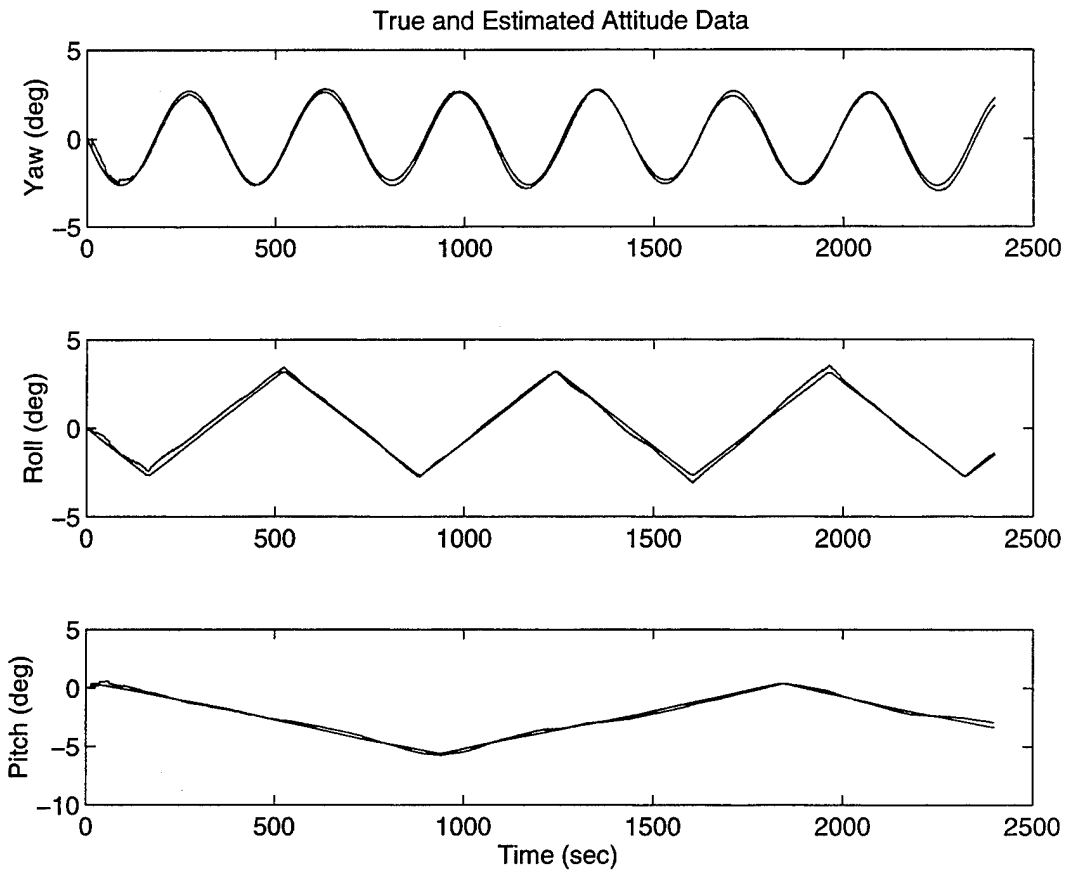


**Fig. 3.13.** True and Estimated Attitude Data.

Figure 3.14 shows Kalman filter error plots for the attitude angles using the extended Kalman filter algorithm and the simulation parameters for run number one in Table 3.1. Note the stepwise nature of the plots that occurs at the GPS update interval of every twelve seconds. Also note that the errors are time correlated due to multipath errors in the GPS measurements. These time correlated errors will be reduced using the measurement differencing algorithm.

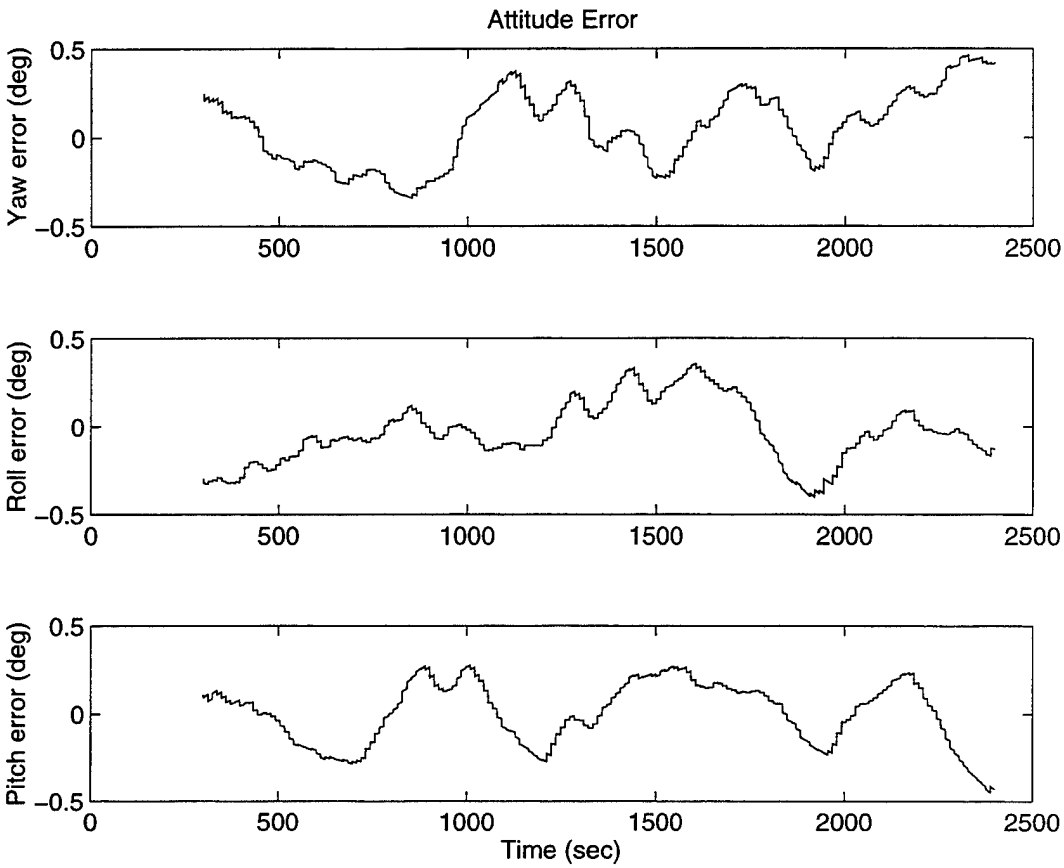


**Fig. 3.14.** Kalman Filter Attitude Error Plot for GPS Ground Test Data.

The errors in the gyro bias estimates using the standard Kalman filter and the GPS ground test data are shown in Fig. 3.15. The time correlated measurement noise in the GPS measurements also results in time correlated estimation errors in the gyro bias states. Filter convergence at the beginning of each run has been eliminated from the plots.

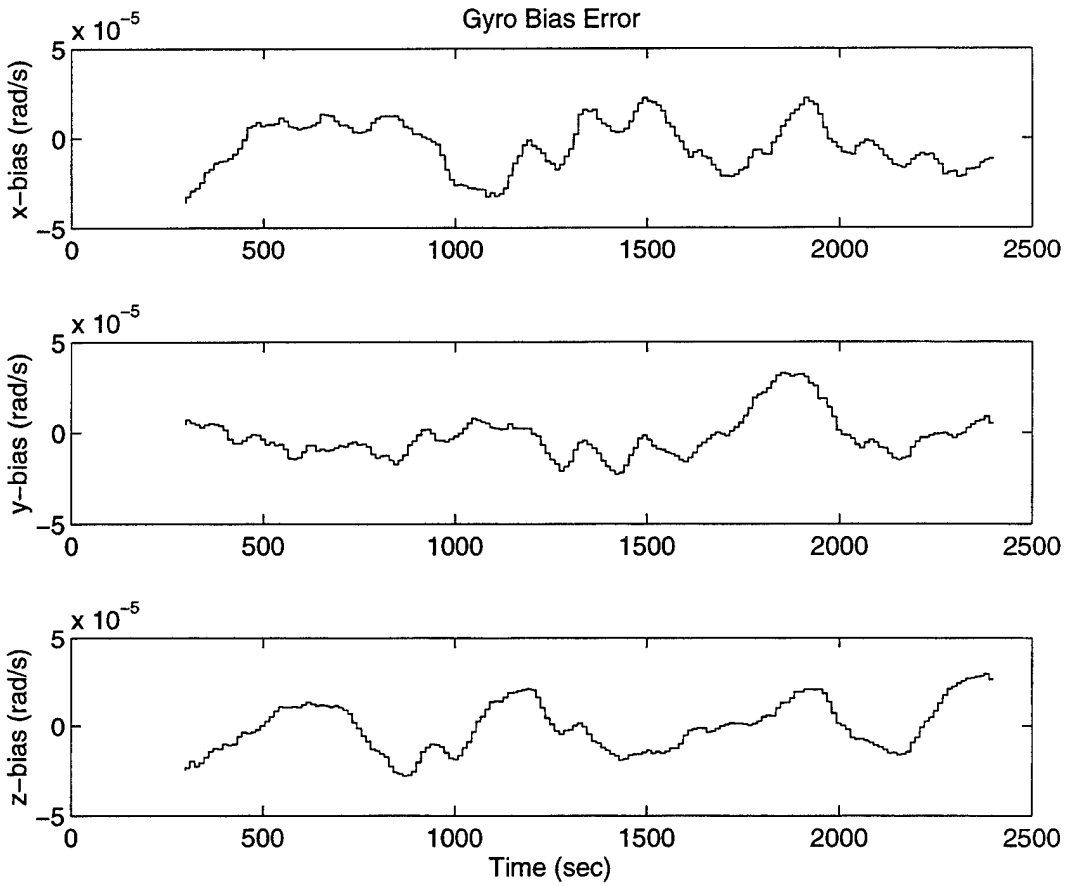


**Fig. 3.15.** Kalman Filter Bias Error Plot for GPS Ground Test Data.

In Figs. 3.16 and 3.17 the standard Kalman filter algorithm is compared to the measurement differencing Kalman filter developed in Section 3.5. Figure 3.16 compares the attitude estimation errors for the two algorithms. Note that the measurement differencing algorithm is affected less by the effects of the multipath errors in the GPS measurements. Similar results for the gyro bias states are shown in Fig. 3.17. Table 3.2 summarizes the computed error statistics for the sample runs shown in Figs. 3.16 and 3.17.

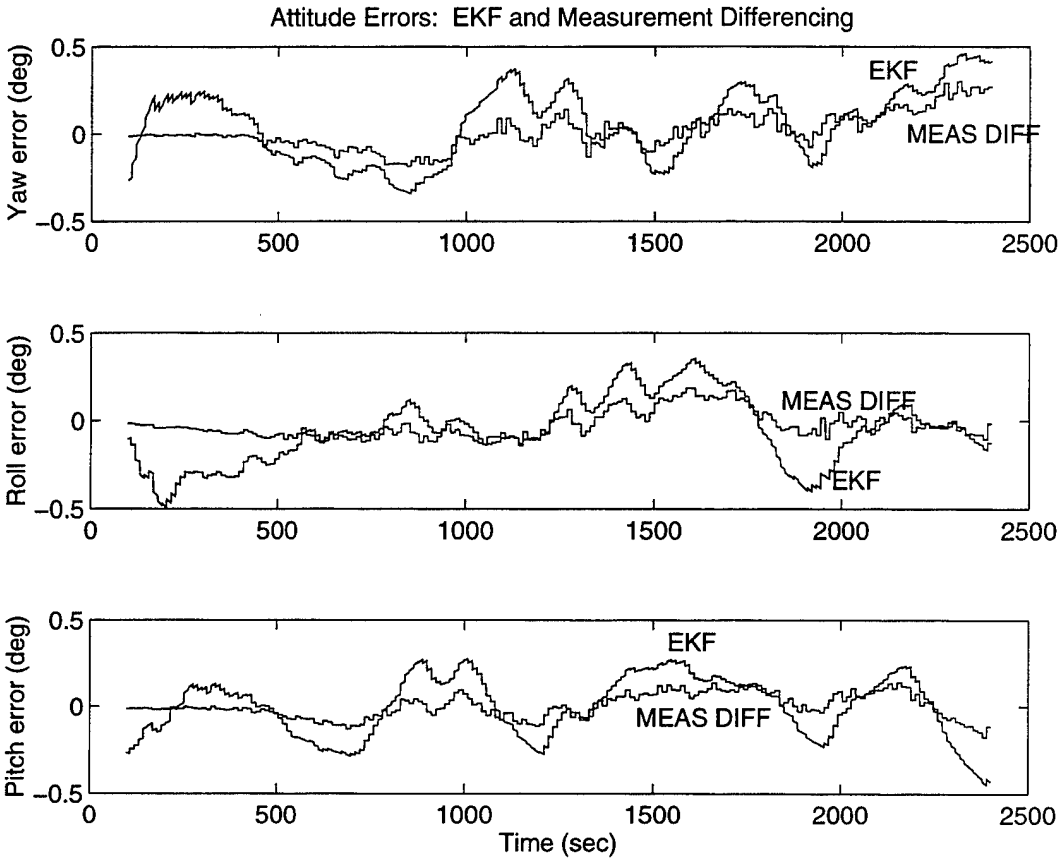


**Fig. 3.16.** Attitude Error Comparison for GPS Ground Test Data. *Graphs show attitude estimation error for the standard and measurement differencing Kalman filter algorithms.*

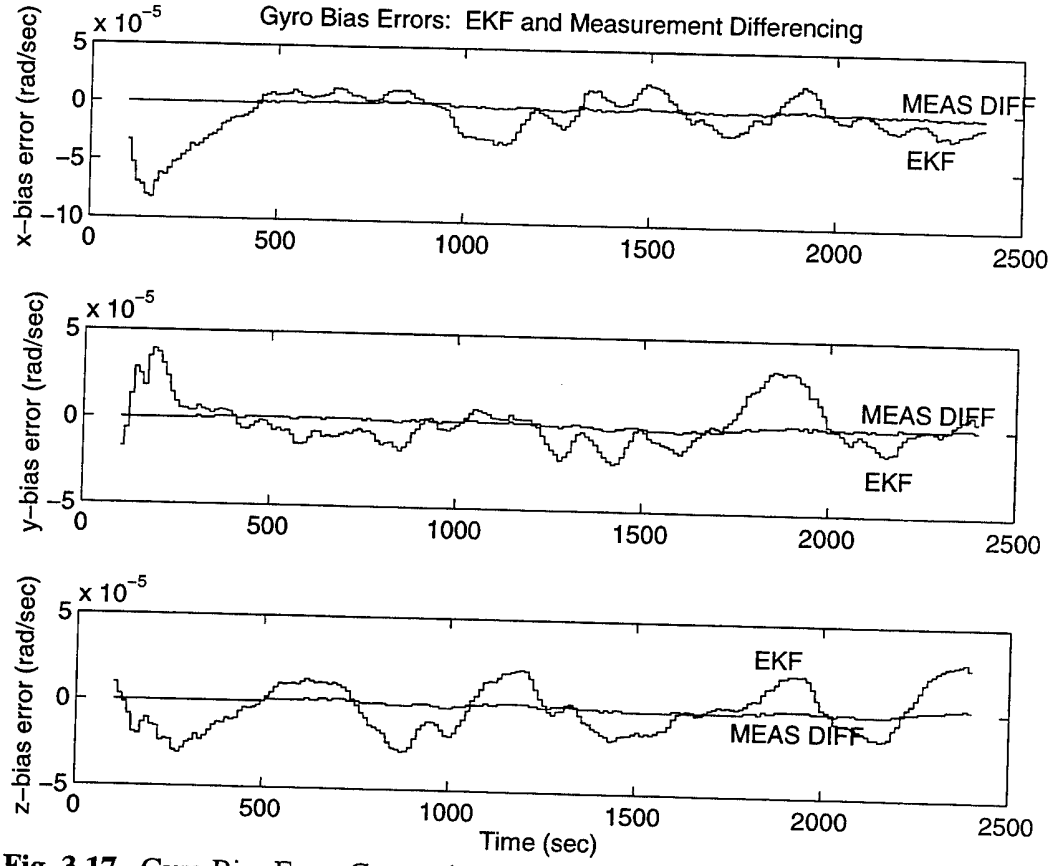


**Fig. 3.17.** Gyro Bias Error Comparison for GPS Ground Test Data. *Graphs show bias estimation error for the standard and measurement differencing Kalman filter algorithms.*

**Table 3.2.** Computed error statistics for Extended Kalman Filter and Measurement Differencing Kalman Filter Algorithms using GPS Ground Test Data.

| | YAW<br>1σ error | ROLL<br>1σ error | PITCH<br>1σ error |
|---|---|---|---|
| KALMAN FILTER | 0.20 deg | 0.19 deg | 0.17 deg |
| MEAS. DIFFERENCING | 0.10 deg | 0.08 deg | 0.07 deg |

One reason for the performance improvements using the measurement differencing algorithm is the way non-white measurement errors are accommodated

in the two approaches. In the standard EKF approach, artificially large process noise is used to allow for the non-white distribution in the measurement errors. In the measurement differencing algorithm, the process noise based on the gyro angle random walk noise parameters is used.

The choice of the time constant for the dynamic model of the time correlated errors given by equations (3.41) and (3.42) is necessary for the implementation of the measurement differencing algorithm. The attitude estimation errors for a range of time constants in the measurement differencing algorithm are shown in Fig. 3.18.

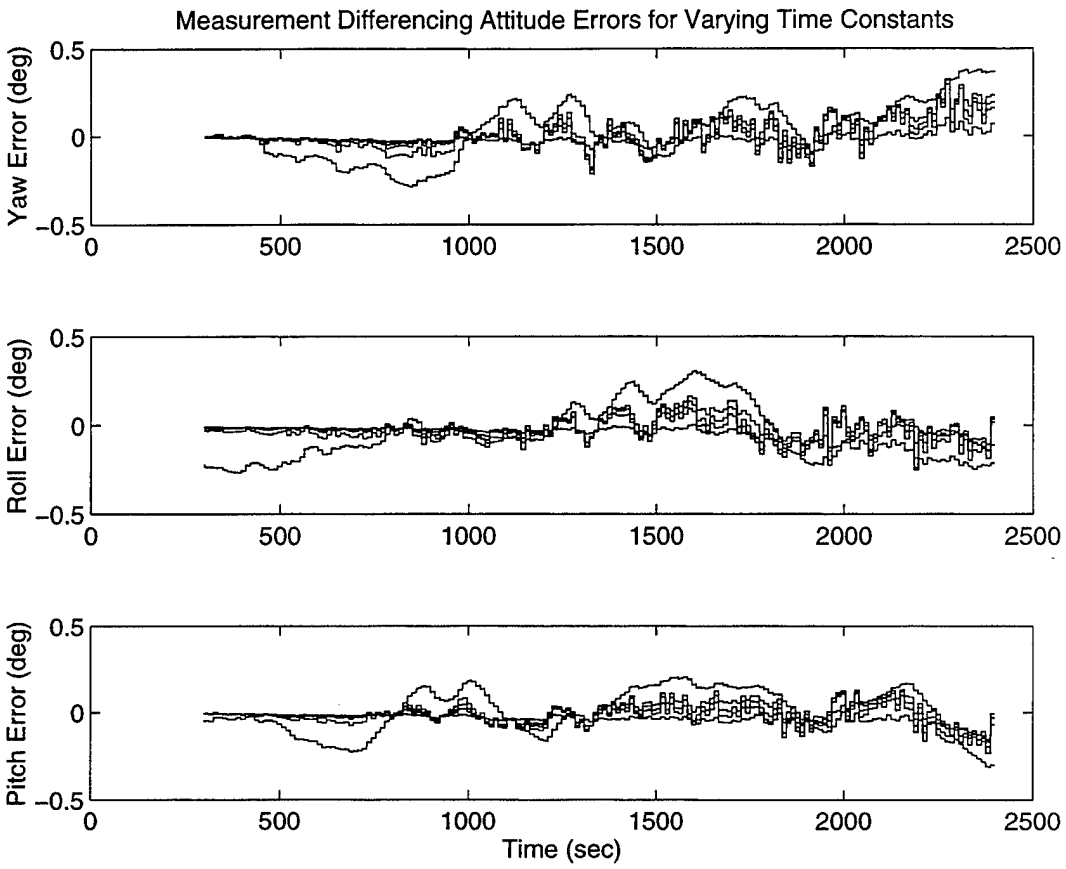


**Fig. 3.18.** Attitude Estimation Errors Using Measurement Differencing Algorithm with Different Time Constants. *Time constant values for the simulations are* $\beta$*=100 sec*$^{-1}$*,* $\beta$*=1/100 sec*$^{-1}$*,* $\beta$*=1/250 sec*$^{-1}$*,* $\beta$*=1/500 sec*$^{-1}$*,* $\beta$*=0 sec*$^{-1}$*. The graph for* $\beta$*=100 sec*$^{-1}$ *shows larger deviations from zero error. The smaller* $\beta$ *values are grouped together with smaller errors.*

The error statistics for the data shown in Fig. 3.18 are compiled in Table 3.3. Note that large $\beta$ approaches the standard Kalman filter formulation. The graphs in Fig. 3.18 and the variances in Table 3.3 show that the $\beta$ values less than about 1/100 $sec^{-1}$ all result in similar performance. Also, the fact that the time constant may not be known exactly does not limit the applicability of the measurement differencing method. Only an approximate value of $\beta$ is needed to provide significantly improved error performance compared with the standard extended Kalman filter formulation.

Attitude estimation results for the standard EKF and the measurement differencing filter are shown in Figs. 3.19 and 3.20 using GPS measurements from RADCAL and the simulation parameters for run two in Table 3.1.

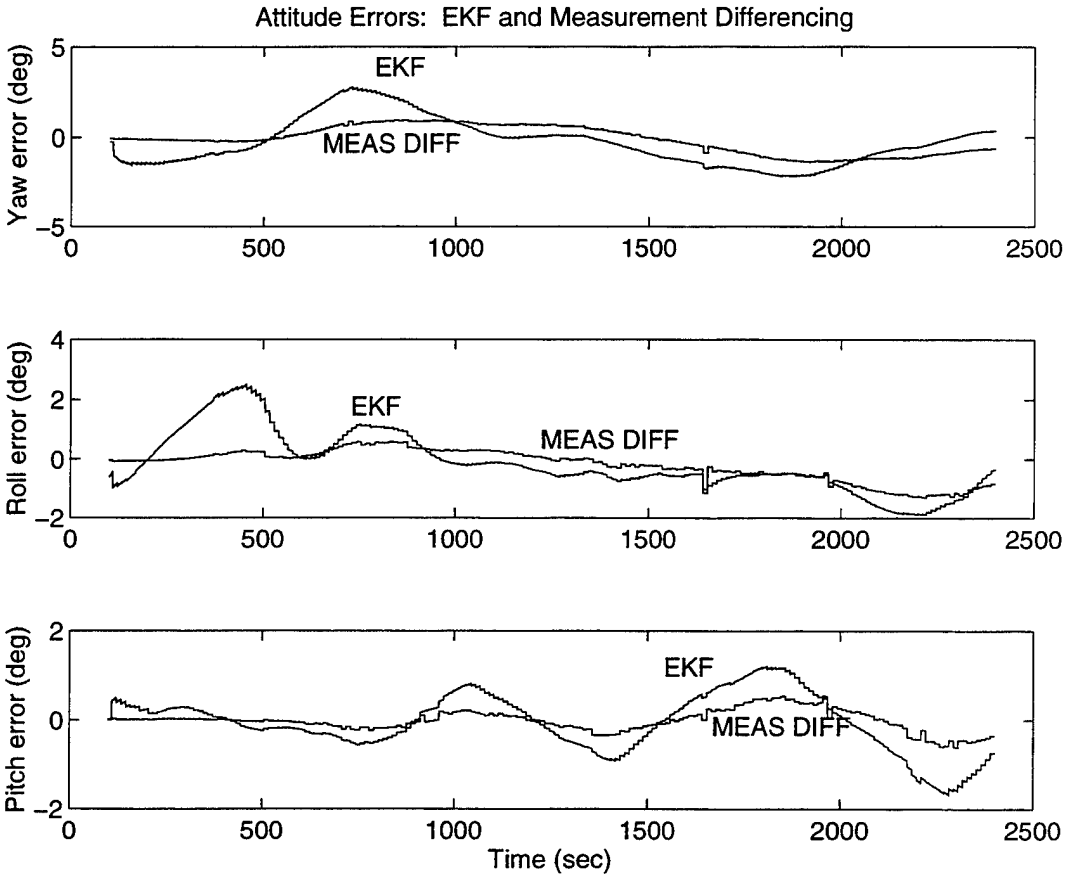


**Fig. 3.19.** Attitude Error Comparison for RADCAL Test Data. *Graphs show attitude estimation error for the standard and measurement differencing Kalman filter algorithms.*

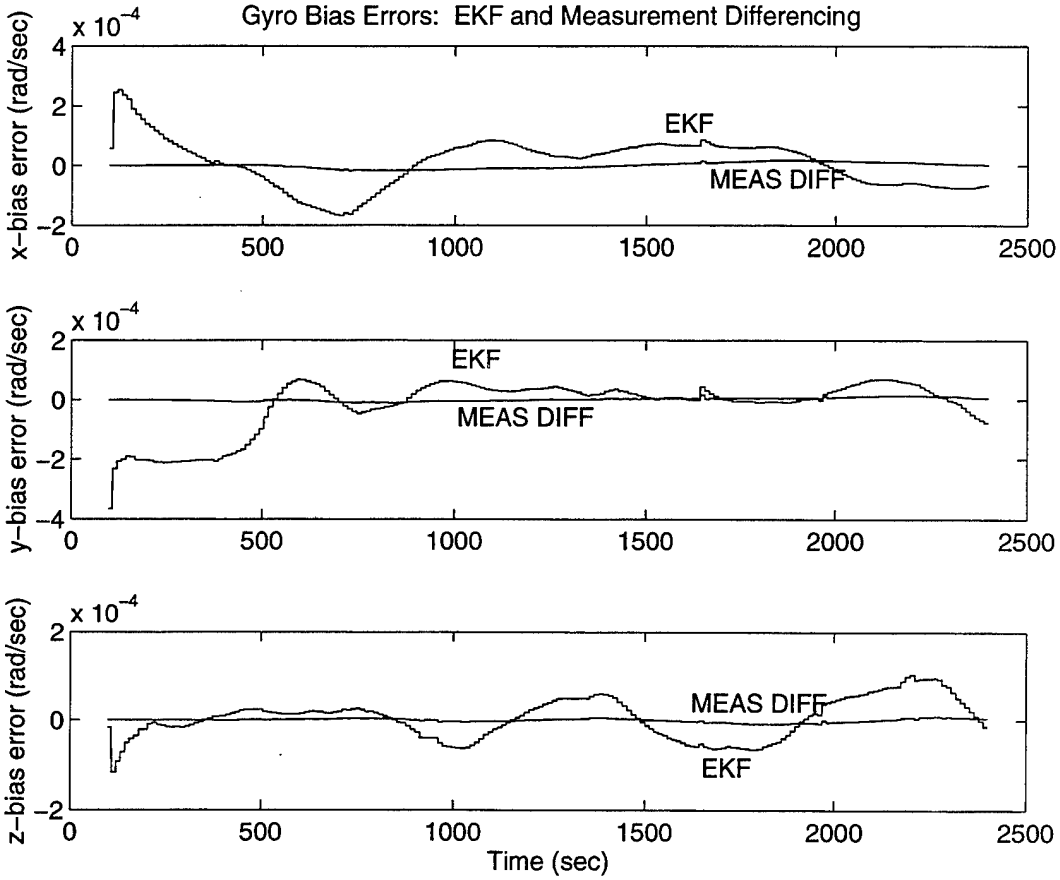


**Fig. 3.20.** Gyro Bias Error Comparison for RADCAL Test Data. *Graphs show bias estimation error for the standard and measurement differencing Kalman filter algorithms.*

As with the ground test GPS data, the measurement differencing approach successfully reduces the effect of GPS errors due to multipath in the combined GPS/FOG solution. Table 3.4 compares the computed error statistics for the filter results using RADCAL data.

**Table 3.4.** Computed error statistics for Extended Kalman Filter and Measurement Differencing Kalman Filter Algorithms using RADCAL Test Data.

| | YAW<br>1σ error | ROLL<br>1σ error | PITCH<br>1σ error |
|---|---|---|---|
| KALMAN FILTER | 1.27 deg | 1.01 deg | 0.65 deg |
| MEAS. DIFFERENCING | 0.74 deg | 0.52 deg | 0.24 deg |

As with the ground test data, the measurement differencing algorithm reduces the standard deviation of the attitude estimation errors by a factor of two for the RADCAL GPS data. Also, extended periods where attitude errors have a non-zero mean are greatly reduced with the measurement differencing approach as can be identified in Fig. 3.19. This feature could prove important in a closed loop attitude control system. Improved performance of measurement differencing approach is due to the fact that the GPS errors can be approximated by a first-order Markov process and that an accurate dynamic model of the vehicle motion is available from the FOG measurements.

**Comparison of Gyro Quality**

One of the keys to the success of the measurement differencing is the availability of an accurate dynamic model to correctly account for the time lag in the

pseudo-measurement. For the spacecraft attitude determination system considered, this dynamic model is derived directly from the gyro measurements. As the accuracy of the gyro measurements decreases, so does the accuracy of the dynamic model.

High accuracy gyros were used for the simulation results using RADCAL GPS measurements shown previously in Figs. 3.19 and 3.20. For comparison, low quality gyros such as piezoelectric gyros were used for the simulation results shown in Fig. 3.21. Note that neither algorithm clearly outperforms the other in this case. These results suggest that for situations where only a poor dynamic model is available, the measurement differencing algorithm may not provide any advantage over the standard EKF.

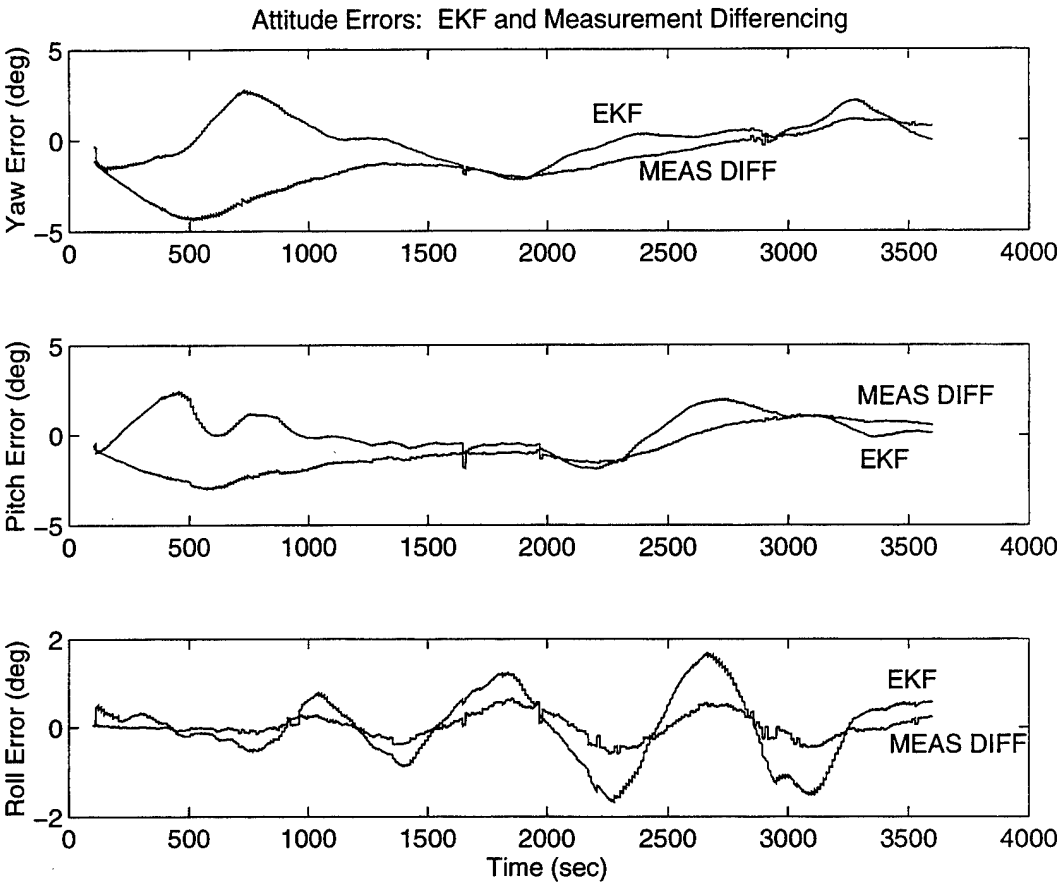


**Fig. 3.21.** Attitude Error Comparison Using Low Quality Gyros. *Graphs show attitude estimation error for the standard and measurement differencing Kalman filter algorithms using RADCAL GPS data.*

## 3.7 Minimizing Receiver On-Time

The mission profile for JAWSAT involves the use of PPT thrusters to perform gradual maneuvering of the spacecraft orbit. To prevent radio frequency interference (RFI) and provide sufficient power for all subsystems, the PPT will not be operated simultaneously with communications transceivers and the GPS receiver.

During thrust maneuvers (which could last several months or even years) pulses will be performed for roughly half of each orbit period, and the GPS receiver and communications equipment will operate for the other half. Since the FOG attitude errors and bias errors grow rather slowly with time, the use of intermittent GPS measurements was studied to see if attitude knowledge could be maintained within JAWSAT requirements.

A parametric covariance analysis was performed to determine how long the GPS receiver can be idle while still maintaining attitude knowledge within 1 deg. The uncertainty in the attitude grows linearly when GPS measurements are not available. For the high quality gyros, a GPS idle time of approximately 5 min. will result in a 3-$\sigma$ error of 5 deg. These 5 min. idle periods do not satisfy the JAWSAT operational constraint to deactivate the GPS receiver for approximately 40 minutes during each orbit that the PPTs are in use.

Based on this analysis, additional measurements from other instruments such as the sun sensors will be needed to estimate gyro drift during the GPS idle period. Incorporation of sun sensor data into the integrated attitude determination algorithms is discussed in subsequent chapters.

## 3.8 Summary and Conclusions

This chapter described an integrated attitude determination system using GPS and FOGs for JAWSAT. JAWSAT is planned to be the first three-axis stabilized educational satellite of its kind [Smith and Liefer, 1993]. The attitude determination system is being designed to incorporate several sensors for improved reliability and technology demonstration. The reasons for designing an integrated attitude determination system for JAWSAT include improved accuracy over stand-alone sensors and failure detection of attitude sensors. This chapter demonstrates a method for improving the accuracy of integrated GPS and gyro attitude measurements using a measurement differencing Kalman filter algorithm.

Results using GPS attitude data from both ground tests using a JAWSAT mock up and on-orbit data from RADCAL were used to evaluate the Kalman filter algorithm and the measurement differencing algorithm. The measurement differencing algorithm significantly reduces attitude estimation errors introduced by GPS multipath for both the ground based and orbital data.

The JAWSAT operational requirement to limit the on-time of the GPS receiver during orbital maneuvering motivates a discussion of including additional sensors in the attitude estimation scheme. The inclusion of digital sun sensor

measurements along with gyros and GPS will be undertaken in the next two chapters.

*Chapter 4:*

# *ATTITUDE DETERMINATION USING DIGITAL SUN SENSORS AND GYROS*

Small satellites typically try to extract the best possible accuracy from low cost, low power instruments. This chapter describes algorithms for spacecraft attitude determination using low cost digital sun sensors in conjunction with gyroscopes for JAWSAT.

The development of attitude determination algorithms using sun sensors and gyroscopes is motivated by the fact that the GPS receiver may not always be available to update the gyro bias parameters as discussed in section 3.7. Furthermore, the availability of sun sensor measurements provides redundancy in the integrated attitude determination system discussed in Chapter 5, building on the concepts presented in this chapter.

A major challenge in the full exploitation of the digital sun sensor measurements is the relatively large quantization levels. Quantization errors in digital sun sensors correspond to the least significant bit of the digital output, approximately 0.5 degrees for the JAWSAT design. Quantization errors of this magnitude are accentuated in the low dynamic environment of a three-axis stabilized spacecraft, and are correlated with vehicle dynamics. The non-white behavior of GPS multipath and

sun sensor quantization errors violate the assumptions of the standard Kalman filter model, rendering the filter-computed covariance matrix an unsatisfactory indication of filter performance. Furthermore, the fact that attitude rotations about the sun line are unobservable by the sun sensor presents a design challenge for maintaining three-axis attitude knowledge within JAWSAT requirements (three-sigma accuracy within ±5 deg or better, if possible). This chapter provides a brief characterization of sun sensor quantization errors followed by an investigation of attitude estimation algorithms tailored to this measurement type.

## 4.1 Digital Sun Sensor Attitude Determination

Virtually every satellite has flown with some sort of sun sensor for attitude estimation [Wertz, 1978, p. 155]. A photodetector is used to determine the angle of incidence of the sun's energy, thereby giving an estimate of the spacecraft orientation. The Sun Sensor Assembly for JAWSAT will be a two-slit sensor with direct digital output. It will be designed and fabricated at the USAF Academy.

The principle of operation of the digital sun sensor relies on strips of photocells located beneath a light entrance slit as shown in Fig. 4.1. A Gray code mask will be overlaid on the photocell strips so that the illumination pattern can be used to determine the angle to the sun [Wertz, 1978]. The composite of photocell

bits that are activated by the incident solar energy comprise the digital word that represents the angle between the sun line and the normal to the sensor face.

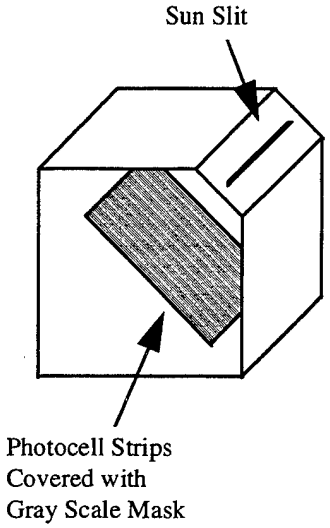


**Fig. 4.1.** Sun sensor assembly for JAWSAT.

Fabrication of the digital sun sensors starts with commercially available photovoltaic cells. Lasers are used to separate elements of a solar cell into electrically isolated strips (as shown in the photograph in Fig. 4.2). A Gray code pattern is etched into a glass plate and mounted on top of the solar cell strips. The voltage output of each strip then generates the digital word output.

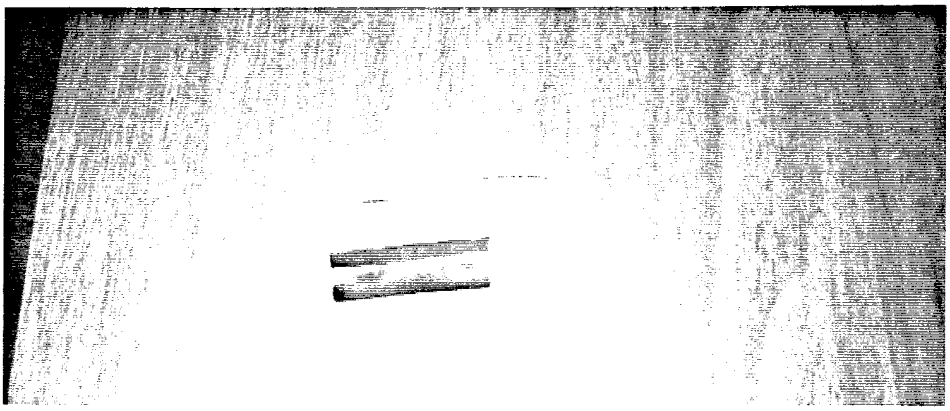

**Fig. 4.2.** Solar cell cut into strips for JAWSAT digital sun sensor. *Solar cell measures approximately 2 cm × 4 cm.*

There are three orthogonal pairs of sun sensors for JAWSAT to provide a field of view of approximately $2\pi$sr. The direct readout from the sensor will be an 8-bit digital word, with the least significant bit representing 0.5 deg. This quantization is expected to be the largest error source.

## 4.2 Sun Sensor Quantization Errors

Quantization errors in the digital sun sensor present a challenge for implementing filtering algorithms. The measurement errors are non-Gaussian, nonlinear, and correlated with the input, all of which violate the assumptions of most stochastic estimation algorithms [Curry, 1970]. Generally, these issues can be ignored when the quantization levels are small or the dynamics of the input signal are large. In this case the quantization errors can be assumed to have a uniform random

distribution [Oppenheim and Schafer, 1989]. For JAWSAT the quantization levels are relatively large and the dynamics are low, causing the uniform distribution assumption to break down.

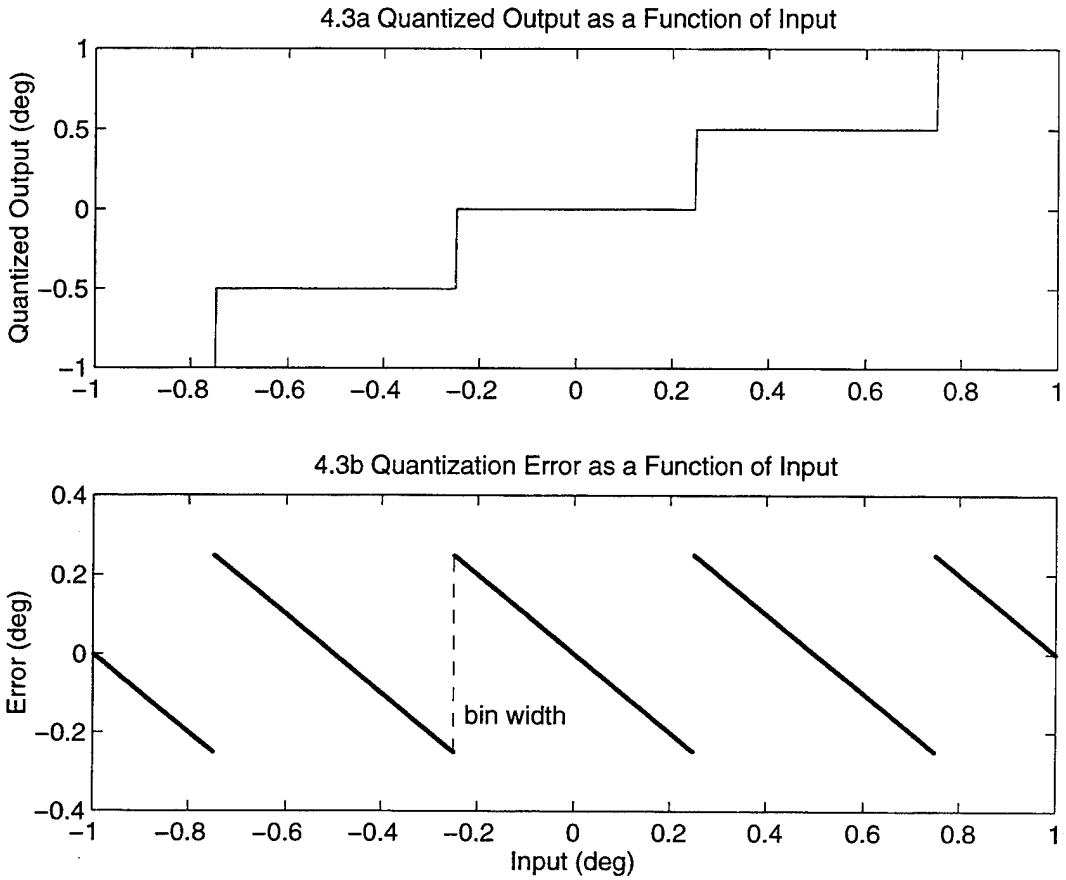


**Fig. 4.3.** Quantization as a function of state. *4.3a illustrates quantizer output as a function of input. 4.3b illustrates error as a deterministic sawtooth function. Figure depicts a quantization bin width of 0.5 deg.*

Analyzing the nonlinear effects of quantization is complicated by the fact that the errors depend on the true state. If the true state is known exactly, then the quantization error can be determined since quantization is a deterministic process. Quantization effects as a function of the true state are shown in Fig. 4.3. Figure 4.3a

shows quantizer output as a function of the input. The "sawtooth" error function of Fig. 4.3b is characteristic of quantizers, although frequently the uniform random distribution assumption is justified. For systems where the dynamics of the signal are known exactly (for example, a single sine wave of known frequency in an audio system), quantization errors can be completely characterized [Maher, 1992; Gray, 1990]. Since the true dynamics of the JAWSAT spacecraft are unknown, a measurement update process that leads to a consistent treatment of the quantization errors is required. In this chapter a "dead zone" method for incorporating sun sensor measurements is proposed.

## 4.3 Attitude Estimation with Sun Sensors and Gyros

Spacecraft attitude estimates are computed using a linearized model of the spacecraft motion that includes attitude and gyro bias parameters. The state vector has seven dimensions: four states for the attitude quaternion, $\bar{q} = \begin{bmatrix} q_1 & q_2 & q_3 & q_4 \end{bmatrix}^T$, and three gyro bias states, $b = \begin{bmatrix} b_1 & b_2 & b_3 \end{bmatrix}^T$, (one for each axis). As in Section 3.3, the filter implementation uses only three of the quaternion states since inclusion of all four gives rise to a singularity in the covariance matrix time update; therefore, a six-state formulation is used following Lefferts *et al.* [1982]. The fourth quaternion state can be computed at any time from the other three to give the full seven dimensional state.

As before, time propagation of the quaternion state estimate and the covariance matrix is performed using gyro angular rate measurements. The sun sensor provides only two independent observations of the three-axis attitude. This causes a condition in the Kalman filter where one or more of the diagonal terms in the covariance matrix tends to increase without bound. As $P$ approaches singularity in this manner, filter divergence or total numerical failure of the recursion relations can occur [Maybeck, 1979].

To help alleviate divergence problems in unobservable problems (as well as to overcome numerical instabilities that arise due to finite word length computations) a class of algorithms known as square root filters has been developed. These algorithms are algebraically equivalent to the Kalman filter, but they operate on a quantity related to the square root of the variance rather than the variance itself. The square roots of the variances have half the dynamic range of the variances, so the square root formulations perform roughly twice as well, in terms of numerical precision, as the conventional filter equations.

The sun sensor results presented in this chapter use the so-called **U-D** filter formulation. Additional information on numerical aspects of Kalman filtering can be found in Brown and Hwang [1992], Maybeck [1979], Bierman and Thornton [1977], and Kaminski *et al.* [1971].

The **U-D** factorization method decomposes the covariance matrix into triangular and diagonal factors as

$$P = UDU^T \tag{4.1}$$

where $U$ is upper triangular and $D$ is diagonal. Algorithms for carrying out this factorization are discussed by Brown and Hwang [1992] and Maybeck [1979]. The main numerical benefit of this method is obtained in the measurement update of the $U$ and $D$ factors rather than the (nearly singular) $P$ matrix. For convenience, the propagation step is summarized below, followed by a discussion of the sun sensor measurement model and update process.

The time propagation for the total attitude quaternion estimate $\hat{\bar{q}}$ from time *k-1* to *k* is obtained from the gyro angular velocity measurements and the attitude kinematics described by

$$\hat{\bar{q}}_k = e^{\frac{1}{2}\Omega^{\times}\Delta t}\hat{\bar{q}}_{k-1} \tag{4.2}$$

where $\Omega^{\times}$ is the cross product matrix based on the gyro angular rate measurements and $\Delta t$ is the time increment.

The time propagation for the covariance matrix is given by

$$P_{k+1}^{-} = \left(\Phi U_k^+\right) D_k^+ \left(\Phi U_k^+\right)^T + \Gamma Q_d \Gamma^T \tag{4.3}$$

where $\Phi$ is the state transition matrix and $Q_d$ is the process noise covariance matrix.

## 4.4 Digital Sun Sensor Measurement Model

Line of sight sensors such as sun sensors measure the projection of the line of sight to the sun onto the sensor axes. The angles expressing the line of sight to the sun in terms of the sun sensor measurement axes are illustrated in Fig. 4.4. The horizontal (H) and vertical (V) sensor axes shown in the figure correspond to the body X and Y axes, respectively.

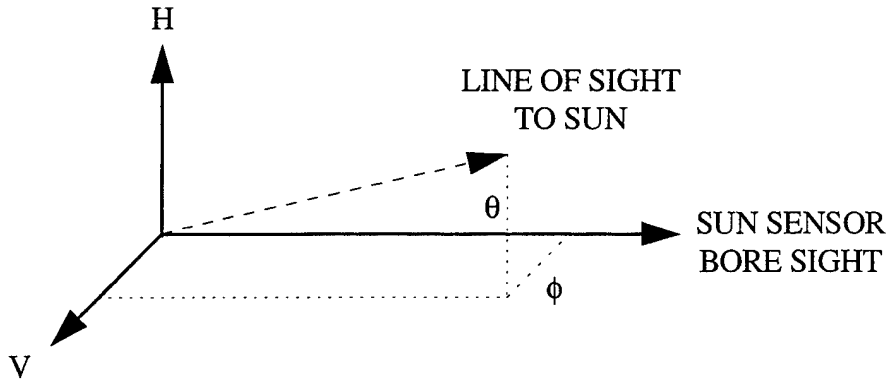


**Fig. 4.4.** Sun sensor coordinate definition.

The angles $\phi$ and $\theta$ are the elevations of the sun in the perpendicular planes formed by the sun sensor axes. These two planes intersect at the sensor boresight. The actual sensor measurements, $u$ and $v$, are related to the elevation angles according to [Wertz, 1978]

$$\begin{aligned} u &= \tan\theta \\ v &= \tan\phi \end{aligned} \tag{4.4}$$

The computed unit vector in the direction of the sun based on the measurements is given as [Sedlak and Chu, 1993]

$$S = \left(1+u^2+v^2\right)^{-1/2}\begin{bmatrix} u \\ v \\ 1 \end{bmatrix} \tag{4.5}$$

and the projection of this unit vector onto the two sensor axes is

$$\wp S = \left(1+u^2+v^2\right)^{-1/2}\begin{bmatrix} u \\ v \end{bmatrix} \tag{4.6}$$

where $\wp$ denotes the projection operation. The error covariance of the projected measurements can be written as

$$R = \sigma^2 B^2 \tag{4.7}$$

where $\sigma^2$ is the standard deviation of the measurement errors and the projection of these errors onto the sensor axes is represented by the matrix [Sedlak and Chu, 1993]

$$B = \left(1+u^2+v^2\right)^{-3/2}\begin{bmatrix}\left(1+u^2\right) & -uv \\ -uv & \left(1+v^2\right)\end{bmatrix} \tag{4.8}$$

Since the true values of $u$ and $v$ are not available in the Kalman filter, the $B$ matrix is approximated using the measured values of $u$ and $v$, as suggested by Sedlak and Chu [1993].

In order to incorporate the sun sensor measurements into a Kalman filter, it remains to relate the sun sensor measurements to the state vector. Following the formulation of Sedlak and Chu [1993] and Vathsal [1987], the predicted observation unit vector is given by

$$\hat{S} = MA\left(\hat{\bar{q}}\right)\hat{V} \tag{4.9}$$

where $M$ is the rotation matrix from the spacecraft body frame to the sensor frame (assumed to be the identity for this analysis), $A$ is the attitude matrix representing the rotation from inertial to body coordinates, and $\hat{V}$ is the estimated sun vector expressed in inertial coordinates.

The measurement residual is the projection of the residual perpendicular to the sensor boresight:

$$\Delta z = \wp\left(S - \hat{S}\right) \tag{4.10}$$

where $S$ is the measured line of sight vector. This projection can be expressed in terms of the quaternion correction states as

$$\Delta z = \begin{bmatrix} -2\left(m_x \times \hat{W}\right)^T \\ -2\left(m_y \times \hat{W}\right)^T \end{bmatrix} \delta q + v \tag{4.11}$$

where

$$\hat{W} \equiv A\left(\hat{\bar{q}}\right)\hat{V} \tag{4.12}$$

and $m_x$ and $m_y$ are unit vectors along the sensor axes, and $v$ is the measurement noise with covariance $R$.

Note that the gyro biases are not directly observed by the sun sensor, so the complete linearized state measurement equation is

$$\Delta z = \begin{bmatrix} -2\left(m_x \times \hat{W}\right)^T & 0_{1\times 3} \\ -2\left(m_y \times \hat{W}\right)^T & 0_{1\times 3} \end{bmatrix} \Delta\tilde{x} + v \tag{4.13}$$

The measurement observation matrix for the Kalman filter is

$$H \equiv \begin{bmatrix} -2\left(m_x \times \hat{W}\right)^T & 0_{1\times 3} \\ -2\left(m_y \times \hat{W}\right)^T & 0_{1\times 3} \end{bmatrix} \tag{4.14}$$

This measurement model for the sun sensors accounts for the fact that rotations about the line to the sun are not observable. The optimal updated state vector is given by

$$\Delta\hat{\tilde{x}}^+ = K\left(\Delta\tilde{z}\right) \tag{4.15}$$

where

$$K = P^- H^T \left(HP^- H^T + R\right)^{-1} \tag{4.16}$$

and the updated covariance is

$$P^+ = U^- \left[ D^- - \frac{1}{\alpha}\left(D^- U^{-T} H^T\right)\left(D^- U^{-T} H^T\right)^T \right] U^{-T} \tag{4.17}$$

where

$$\alpha \equiv HP^{-}H^{T} + R \tag{4.18}$$

for scalar measurements.

The updated total state can be obtained as in Lefferts *et al.* [1982], using the following relations (where superscript "+" indicates updated values, superscript "-" indicates predicted values, and "$\otimes$" denotes quaternion composition)

$$\Delta\hat{\tilde{x}}^{+} \equiv \begin{bmatrix} \delta\hat{q}^{+} \\ \Delta\hat{b}^{+} \end{bmatrix} \tag{4.19}$$

$$\delta\hat{\bar{q}}^{+} \equiv \begin{bmatrix} \delta\hat{q}^{+} \\ 1 \end{bmatrix} \tag{4.20}$$

$$\hat{\bar{q}}^{+} = \delta\hat{\bar{q}}^{+} \otimes \hat{\bar{q}}^{-} \tag{4.21}$$

$$\hat{b}^{+} = \hat{b}^{-} + \Delta\hat{b}^{+}. \tag{4.22}$$

## 4.5 Dead Zone Filter

What is the best way to incorporate the digital sun sensor measurements into the filter? One straightforward approach is to just treat the center of each quantization level as the observation at each measurement interval, as suggested by the form of the measurement update equations in the previous subsection. The measurement error will then be equal to the quantization error, and the measurement residual will be equal to this error plus the prediction error. A potential difficulty with this is that as the true attitude nears the edge of the bin, the sun sensor measurement will pull the solution in the wrong direction. This is also likely to lead to degradation in the bias estimates. Furthermore, the sun sensor provides only two linearly independent measurements, limiting the observability of the three-dimensional attitude, particularly in a sun synchronous orbit.

One way to deal with the quantization errors is to implement a "dead zone" [*e.g.*, Evans *et al.*, 1994] wherein as long as the predicted and observed sun sensor measurements lie within the same bin, the measurement residual is set to zero. If they do not agree, the observation is set either to the center of the bin or to the edge of the bin. The latter approach has been selected after observing that most of the time when the predicted and observed do not agree it is because both are near the edge of a bin. In this approach the measurement residual is taken to be zero when they agree and by the following expression when they do not.

$$\Delta z = \wp S - \Delta \,\mathrm{round}\left(\frac{1}{\Delta}\left(\wp \hat{S}\right)\right) \tag{4.23}$$

where round$(\cdot)$ represents the nonlinear "round to nearest integer" function and $\Delta$ is the quantization bin width. Since quantization errors are deterministic it is possible to predict the quantized measurement. Regardless of whether the measurement residual is zero, the covariance is updated to reflect the information gained from the sun sensor measurement. Note that the predicted measurement is not simply $H\hat{x}^-$ as in the standard Kalman filter, but instead the second term in equation (4.23) uses the deterministic "round" function to form the measurement residual.

Conceptually, it is desirable to use all the information available from the sun sensor measurements in a filtering algorithm that is mathematically consistent with the measurement errors. With the dead zone formulation, the digital sun sensor essentially acts as a sun presence detector within each quantization level. This sun presence information can be used in two ways, depending on whether any bin switching in the actual or predicted observation has occurred.

An alternative to the "dead zone" approach for incorporating quantized sun sensor measurements is to treat the errors as unknown but bounded. In other words, no assumptions about the statistics of the errors are assumed, but the magnitude of

the errors is known to be bounded by the quantization bin width. This notion of unknown but bounded processes was first incorporated into a state estimation context by Schweppe [1973, 1968]. Recent applications and refinements of these techniques are described in the review articles by Combettes [1993] and Walter and Piet-Lahanier [1990]. A difficulty with these methods for sequential state estimation is that they can lead to excessively conservative error bounds on the state estimates.

Several authors have proposed the application of set membership estimation to quantization errors in various A/D sampling systems such as a digital sun sensor [*e.g.*, Cerone, 1993; Combettes, 1993; Rao and Huang, 1992; Belaforte *et al.*, 1990; Walter and Piet-Lahanier, 1990; Fogel and Huang, 1982; Schweppe, 1973]. None of these papers, however, presents any numerical or empirical results for state estimation using quantized measurements. Chesley and Axelrad [1995] showed that existing sequential algorithms using ellipsoidal bounding sets are generally impractical for spacecraft attitude estimation using the JAWSAT digital sun sensor due to the excessively conservative error bounds on the state estimates. Preliminary numerical evaluations of a new algorithm due to Hong [1993] that uses confidence intervals associated with bounding sets also seem to suffer the same excessively conservative error bounds.

## 4.6 Simulation Results and Discussion

The dead zone and EKF algorithms described in this chapter were implemented in a MATLAB simulation. For the purpose of emphasizing the observability limitations of the sun sensor, results are first presented for a sun-synchronous, dawn-dusk orbit. In this configuration the sun sensor suffers does not observe the pitch axis. The EKF algorithm should be expected to suffer numerical instability caused by the lack of observability which could cause the estimates of all filter states to diverge [Brown and Hwang, 1992].

Figure 4.5 shows the attitude estimation errors for the extended Kalman filter. Note that the filter estimates diverge after a short time and that the divergence occurs most rapidly in the pitch axis which is unobservable.

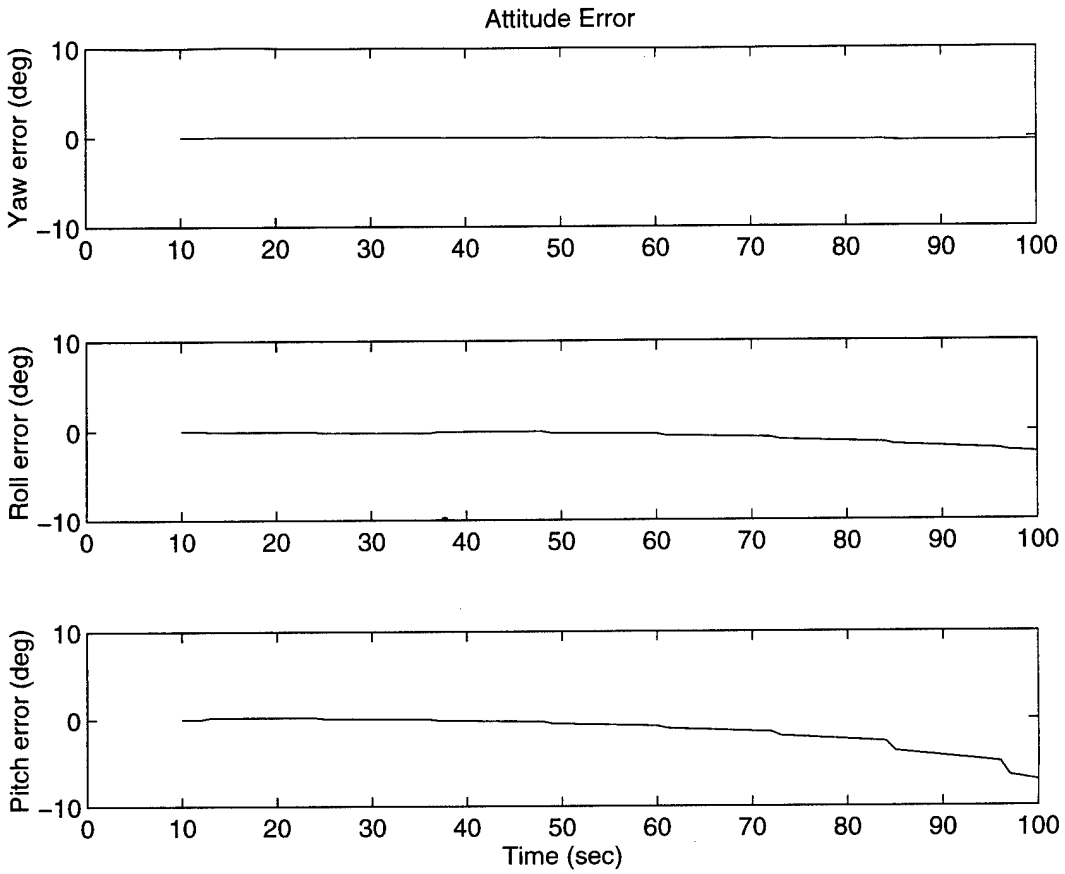


**Fig. 4.5.** Attitude Estimation Error: Standard EKF Algorithm. *Sun sensor measurements are based on a dawn-dusk sun synchronous orbit.*

The measurement updates based on the quantized measurements emphasize the center of the measurement bin. Since the true state is not always at the center of the bin, measurements incorporated in this way tend to drive the filter away from the correct estimate.

The dead zone filter results for the dawn-dusk sun synchronous orbit are presented in Fig. 4.6. The dead zone filter helps reduce the effects of introducing biased measurements due to the coarse quantization in the digital sun sensor.

However, the pitch axis is never observed in this orbit which ultimately causes this filter to diverge as well.

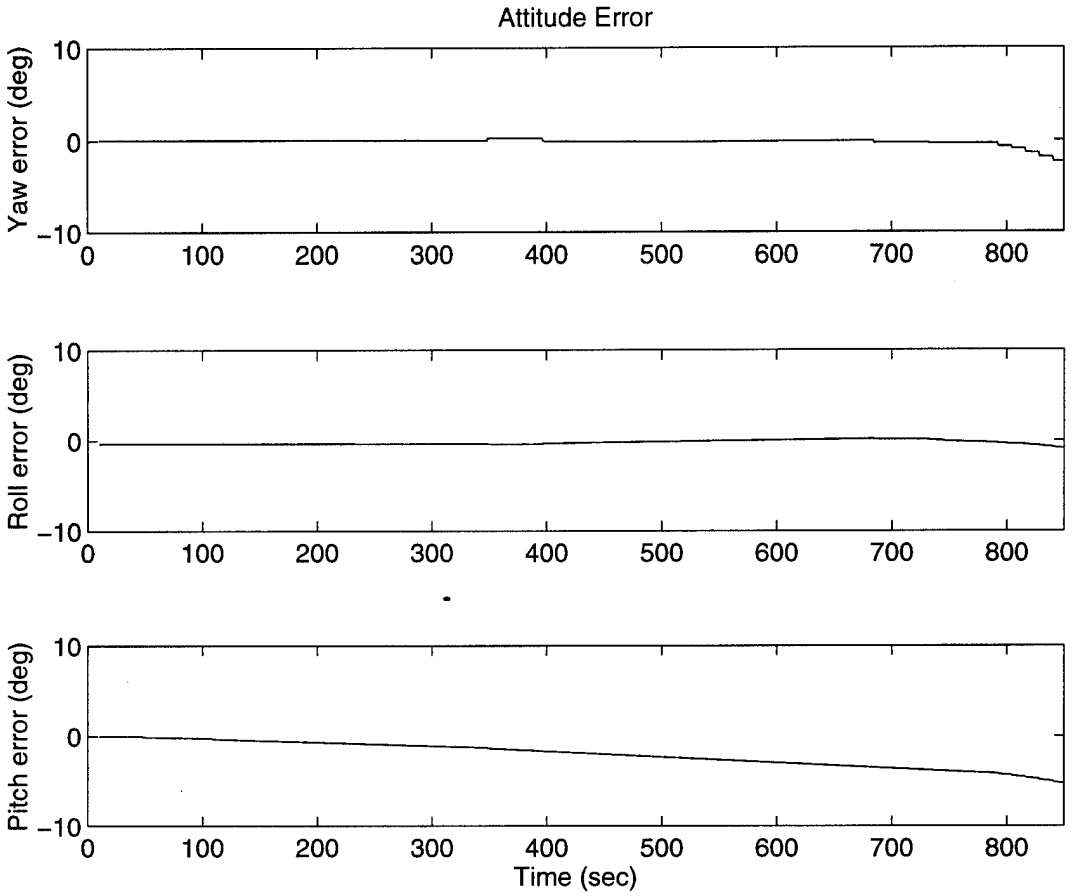


**Fig. 4.6.** Attitude Estimation Error: Dead Zone Algorithm. *Sun sensor measurements are based on a dawn-dusk sun synchronous orbit.*

The dawn-dusk orbit illustrates the worst case possible for the combination of digital sun sensors and gyros. These results demonstrate that errors grow most rapidly in the unobservable axis, and that the dead zone approach improves filter performance for the large quantization levels present in the digital sun sensor. These results also demonstrate that if JAWSAT is to be placed in a dawn-dusk orbit,

additional measurements from an Earth horizon scanner or three-axis magnetometer will be needed to maintain attitude determination accuracy when GPS measurements are not available.

Although final orbit parameters for JAWSAT have not been established, the baseline design for JAWSAT was a noon-midnight sun synchronous orbit. Since the sun direction does not remain along the same axis as the spacecraft travels along the noon-midnight orbit, the observability limitations in this case should be somewhat alleviated. In other words, the information lost in the unobservable direction is distributed among more than one attitude state.

Figure 4.7 shows the attitude estimation errors for the standard Kalman filter algorithm using digital sun sensors and gyros in the noon-midnight orbit. The simulation run begins with the spacecraft above the North Pole so that the roll axis is unobservable initially. Note that the standard filter diverges quite rapidly, as it did for the dawn-dusk case (see Fig. 4.5). However, in Fig. 4.7 the errors grow most rapidly in the unobservable roll direction, as expected. The incorporation of the quantized measurements causes the filter to diverge before the satellite motion can be used to gain any information in the roll axis.

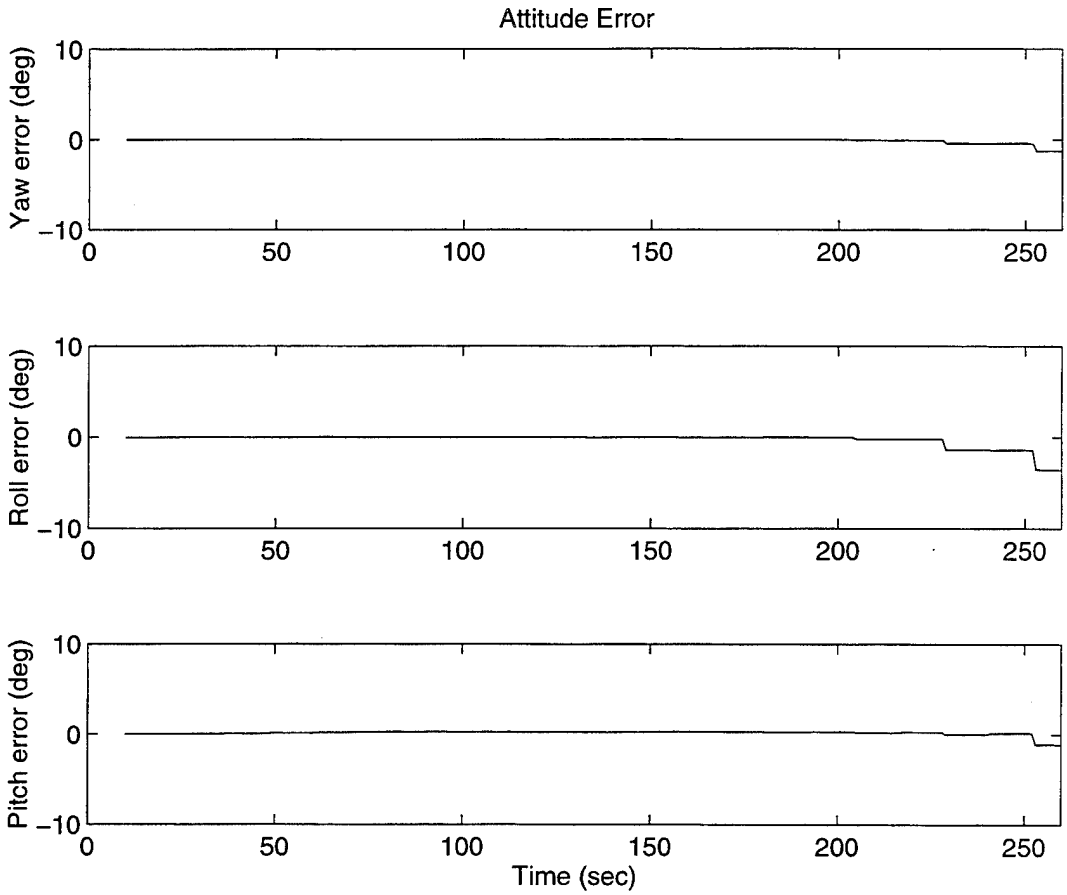


**Fig. 4.7.** Attitude Estimation Error: Standard EKF Algorithm. *Sun sensor measurements are based on a noon-midnight sun synchronous orbit.*

Attitude estimation errors for the dead zone algorithm in the noon-midnight orbit are shown in Fig. 4.8. The results show that the dead zone algorithm operates for at 60 min. without diverging in the noon-midnight orbit. After about 60 min. the spacecraft would enter an eclipse period and GPS measurements would be used to update the attitude filter.

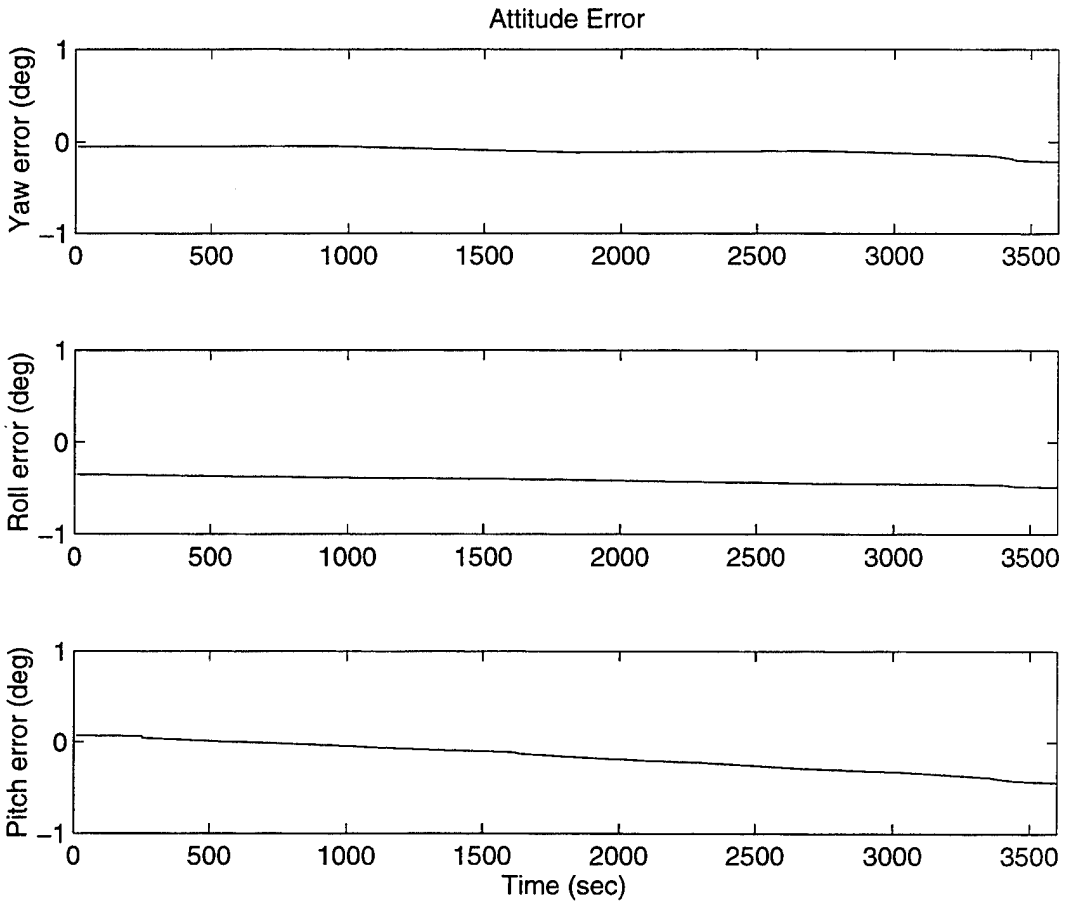


**Fig. 4.8.** Attitude Estimation Error: Dead Zone Algorithm. *Sun sensor measurements are based on a noon-midnight sun synchronous orbit.*

The computed filter covariance describes the quaternion states and is not directly related to the yaw, roll, and pitch angles. However, the computed covariance for the attitude states remains bounded throughout the run. In fact, the computed 1-$\sigma$ uncertainties in the attitude quaternion states remain less than 5 deg for the time period simulated.

The combination of somewhat improved observability in the high noon orbit and the use of measurement updates based on the dead zone result in an algorithm that satisfies JAWSAT mission requirements during planned outages of the GPS receiver. Further analysis will be required when the final orbit parameters of JAWSAT are decided, particularly if the orbit is nearly dawn-dusk.

## 4.7 Summary and Conclusions

Recursive state estimation algorithms have been described for a small satellite attitude determination system using digital sun sensors and gyros. The filters discussed include an extended Kalman filter and a modified filter that employs a "dead zone" for the sun sensor measurements where only sun presence information is used within each quantization bin. Measurement updates are based on measurement residuals that exceed the quantization bin width.

Large quantization errors in the digital sun sensors cause the standard Kalman filter algorithm to diverge since the measurements are biased toward the center of the quantization bin. The dead zone filter overcomes these problems by providing measurement updates based on bin switching rather than the center of each bin. The dead zone filter provides stable attitude estimates in the noon-midnight orbit planned for JAWSAT.

The combination of sun sensors and gyros is generally unobservable [Vathsal, 1987]. Additional measurements are needed to maintain filter stability, either during solar eclipse periods or poor observability conditions. Additional measurements from GPS will be incorporated in an integrated attitude estimation method in Chapter 5. As an intermediate step, this chapter has considered a dead zone filter that is adequate for attitude determination using only sun sensors and gyros during intermittent outages of the GPS attitude measurements.

*Chapter 5:*

# *INTEGRATED GPS ATTITUDE DETERMINATION*

Multisensor state estimation and failure detection has received considerable interest for aerospace applications where an optimal estimate is required based on measurements from several sensors. In fact, the sensor "measurements" may actually be the output from a Kalman filter contained within a given sensor, such as a GPS receiver [Carlson, 1990]. As several off-the-shelf components are combined to form an overall system, the methods for integrating measurements from these distributed systems requires careful attention.

This chapter discusses integrated filtering algorithms for the JAWSAT attitude determination system. First, a centralized Kalman filter methodology is discussed and the shortcomings of this method are summarized. Then a distributed Kalman filter approach, namely the federated filter algorithm, is introduced. Finally, a federated filter based on time-correlated measurement errors due to GPS multipath is developed, results from the algorithm are presented, and implications for an integrated spacecraft attitude determination system are discussed.

## 5.1 Centralized Kalman Filtering

A straightforward extension of the algorithms presented in Chapters 3 and 4 is to form state estimates using multiple sensors in a single, globally optimal Kalman filter that incorporates a separate measurement update step for each sensor. For the JAWSAT attitude determination system, this involves updates based on sun sensor and GPS attitude measurements.

The centralized filter algorithm is summarized in Fig. 5.1, where GPS measurement differencing can be employed as desired.

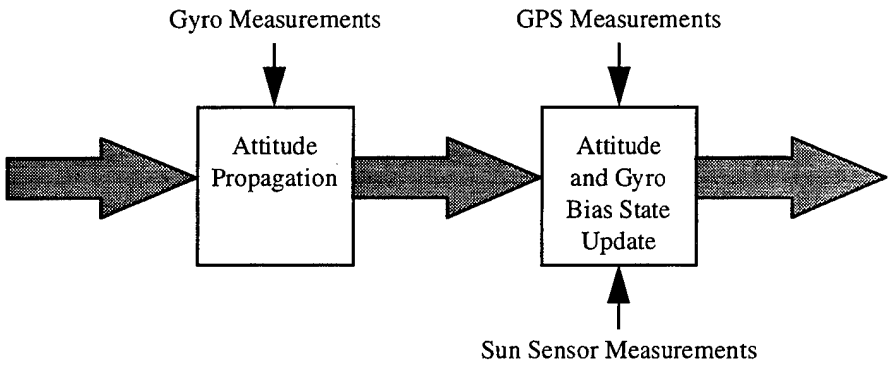


**Fig. 5.1.** Centralized Kalman filter algorithm

The centralized Kalman filter approach has several shortcomings which are described by Carlson and Berarducci [1994]. These include: heavy computational loads, poor fault tolerance, and inability to correctly process prefiltered data. These shortcomings are all critical concerns for low cost satellites, where it is desirable to minimize computational loads, sensor failures are more likely, and prefiltered data

from gyros or GPS is likely to be available from off-the-shelf sensors. Therefore, consideration will be given to decentralized filtering methods for the integrated attitude determination system for JAWSAT.

## 5.2 Decentralized Kalman Filtering

Decentralized or distributed Kalman filtering methods have been developed to exploit parallel processing technology, fault tolerant system design, and integration of multiple specialized sensors [Carlson and Berarducci, 1994]. The basic idea of decentralized filtering is to divide the global system information among local sensors associated with each of the contributing sensors. Research on decentralized estimation using distinct local filters to process measurements traces back to Speyer's [1979] formulation. Subsequent developments are summarized by Kerr [1987]. Recent developments in the decentralized filtering problem include the estimate fusion approach of Carpenter and Bishop [1995, 1994, 1993]. They develop a means for fusing estimates from two separate filters, but they do not generalize to the case of more than two contributing sensors. Pao [1994] develops a fusion algorithm for tracking multiple targets using measurements from distributed sensors. Her approach is specifically tailored to a tracking radar environment where unique state vectors are desired for each separate target, and is not readily extended to spacecraft attitude estimation. Additional studies [*e.g.*, Berg and Durrant-Whyte,

1992; Bailey and Sims, 1990; Hashemipour *et al.*, 1988; Bierman and Belzer, 1985; and Castanon and Teneketzis, 1985] have developed decentralized filtering algorithms for various applications. None of these existing studies has considered the use of a quaternion attitude representation in the state vector.

A particularly attractive method for performing decentralized filtering for navigation systems is the so-called "federated" Kalman filter that has been developed by Carlson [1990, 1988]. The advantages of the federated filter include the following: the local filters are constructed such that the cross correlation between local filters are eliminated; local estimators are able to share common information which can be combined in a rigorous manner to form a global best estimate; "off-the-shelf" sensors, including those with embedded Kalman filters, can be combined in a consistent, rigorous manner. This approach is very well suited to navigation applications since a master filter propagation step can be performed based on measurements from gyros or an inertial navigation system. In this chapter the federated filter approach is extended to reduce the effects of GPS multipath errors in the integrated system developed for the JAWSAT attitude determination system.

The crux of the federated filter is the ability to combine measurements from distinct local filters into a globally optimal solution. If the local filters are constructed to allow for this distribution of information, then the overall filter covariance, $P_f$, and the global state estimate, $\hat{x}_f$, can be constructed from the local

filter covariance and state estimates, $P_i$ and $\hat{x}_i$ where $i = 1,\ldots,N$ and $N$ is the total number of partitions. The optimal combination of these distributed estimates is given by [Kerr, 1987]

$$P_f = \left(P_1^{-1} + \ldots + P_N^{-1}\right)^{-1} \tag{5.1}$$

$$\hat{x}_f = P_f\left(P_1^{-1}\hat{x}_1 + \ldots + P_N^{-1}\hat{x}_N\right) \tag{5.2}$$

The details of how these separate estimates are constructed so that equations (5.1)-(5.2) result in a valid global estimate will be addressed further in the next section.

Recent investigations of the federated filter method include Carlson and Berarducci [1994], Lawrence and Berarducci [1994], Gao *et al.* [1993, 1992], Moorman and Bullock [1993], Felter [1992], and Broatch and Henley [1991]. These studies all focus on integrated navigation applications, rather than attitude estimation. Implementation of a federated filter for a quaternion attitude representation requires a modification of the master filter fusion equations. This extension of the original federated filter is discussed in Section 5.5.

## 5.3 Federated Kalman Filter Algorithm

Motivated by the shortcomings of centralized Kalman filters outlined in the previous section, Carlson [1990, 1988] developed the federated filter to address many of these concerns. The federated filter builds on several earlier developments in decentralized filtering, particularly the developments by Kerr [1987], Bierman and Belzer [1985], Chang [1980], and Speyer [1979]. The federated filter distributes the global system information among the local filters associated with each contributing sensor. These distinct local filter estimates can recombined in an optimal way, or in a conservatively suboptimal way, depending on the implementation selected.

The local filter estimates are constructed from the global (centralized) Kalman filter using rigorous information sharing principles [Carlson, 1990]. The basic approach of this method is to form a global state vector, $x$, that includes the states from each of the local filters, $x_i$ for $i = 1,\ldots,N$, as

$$x = \begin{bmatrix} x_1 \\ \vdots \\ x_N \end{bmatrix} \tag{5.3}$$

with global covariance

$$P = \begin{bmatrix} P_{11} & \cdots & P_{1N} \\ \vdots & \ddots & \vdots \\ P_{N1} & \cdots & P_{NN} \end{bmatrix} \tag{5.4}$$

where $P_{ii}$ is the covariance matrix for the state vector $x_i$, and $P_{ij}$ for $i \neq j$ is the cross covariance of state $x_i$ with state $x_j$.

Then, it can be shown that the measurement update equations for local filter $i$ are given by the standard Kalman filter equations [Carlson, 1990], namely

$$\begin{aligned} x_i^+ &= x_i^- + K_i\left(z_i - H_i x_i^-\right) \\ P_{ii}^+ &= \left(I - K_i H_i\right) P_{ii}^- \end{aligned} \tag{5.5}$$

(5.6)

where

$$K_i = P_{ii}^- H_i^T \left(H_i P_{ii}^- H_i^T + R_i\right)^{-1} \tag{5.7}$$

The global propagation step can be written as [Carlson, 1990]

$$\begin{bmatrix} x_1 \\ \vdots \\ x_N \end{bmatrix}_{k+1} = \begin{bmatrix} \Phi_{11} & \cdots & 0 \\ \vdots & \ddots & \vdots \\ 0 & \cdots & \Phi_{NN} \end{bmatrix} \begin{bmatrix} x_1 \\ \vdots \\ x_N \end{bmatrix}_k + \begin{bmatrix} \Gamma_1 \\ \vdots \\ \Gamma_N \end{bmatrix} w \tag{5.8}$$

$$\begin{bmatrix} P_{11} & \cdots & P_{1N} \\ \vdots & \ddots & \vdots \\ P_{N1} & \cdots & P_{NN} \end{bmatrix}_{k+1} = \begin{bmatrix} \Phi_{11} & \cdots & 0 \\ \vdots & \ddots & \vdots \\ 0 & \cdots & \Phi_{NN} \end{bmatrix} \begin{bmatrix} P_{11} & \cdots & P_{1N} \\ \vdots & \ddots & \vdots \\ P_{N1} & \cdots & P_{NN} \end{bmatrix}_k \begin{bmatrix} \Phi_{11} & \cdots & 0 \\ \vdots & \ddots & \vdots \\ 0 & \cdots & \Phi_{NN} \end{bmatrix}^T + \begin{bmatrix} \Gamma_1 \\ \vdots \\ \Gamma_N \end{bmatrix} Q \begin{bmatrix} \Gamma_1^T & \cdots & \Gamma_N^T \end{bmatrix} \tag{5.9}$$

It is clear from equation (5.8) that the state vector propagation can be partitioned into local filter computations using the standard Kalman filter equation, that is,

$$x_{i_{k+1}} = \Phi_{ii} x_{i_k} + \Gamma_i w \tag{5.10}$$

There are two problems, however, with partitioning the covariance propagation, one related to the *a priori* covariance, and the other related to the process noise. The problem is the appearance of nonzero matrices in the off-diagonal positions in equation (5.9). The problem can be solved by a formulation of equation (5.9) that contains all block diagonal matrices which can be readily separated into local filter estimates. Following the derivation introduced by Carlson [1988], note that the last term in equation (5.9) can be rewritten as

$$\begin{bmatrix} \Gamma_1 & \cdots & 0 \\ \vdots & \ddots & \vdots \\ 0 & \cdots & \Gamma_N \end{bmatrix} \begin{bmatrix} Q & \cdots & Q \\ \vdots & \ddots & \vdots \\ Q & \cdots & Q \end{bmatrix} \begin{bmatrix} \Gamma_1^T & \cdots & 0 \\ \vdots & \ddots & \vdots \\ 0 & \cdots & \Gamma_N^T \end{bmatrix} \tag{5.11}$$

Next, the matrix upper bound theorem [Carlson, 1990] is applied,

$$\begin{bmatrix} Q & \cdots & Q \\ \vdots & \ddots & \vdots \\ Q & \cdots & Q \end{bmatrix} \leq \begin{bmatrix} \gamma_1 Q & \cdots & 0 \\ \vdots & \ddots & \vdots \\ 0 & \cdots & \gamma_N Q \end{bmatrix} \tag{5.12}$$

where $0 \leq \frac{1}{\gamma_i} \leq 1$ for all $i$ and $\sum_{i=1}^{N} \frac{1}{\gamma_i} = 1$.

The matrix inequality in equation (5.12) indicates that the larger matrix is "more positive semi-definite" than the smaller matrix. Stated more precisely,

$$\begin{bmatrix} \gamma_1 Q & \cdots & 0 \\ \vdots & \ddots & \vdots \\ 0 & \cdots & \gamma_N Q \end{bmatrix} - \begin{bmatrix} Q & \cdots & Q \\ \vdots & \ddots & \vdots \\ Q & \cdots & Q \end{bmatrix} \geq 0 \tag{5.13}$$

where the symbol $\geq 0$ in equation (5.13) indicates positive semidefiniteness. (A positive semi-definite matrix has all eigenvalues greater than or equal to zero.)

The terms $\gamma_i$ in equation (5.13) are defined such that $0 \leq \frac{1}{\gamma_i} \leq 1$ for all $i$ and $\sum_{i=1}^{N} \frac{1}{\gamma_i} = 1$. This leads to a conservative block diagonal form for the global process noise.

In order to fully block diagonalize equation (5.9), a similar upper bounding procedure is applied to the *a priori* covariance matrix. Note that once the initial global covariance matrix has been diagonalized at time zero, the structure of equation (5.9) dictates that the off-diagonal terms must remain identically zero [Carlson, 1990]. Thus, the covariance propagation for partition $i$ can be expressed as

$$P_{ii_{k+1}} = \Phi_{ii} P_{ii_k} \Phi_{ii}^T + \Gamma_i \gamma_i Q \Gamma_i^T \tag{5.14}$$

where $\gamma_i$ represents the share of the global information allotted to local filter $i$ (usually $\gamma_i = N$ for all $i$).

Various implementation options for sharing information in the federated filter are described by Carlson and Berarducci [1994, 1993], depending on the desired level of optimality or fault tolerance. The differences between these information sharing methods depend on the amount of filter "memory" associated with the master filter and local filters. In the federated filters discussed for the JAWSAT attitude determination system discussed in this chapter, the "fusion reset" mode is used. In this configuration the global filter retains the long term memory and the local filters are reset at each measurement epoch with global state and covariance information from the master filter [Carlson and Berarducci, 1994]. This implementation was selected since allowing the sun sensor local filter to operate for extended periods

without reset leads to divergence due to the observability limitations discussed in Chapter 4.

The advantage of the fusion reset mode are that the local filters operate at higher accuarcies due to the incorporation of information from other sensors through the master fusion reset. This improved accuracy for the local filters prevents the limited observabilty inherent in the digital sun sensors from degrading the overall results.

In summary, the fusion reset mode is the most accurate of the data processing modes in the federated filter formulation. A disadvantage of this approach is that the fusion updates from the local filters to the master filter must occur simultaneously. This could limit the usefulness of this approach in real time applications. The other notable disadvantage of this approach is the fact that the fusion reset mode has the poorest fault detection and failure identification characteristics of any of the data fusion modes. For a discussion of the relative merits of other data fusion modes, see Carlson and Berarducci [1994]. An evaluation of fault tolerance and failure detection for the JAWSAT attitude determination system is discussed in Chapter 7 as a subject for future research.

The federated Kalman filter provides flexible implementation options for maximum accuracy, maximum fault tolerance, or an intermediate combination of

accuracy and fault tolerance. In any implementation, federated filter estimates are conservatively suboptimal at worst. Further, the information lost by processing measurements in a suboptimal way can be characterized rigorously.

## 5.4 Federated Kalman Filtering with Time-Correlated Measurement Errors

GPS based attitude determination provides a contributing sensor that can be characterized by correlated measurement errors. This section provides a derivation of a federated filter that includes GPS attitude measurements in an algorithm that considers time-correlated errors. The new algorithm is not strictly optimal, since a matrix approximation is required to construct distinct local filter estimates. Recall that the standard filter implementation is not optimal, either, since the assumption of Gaussian measurement errors has been violated. Performance comparisons highlighting the benefits of the new algorithm will be presented in the next section.

The basic approach in the derivation of a Federated Kalman Filter for measurements containing time-correlated errors is to use measurement differencing (single differencing over a time step) in local filters to "whiten" the errors in the measurement difference pseudo-measurement. A matrix upper bound is then employed to determine an approximate conservative local filter. In the derivations that follow, all the local filter partitions are assumed to have the same state vector, as

is the case for the JAWSAT filter design. This need not be true in general, but this is easily accommodated with a slightly more cumbersome notation and careful accounting of global and local state variables [see Carlson, 1990].

The problem is to estimate the state vector $x$ in a linear system described by:

$$x_{k+1} = \Phi x_k + \Gamma w_k \tag{5.15}$$

$$z_i = \mathbf{H}_i x + \omega_{i_k} \tag{5.16}$$

$$\omega_{i_k} = \Psi \omega_{i_{k-1}} + v_{i_k} \tag{5.17}$$

where $\Phi$ is the state transition matrix from $x_k$ (some prior time) to $x_{k+1}$, $\Gamma$ is the noise distribution matrix, $z_i$ is the measurement from sensor $i$, $\mathbf{H}_i$ is the observation matrix for sensor $i$, $\omega_i$ is the time-correlated measurement noise described by state transition matrix $\Psi$, and $w$ and $v_i$ are white noise driving sequences.

Note that it has been assumed that there is no correlation of measurement errors from separate sensors. (This assumption is reasonable for the JAWSAT sensor suite, but there may be some cases where sensors will be contaminated by the same non-white error source, *e.g.*, visible spectrum sensors contaminated by the same sun glint [see Roy and Iltes, 1991].)

The error statistics of the above quantities are:

$$E[w] = 0 \tag{5.18}$$

$$E[ww^T] = Q \tag{5.19}$$

$$E[v_i] = 0 \tag{5.20}$$

$$E[v_i v_i^T] = \overline{Q_i} \tag{5.21}$$

Next, the global filter variables are defined to include the states from $i = 1,\ldots,N$ sensors, as follows

$$x = \begin{bmatrix} x_1 \\ x_2 \\ \vdots \\ x_N \end{bmatrix} \tag{5.22}$$

$$\mathbf{P} = \begin{bmatrix} \mathbf{P_{11}} & \cdots & \mathbf{P}_{1N} \\ \vdots & \ddots & \vdots \\ \mathbf{P}_{N1} & \cdots & \mathbf{P}_{NN} \end{bmatrix} \tag{5.23}$$

Note that the local state vectors, $x_i$, are assumed to all contain exactly the same states for ease of notation in the following derivation. As shown by Carlson [1990], if the local estimates can be formulated such that they are uncorrelated (*i.e.*, $\mathbf{P}_{ij} = 0, i \neq j$), then the globally optimal state and covariance can be expressed as

$$\mathbf{P}_{mm} = \left[\mathbf{P}_{11}^{-1} + \ldots + \mathbf{P}_{NN}^{-1}\right]^{-1} \tag{5.24}$$

$$\hat{x}_M = \mathbf{P}_{mm}\left[\mathbf{P}_{11}^{-1}\hat{x}_1 + \ldots + \mathbf{P}_{NN}^{-1}\hat{x}_N\right]^{-1} \tag{5.25}$$

Thus, the crucial part of the federated filter formulation is to form local filter estimates which can be globally combined in this way. This will be performed in the following steps:

- The global optimal estimate will be expressed in terms of measurement differencing for each sensor;
- The global time update will be formulated so that estimates may be combined using the above fusion equations; and
- The global measurement update will be shown to be approximately equal to distinct local filter updates which can be accomplished independently.

Directing attention to the problem of measurement differencing, the global state vector propagation is expressed in matrix form as:

$$\begin{bmatrix} x_1 \\ \vdots \\ x_N \end{bmatrix}_{k+1} = \begin{bmatrix} \Phi_{11} & \cdots & 0 \\ \vdots & \ddots & \vdots \\ 0 & \cdots & \Phi_{NN} \end{bmatrix} \begin{bmatrix} x_1 \\ \vdots \\ x_N \end{bmatrix}_k + \begin{bmatrix} \Gamma_1 \\ \vdots \\ \Gamma_N \end{bmatrix} w \tag{5.26}$$

$$\begin{bmatrix} \mathbf{P}_{11} & \cdots & \mathbf{P}_{1N} \\ \vdots & \ddots & \vdots \\ \mathbf{P}_{N1} & \cdots & \mathbf{P}_{NN} \end{bmatrix}_{k+1} = \begin{bmatrix} \Phi_{11} & \cdots & 0 \\ \vdots & \ddots & \vdots \\ 0 & \cdots & \Phi_{NN} \end{bmatrix} \begin{bmatrix} \mathbf{P}_{11} & \cdots & \mathbf{P}_{1N} \\ \vdots & \ddots & \vdots \\ \mathbf{P}_{N1} & \cdots & \mathbf{P}_{NN} \end{bmatrix}_k \begin{bmatrix} \Phi_{11}^T & \cdots & 0 \\ \vdots & \ddots & \vdots \\ 0 & \cdots & \Phi_{NN}^T \end{bmatrix} + \begin{bmatrix} \Gamma_1 \\ \vdots \\ \Gamma_N \end{bmatrix} \mathbf{Q} \begin{bmatrix} \Gamma_1^T & \cdots & \Gamma_N^T \end{bmatrix} \tag{5.27}$$

$$z_i = \begin{bmatrix} 0 & \cdots & H_i & \cdots & 0 \end{bmatrix} \begin{bmatrix} x_1 \\ \vdots \\ x_N \end{bmatrix} + \omega_i \tag{5.28}$$

where $i$ is the sensor index and $k$ is the time index. The measurement equation indicates that measurements are available from individual, independent sensors only.

Note that the measurement errors, $\omega_i$, are not white, but are correlated in time. Thus, the measurement error can be expressed as

$$\omega_{i_{k+1}} = \Psi_i \omega_{i_k} + v_{i_k} \tag{5.29}$$

where $v_i$ is a white measurement error vector. Note that for a sensor corrupted only by white measurement noise, $\Psi_i \equiv 0$.

The presence of time-correlated measurement errors was circumvented in the standard Kalman filter by forming a pseudo-measurement from the difference of successive measurements (see Chapter 3). Proceeding similarly for the multisensor case, the measurement difference is formed

$$\zeta_{i_k} = (z_i)_{k+1} - \Psi_i (z_i)_k \tag{5.30}$$

where $i$ is the sensor index and $k$ is the time step index. The measurement vectors from the different sensors are concatenated as

$$\begin{bmatrix} \zeta_1 \\ \vdots \\ \zeta_N \end{bmatrix}_k = \begin{bmatrix} z_1 \\ \vdots \\ z_N \end{bmatrix}_{k+1} - \begin{bmatrix} \Psi_1 & \cdots & 0 \\ \vdots & \ddots & \vdots \\ 0 & \cdots & \Psi_N \end{bmatrix} \begin{bmatrix} z_1 \\ \vdots \\ z_N \end{bmatrix}_k \tag{5.31}$$

Using the measurement equations and state transition relation gives

$$\begin{bmatrix} \zeta_1 \\ \vdots \\ \zeta_N \end{bmatrix}_k = \begin{bmatrix} H_1 & \cdots & 0 \\ \vdots & \ddots & \vdots \\ 0 & \cdots & H_N \end{bmatrix} \left\{ \begin{bmatrix} \Phi_{11} & \cdots & 0 \\ \vdots & \ddots & \vdots \\ 0 & \cdots & \Phi_{NN} \end{bmatrix} \begin{bmatrix} x_1 \\ \vdots \\ x_N \end{bmatrix} + \begin{bmatrix} \Gamma_1 \\ \vdots \\ \Gamma_N \end{bmatrix} w \right\} + \begin{bmatrix} \Psi_1 & \cdots & 0 \\ \vdots & \ddots & \vdots \\ 0 & \cdots & \Psi_N \end{bmatrix} \begin{bmatrix} \omega_1 \\ \vdots \\ \omega_N \end{bmatrix} + \begin{bmatrix} v_1 \\ \vdots \\ v_N \end{bmatrix}$$
$$- \begin{bmatrix} \Psi_1 & \cdots & 0 \\ \vdots & \ddots & \vdots \\ 0 & \cdots & \Psi_N \end{bmatrix} \left\{ \begin{bmatrix} H_1 & \cdots & 0 \\ \vdots & \ddots & \vdots \\ 0 & \cdots & H_N \end{bmatrix} \begin{bmatrix} x_1 \\ \vdots \\ x_N \end{bmatrix} + \begin{bmatrix} \omega_1 \\ \vdots \\ \omega_N \end{bmatrix} \right\} \tag{5.32}$$

Thus,

$$\begin{bmatrix} \zeta_1 \\ \vdots \\ \zeta_N \end{bmatrix}_k = \left\{ \begin{bmatrix} H_1 & \cdots & 0 \\ \vdots & \ddots & \vdots \\ 0 & \cdots & H_N \end{bmatrix} \begin{bmatrix} \Phi_{11} & \cdots & 0 \\ \vdots & \ddots & \vdots \\ 0 & \cdots & \Phi_{NN} \end{bmatrix} - \begin{bmatrix} \Psi_1 & \cdots & 0 \\ \vdots & \ddots & \vdots \\ 0 & \cdots & \Psi_N \end{bmatrix} \begin{bmatrix} H_1 & \cdots & 0 \\ \vdots & \ddots & \vdots \\ 0 & \cdots & H_N \end{bmatrix} \right\} \begin{bmatrix} x_1 \\ \vdots \\ x_N \end{bmatrix}$$
$$+ \left\{ \begin{bmatrix} H_1 & \cdots & 0 \\ \vdots & \ddots & \vdots \\ 0 & \cdots & H_N \end{bmatrix} \begin{bmatrix} \Gamma_1 \\ \vdots \\ \Gamma_N \end{bmatrix} w + \begin{bmatrix} v_1 \\ \vdots \\ v_N \end{bmatrix} \right\} \tag{5.33}$$

This can be rewritten as

$$\begin{bmatrix} \zeta_1 \\ \vdots \\ \zeta_N \end{bmatrix}_k = \begin{bmatrix} H_1^* & \cdots & 0 \\ \vdots & \ddots & \vdots \\ 0 & \cdots & H_N^* \end{bmatrix} \begin{bmatrix} x_1 \\ \vdots \\ x_N \end{bmatrix} + \begin{bmatrix} \varepsilon_1 \\ \vdots \\ \varepsilon_N \end{bmatrix} \tag{5.34}$$

where the definitions of $H_i^*$ and $\varepsilon_i$ are given as

$$H_i^* \equiv H_i \Phi_i - \Psi_i H_i \tag{5.35}$$

$$\varepsilon_i \equiv H_i \Gamma_i w + v_i \tag{5.36}$$

Note that $\varepsilon_i$ is a white measurement error sequence, but it is correlated with the process noise $w$. This correlation is described by the covariance matrix

$$\begin{aligned} \mathbf{C} &= E\left[ w \left\{ \begin{bmatrix} H_1 & \cdots & 0 \\ \vdots & \ddots & \vdots \\ 0 & \cdots & H_N \end{bmatrix} \begin{bmatrix} \Gamma_1 \\ \vdots \\ \Gamma_N \end{bmatrix} w + \begin{bmatrix} v_1 \\ \vdots \\ v_N \end{bmatrix} \right\}^T \right] \\ &= E\left[ w w^T \begin{bmatrix} \Gamma_1^T & \cdots & \Gamma_N^T \end{bmatrix} \begin{bmatrix} H_1^T & \cdots & 0 \\ \vdots & \ddots & \vdots \\ 0 & \cdots & H_N^T \end{bmatrix} \right] + E\left[ w \begin{bmatrix} v_1^T & \cdots & v_1^T \end{bmatrix} \right] \\ &= \mathbf{Q} \begin{bmatrix} \Gamma_1^T & \cdots & \Gamma_N^T \end{bmatrix} \begin{bmatrix} H_1^T & \cdots & 0 \\ \vdots & \ddots & \vdots \\ 0 & \cdots & H_N^T \end{bmatrix} \\ \mathbf{C} &= \mathbf{Q} \begin{bmatrix} \Gamma_1^T H_1^T & \cdots & \Gamma_N^T H_N^T \end{bmatrix} \end{aligned} \tag{5.37}$$

Note that the (pseudo) measurement noise covariance is given by

$$\begin{aligned}\mathbf{R}_{ij} &= E\left[\varepsilon_i \varepsilon_j{}^T\right] \\ &= E\left[\left(H_i\Gamma_i w + v_i\right)\left(H_j\Gamma_j w + v_j\right)^T\right] \\ &= H_i\Gamma_i\mathbf{Q}_i\Gamma_j{}^T H_j{}^T + \overline{\mathbf{Q}}_{ij}\end{aligned} \tag{5.38}$$

Recall that $E\left[ww^T\right] = \mathbf{Q}$ and $E\left[v_i v_j{}^T\right] = \overline{\mathbf{Q}}_{ij}$. Thus,

$$\mathbf{R} = \begin{bmatrix} \left(H_1\Gamma_1\mathbf{Q}\Gamma_1{}^T H_1{}^T + \overline{\mathbf{Q}}_{11}\right) & \cdots & \left(H_1\Gamma_1\mathbf{Q}\Gamma_N{}^T H_N{}^T + \overline{\mathbf{Q}}_{1N}\right) \\ \vdots & \ddots & \vdots \\ \left(H_N\Gamma_N\mathbf{Q}\Gamma_1{}^T H_1{}^T + \overline{\mathbf{Q}}_{N1}\right) & \cdots & \left(H_N\Gamma_N\mathbf{Q}\Gamma_N{}^T H_N{}^T + \overline{\mathbf{Q}}_{NN}\right) \end{bmatrix} \tag{5.39}$$

Approximate federated filter estimates that use the information present in the time-correlated measurements can now be formulated.

**State Propagation**

Having formulated the global measurement difference, the global time propagation step will be considered. Following Bryson and Ho [1975] for the single sensor case, the standard Kalman filter time update equation can be adjoined as follows

$$\begin{bmatrix} x_1 \\ \vdots \\ x_N \end{bmatrix}_{k+1} = \begin{bmatrix} \Phi_{11} & \cdots & 0 \\ \vdots & \ddots & \vdots \\ 0 & \cdots & \Phi_{NN} \end{bmatrix} \begin{bmatrix} x_1 \\ \vdots \\ x_N \end{bmatrix}_k + \begin{bmatrix} \Gamma_1 \\ \vdots \\ \Gamma_N \end{bmatrix} w + \mathbf{D} \left\{ \begin{bmatrix} \zeta_1 \\ \vdots \\ \zeta_N \end{bmatrix} - \begin{bmatrix} H_1^* & \cdots & 0 \\ \vdots & \ddots & \vdots \\ 0 & \cdots & H_N^* \end{bmatrix} \begin{bmatrix} x_1 \\ \vdots \\ x_N \end{bmatrix} - \begin{bmatrix} \varepsilon_1 \\ \vdots \\ \varepsilon_N \end{bmatrix} \right\} \tag{5.40}$$

where all that has been done is to add zero to equation (5.8) in the form of equation (5.28) times some unknown matrix multiplier, **D**. Rearranging terms yields

$$\begin{bmatrix} x_1 \\ \vdots \\ x_N \end{bmatrix}_{k+1} = \left\{ \begin{bmatrix} \Phi_{11} & \cdots & 0 \\ \vdots & \ddots & \vdots \\ 0 & \cdots & \Phi_{NN} \end{bmatrix} - \mathbf{D} \begin{bmatrix} H_1^* & \cdots & 0 \\ \vdots & \ddots & \vdots \\ 0 & \cdots & H_N^* \end{bmatrix} \right\} \begin{bmatrix} x_1 \\ \vdots \\ x_N \end{bmatrix}_k + \mathbf{D} \begin{bmatrix} \zeta_1 \\ \vdots \\ \zeta_N \end{bmatrix}_k + \left\{ \begin{bmatrix} \Gamma_1 \\ \vdots \\ \Gamma_N \end{bmatrix} w - \mathbf{D} \begin{bmatrix} \varepsilon_1 \\ \vdots \\ \varepsilon_N \end{bmatrix} \right\} \tag{5.41}$$

The noise term in this equation is defined as

$$w' = \begin{bmatrix} \Gamma_1 \\ \vdots \\ \Gamma_N \end{bmatrix} w - \mathbf{D} \begin{bmatrix} \varepsilon_1 \\ \vdots \\ \varepsilon_N \end{bmatrix} \tag{5.42}$$

It is desired that the term $w'$ be additive white noise with zero correlation to the measurement noises, $\varepsilon_i$, so this term is considered separately.

$w'$ is correlated to the measurement noise $\begin{bmatrix} \varepsilon_1 \\ \vdots \\ \varepsilon_N \end{bmatrix}$ according to

$$E\left\{\left(\begin{bmatrix}\Gamma_1\\ \vdots\\ \Gamma_N\end{bmatrix}w-\mathbf{D}\begin{bmatrix}\varepsilon_1\\ \vdots\\ \varepsilon_N\end{bmatrix}\right)(\varepsilon_i)^T\right\}=\begin{bmatrix}\Gamma_1\\ \vdots\\ \Gamma_N\end{bmatrix}[\mathbf{C}_1\ \cdots\ \mathbf{C}_N]-\begin{bmatrix}\mathbf{D}_{11} & \cdots & \mathbf{D}_{1N}\\ \vdots & \ddots & \vdots\\ \mathbf{D}_{N1} & \cdots & \mathbf{D}_{NN}\end{bmatrix}\begin{bmatrix}\mathbf{R}_{11} & \cdots & \mathbf{R}_{NN}\\ \vdots & \ddots & \vdots\\ \mathbf{R}_{NN} & \cdots & \mathbf{R}_{NN}\end{bmatrix} \tag{5.43}$$

The correlation between global measurement and process error terms will be identically zero if $\mathbf{D}$ is chosen so that the following condition is satisfied:

$$\begin{bmatrix}\Gamma_1\mathbf{C}_1 & \cdots & \Gamma_1\mathbf{C}_N\\ \vdots & \ddots & \vdots\\ \Gamma_N\mathbf{C}_1 & \cdots & \Gamma_N\mathbf{C}_N\end{bmatrix}-\begin{bmatrix}\mathbf{D}_{11} & \cdots & \mathbf{D}_{1N}\\ \vdots & \ddots & \vdots\\ \mathbf{D}_{N1} & \cdots & \mathbf{D}_{NN}\end{bmatrix}\begin{bmatrix}\mathbf{R}_{11} & \cdots & \mathbf{R}_{1N}\\ \vdots & \ddots & \vdots\\ \mathbf{R}_{N1} & \cdots & \mathbf{R}_{NN}\end{bmatrix}=0 \tag{5.44}$$

Therefore,

$$\begin{bmatrix}\mathbf{D}_{11} & \cdots & \mathbf{D}_{1N}\\ \vdots & \ddots & \vdots\\ \mathbf{D}_{N1} & \cdots & \mathbf{D}_{NN}\end{bmatrix}=\begin{bmatrix}\Gamma_1\mathbf{C}_1 & \cdots & \Gamma_1\mathbf{C}_N\\ \vdots & \ddots & \vdots\\ \Gamma_N\mathbf{C}_1 & \cdots & \Gamma_N\mathbf{C}_N\end{bmatrix}\begin{bmatrix}\mathbf{R}_{11} & \cdots & \mathbf{R}_{1N}\\ \vdots & \ddots & \vdots\\ \mathbf{R}_{N1} & \cdots & \mathbf{R}_{NN}\end{bmatrix}^{-1} \tag{5.45}$$

Note that the matrix inversion always exists provided the measurements are noisy. Using this choice for $\mathbf{D}$ as defined in equation (5.45), the time propagation equations for the state estimate have the form

$$\begin{bmatrix} \hat{x}_1 \\ \vdots \\ \hat{x}_N \end{bmatrix}_{k+1} = \left\{ \begin{bmatrix} \Phi_{11} & \cdots & 0 \\ \vdots & \ddots & \vdots \\ 0 & \cdots & \Phi_{NN} \end{bmatrix} - \begin{bmatrix} \mathbf{D}_{11} & \cdots & \mathbf{D}_{1N} \\ \vdots & \ddots & \vdots \\ \mathbf{D}_{N1} & \cdots & \mathbf{D}_{NN} \end{bmatrix} \begin{bmatrix} H_1^* & \cdots & 0 \\ \vdots & \ddots & \vdots \\ 0 & \cdots & H_N^* \end{bmatrix} \right\} \begin{bmatrix} \hat{x}_1 \\ \vdots \\ \hat{x}_N \end{bmatrix}_k + \begin{bmatrix} \mathbf{D}_{11} & \cdots & \mathbf{D}_{1N} \\ \vdots & \ddots & \vdots \\ \mathbf{D}_{N1} & \cdots & \mathbf{D}_{NN} \end{bmatrix} \begin{bmatrix} \zeta_1 \\ \vdots \\ \zeta_N \end{bmatrix}_k \tag{5.46}$$

Note that the Gaussian, zero-mean, white noise terms are not propagated. These terms are just a linear combination of Gaussian, zero-mean, white noise terms with expectation zero. Specifically,

$$\mathrm{E}[w'] = \mathrm{E}\left[G\mathbf{Q}G^T H^T \mathbf{R}^{-1} HGv + G\mathbf{Q}G^T H^T \mathbf{R}^{-1} w\right] = 0 \tag{5.47}$$

The time update equation for the covariance matrix is

$$\begin{bmatrix} \mathbf{P}_{11} & \cdots & \mathbf{P}_{1N} \\ \vdots & \ddots & \vdots \\ \mathbf{P}_{N1} & \cdots & \mathbf{P}_{NN} \end{bmatrix}_{k+1} = \left\{ \begin{bmatrix} \Phi_{11} & \cdots & 0 \\ \vdots & \ddots & \vdots \\ 0 & \cdots & \Phi_{NN} \end{bmatrix} - \begin{bmatrix} \mathbf{D}_{11} & \cdots & \mathbf{D}_{11} \\ \vdots & \ddots & \vdots \\ \mathbf{D}_{11} & \cdots & \mathbf{D}_{NN} \end{bmatrix} \begin{bmatrix} H_1^* & \cdots & 0 \\ \vdots & \ddots & \vdots \\ 0 & \cdots & H_N^* \end{bmatrix} \right\} \begin{bmatrix} \mathbf{P}_{11} & \cdots & \mathbf{P}_{1N} \\ \vdots & \ddots & \vdots \\ \mathbf{P}_{N1} & \cdots & \mathbf{P}_{NN} \end{bmatrix}_k$$

$$\left\{ \begin{bmatrix} \Phi_{11} & \cdots & 0 \\ \vdots & \ddots & \vdots \\ 0 & \cdots & \Phi_{NN} \end{bmatrix} - \begin{bmatrix} \mathbf{D}_{11} & \cdots & \mathbf{D}_{1N} \\ \vdots & \ddots & \vdots \\ \mathbf{D}_{N1} & \cdots & \mathbf{D}_{NN} \end{bmatrix} \begin{bmatrix} H_1^* & \cdots & 0 \\ \vdots & \ddots & \vdots \\ 0 & \cdots & H_N^* \end{bmatrix} \right\}^T$$

$$+ \begin{bmatrix} \mathbf{D}_{11} & \cdots & \mathbf{D}_{1N} \\ \vdots & \ddots & \vdots \\ \mathbf{D}_{N1} & \cdots & \mathbf{D}_{NN} \end{bmatrix} \begin{bmatrix} \mathbf{R}_{11} & \cdots & \mathbf{R}_{1N} \\ \vdots & \ddots & \vdots \\ \mathbf{R}_{N1} & \cdots & \mathbf{R}_{NN} \end{bmatrix} \left\{ \begin{bmatrix} \mathbf{D}_{11} & \cdots & \mathbf{D}_{1N} \\ \vdots & \ddots & \vdots \\ \mathbf{D}_{N1} & \cdots & \mathbf{D}_{NN} \end{bmatrix} \right\}^T$$

$$+ \begin{bmatrix} \Gamma_1 \\ \vdots \\ \Gamma_N \end{bmatrix} \mathbf{Q} \begin{bmatrix} \Gamma_1^T & \cdots & \Gamma_N^T \end{bmatrix} \tag{5.48}$$

At this point there is no clear way to partition the computations into local filters and recombine the estimates using equations (5.1-5.2). The portions of the global propagation equations that do not partition cleanly are those terms due to the off-diagonal block terms of the **Q**, **D** and **P** matrices. The procedure followed will be to find suitable bounds or approximations to treat each of these in turn. For the covariance matrix **Q**, first the last term is rewritten as (following Carlson [1988])

$$\begin{bmatrix} \Gamma_1 \\ \vdots \\ \Gamma_N \end{bmatrix} \mathbf{Q} \begin{bmatrix} \Gamma_1^T & \cdots & \Gamma_N^T \end{bmatrix} = \begin{bmatrix} \Gamma_1 & \cdots & 0 \\ \vdots & \ddots & \vdots \\ 0 & \cdots & \Gamma_N \end{bmatrix} \begin{bmatrix} \mathbf{Q} & \cdots & \mathbf{Q} \\ \vdots & \ddots & \vdots \\ \mathbf{Q} & \cdots & \mathbf{Q} \end{bmatrix} \begin{bmatrix} \Gamma_1^T & \cdots & 0 \\ \vdots & \ddots & \vdots \\ 0 & \cdots & \Gamma_N^T \end{bmatrix} \tag{5.49}$$

Then the upper bounding is applied as in Section 5.3:

$$\begin{bmatrix} \mathbf{Q} & \cdots & \mathbf{Q} \\ \vdots & \ddots & \vdots \\ \mathbf{Q} & \cdots & \mathbf{Q} \end{bmatrix} \leq \begin{bmatrix} \gamma_i \mathbf{Q} & \cdots & 0 \\ \vdots & \ddots & \vdots \\ 0 & \cdots & \gamma_i \mathbf{Q} \end{bmatrix} \tag{5.50}$$

where the scalar quantities $\gamma_i$ have the same properties as before (*i.e.*, $0 \leq \frac{1}{\gamma_i} \leq 1$ for all $i$ and $\sum_{i=1}^{N} \frac{1}{\gamma_i} = 1$). This has the effect that each partition conservatively adds process noise in the time update step (since all of the block matrices are positive semi-definite).

**Block Diagonal Approximation of the State Propagation**

The **D** matrix proves to be the most problematic aspect of this formulation, since it cannot be directly partitioned into a block diagonal matrix. Therefore, a block diagonal approximation of **D** will be formed so that the global update and propagation equations can be partitioned. This is accomplished by employing the upper bounding procedure used for the **Q** matrix above.

Recall that **D** was defined above as

$$\begin{bmatrix} \mathbf{D}_{11} & \cdots & \mathbf{D}_{1N} \\ \vdots & \ddots & \vdots \\ \mathbf{D}_{N1} & \cdots & \mathbf{D}_{NN} \end{bmatrix} = \begin{bmatrix} \Gamma_1\mathbf{C}_1 & \cdots & \Gamma_1\mathbf{C}_N \\ \vdots & \ddots & \vdots \\ \Gamma_N\mathbf{C}_1 & \cdots & \Gamma_N\mathbf{C}_N \end{bmatrix} \begin{bmatrix} \mathbf{R}_{11} & \cdots & \mathbf{R}_{1N} \\ \vdots & \ddots & \vdots \\ \mathbf{R}_{N1} & \cdots & \mathbf{R}_{NN} \end{bmatrix}^{-1} \tag{5.51}$$

Block diagonal approximations for each of the two terms will be considered. First **R**

$$\mathbf{R} = \begin{bmatrix} \left(H_1\Gamma_1\mathbf{Q}\Gamma_1{}^T H_1{}^T + \overline{\mathbf{Q}}_{11}\right) & \cdots & \left(H_1\Gamma_1\mathbf{Q}\Gamma_N{}^T H_N{}^T + \overline{\mathbf{Q}}_{1N}\right) \\ \vdots & \ddots & \vdots \\ \left(H_N\Gamma_N\mathbf{Q}\Gamma_1{}^T H_1{}^T + \overline{\mathbf{Q}}_{N1}\right) & \cdots & \left(H_N\Gamma_N\mathbf{Q}\Gamma_N{}^T H_N{}^T + \overline{\mathbf{Q}}_{NN}\right) \end{bmatrix} \tag{5.52}$$

Since the inverse of **R** appears in the propagation equations (through the definition of the **D** matrix), a lower bound on **R** that is block diagonal is required. A lower bound on **R** will give an upper bound on its inverse, thereby conservatively adding process noise at each propagation step. A straightforward lower bound on **R** is given by

$$\mathbf{R} \geq \begin{bmatrix} \overline{\mathbf{Q}}_{11} & \cdots & 0 \\ \vdots & \ddots & \vdots \\ 0 & \cdots & \overline{\mathbf{Q}}_{NN} \end{bmatrix} \tag{5.53}$$

Thus if **R** is approximated by its lower bound given in equation (5.55), the information content of each measurement will be estimated conservatively. For the case of the JAWSAT attitude determination system, little is lost in this approximation since the process noise (represented by the gyro measurement errors) is small compared to the sensor measurement noise.

Next, consider the $\Gamma\mathbf{C}$ terms

$$\begin{bmatrix} \Gamma_1\mathbf{C}_1 & \cdots & \Gamma_1\mathbf{C}_N \\ \vdots & \ddots & \vdots \\ \Gamma_N\mathbf{C}_1 & \cdots & \Gamma_N\mathbf{C}_N \end{bmatrix} = \begin{bmatrix} \Gamma_1\mathbf{Q}\Gamma_1{}^T H_1{}^T & \cdots & \Gamma_1\mathbf{Q}\Gamma_N{}^T H_N{}^T \\ \vdots & \ddots & \vdots \\ \Gamma_N\mathbf{Q}\Gamma_1{}^T H_1{}^T & \cdots & \Gamma_N\mathbf{Q}\Gamma_N{}^T H_N{}^T \end{bmatrix}$$

$$= \begin{bmatrix} \Gamma_1 & \cdots & 0 \\ \vdots & \ddots & \vdots \\ 0 & \cdots & \Gamma_N \end{bmatrix} \begin{bmatrix} \mathbf{Q} & \cdots & \mathbf{Q} \\ \vdots & \ddots & \vdots \\ \mathbf{Q} & \cdots & \mathbf{Q} \end{bmatrix} \begin{bmatrix} \Gamma_1{}^T & \cdots & 0 \\ \vdots & \ddots & \vdots \\ 0 & \cdots & \Gamma_N{}^T \end{bmatrix} \begin{bmatrix} H_1{}^T & \cdots & 0 \\ \vdots & \ddots & \vdots \\ 0 & \cdots & H_N{}^T \end{bmatrix}$$

(5.54)

The upper bound theorem is applied to this equation to give

$$\begin{bmatrix} \Gamma_1\mathbf{C}_1 & \cdots & \Gamma_1\mathbf{C}_N \\ \vdots & \ddots & \vdots \\ \Gamma_N\mathbf{C}_1 & \cdots & \Gamma_N\mathbf{C}_N \end{bmatrix} \leq \begin{bmatrix} \Gamma_1 & \cdots & 0 \\ \vdots & \ddots & \vdots \\ 0 & \cdots & \Gamma_N \end{bmatrix} \begin{bmatrix} \gamma_1\mathbf{Q} & \cdots & 0 \\ \vdots & \ddots & \vdots \\ 0 & \cdots & \gamma_N\mathbf{Q} \end{bmatrix} \begin{bmatrix} \Gamma_1{}^T & \cdots & 0 \\ \vdots & \ddots & \vdots \\ 0 & \cdots & \Gamma_N{}^T \end{bmatrix} \begin{bmatrix} H_1{}^T & \cdots & 0 \\ \vdots & \ddots & \vdots \\ 0 & \cdots & H_N{}^T \end{bmatrix}$$

(5.55)

In order to partition the results, a suboptimal approximation of the correlation between the global process and measurement noises is desired. The measurement differencing federated filter uses some of the information about the correlated measurements in a conservative way (within the limits of the approximation used). Recall that a standard Kalman Filter or standard Federated Kalman Filter is tacitly suboptimal since the time correlation of the measurements is simply ignored.

To perform partitioning, an approximation for **R** has been assumed to give

$$\mathbf{R} \approx \begin{bmatrix} \overline{\mathbf{Q}}_{11} & \cdots & 0 \\ \vdots & \ddots & \vdots \\ 0 & \cdots & \overline{\mathbf{Q}}_{NN} \end{bmatrix} \tag{5.56}$$

and

$$\begin{bmatrix} \Gamma_1 \mathbf{C}_1 & \cdots & \Gamma_1 \mathbf{C}_N \\ \vdots & \ddots & \vdots \\ \Gamma_N \mathbf{C}_1 & \cdots & \Gamma_N \mathbf{C}_N \end{bmatrix} \approx \begin{bmatrix} \Gamma_1 \gamma_1 \mathbf{Q} \Gamma_1^T H_1^T & \cdots & 0 \\ \vdots & \ddots & \vdots \\ 0 & \cdots & \Gamma_N \gamma_N \mathbf{Q} \Gamma_N^T H_N^T \end{bmatrix} \tag{5.57}$$

Therefore, the approximation for $\mathbf{D}$ is $\mathbf{D}_a$ which is defined as

$$\mathbf{D}_a \equiv \begin{bmatrix} \Gamma_1 \gamma_1 \mathbf{Q} \Gamma_1^T H_1^T & \cdots & 0 \\ \vdots & \ddots & \vdots \\ 0 & \cdots & \Gamma_N \gamma_N \mathbf{Q} \Gamma_N^T H_N^T \end{bmatrix} \begin{bmatrix} \overline{\mathbf{Q}}_{11}^{-1} & \cdots & 0 \\ \vdots & \ddots & \vdots \\ 0 & \cdots & \overline{\mathbf{Q}}_{NN}^{-1} \end{bmatrix} \tag{5.58}$$

The global time propagation equations based on the approximated values for $\mathbf{D}_a$ and $\mathbf{R}$ are now presented

$$\begin{bmatrix} \hat{x}_1 \\ \vdots \\ \hat{x}_N \end{bmatrix}_{k+1} = \left\{ \begin{bmatrix} \Phi_{11} & \cdots & 0 \\ \vdots & \ddots & \vdots \\ 0 & \cdots & \Phi_{NN} \end{bmatrix} - \begin{bmatrix} \mathbf{D}_{a_{11}} & \cdots & 0 \\ \vdots & \ddots & \vdots \\ 0 & \cdots & \mathbf{D}_{a_{NN}} \end{bmatrix} \begin{bmatrix} H_1^* & \cdots & 0 \\ \vdots & \ddots & \vdots \\ 0 & \cdots & H_N^* \end{bmatrix} \right\} \begin{bmatrix} \hat{x}_1 \\ \vdots \\ \hat{x}_N \end{bmatrix}_k + \begin{bmatrix} \mathbf{D}_{a_{11}} & \cdots & 0 \\ \vdots & \ddots & \vdots \\ 0 & \cdots & \mathbf{D}_{a_{NN}} \end{bmatrix} \begin{bmatrix} \zeta_1 \\ \vdots \\ \zeta_N \end{bmatrix}_k \tag{5.59}$$

$$\begin{aligned} \begin{bmatrix} \mathbf{P}_{11} & \cdots & \mathbf{P}_{1N} \\ \vdots & \ddots & \vdots \\ \mathbf{P}_{N1} & \cdots & \mathbf{P}_{NN} \end{bmatrix}_{k+1} &= \left\{ \begin{bmatrix} \Phi_{11} & \cdots & 0 \\ \vdots & \ddots & \vdots \\ 0 & \cdots & \Phi_{NN} \end{bmatrix} - \begin{bmatrix} \mathbf{D}_{a_{11}} & \cdots & 0 \\ \vdots & \ddots & \vdots \\ 0 & \cdots & \mathbf{D}_{a_{NN}} \end{bmatrix} \begin{bmatrix} H_1^* & \cdots & 0 \\ \vdots & \ddots & \vdots \\ 0 & \cdots & H_N^* \end{bmatrix} \right\} \begin{bmatrix} \mathbf{P}_{11} & \cdots & \mathbf{P}_{1N} \\ \vdots & \ddots & \vdots \\ \mathbf{P}_{N1} & \cdots & \mathbf{P}_{NN} \end{bmatrix}_k \\ &\left\{ \begin{bmatrix} \Phi_{11} & \cdots & 0 \\ \vdots & \ddots & \vdots \\ 0 & \cdots & \Phi_{NN} \end{bmatrix} - \begin{bmatrix} \mathbf{D}_{a_{11}} & \cdots & 0 \\ \vdots & \ddots & \vdots \\ 0 & \cdots & \mathbf{D}_{a_{NN}} \end{bmatrix} \begin{bmatrix} H_1^* & \cdots & 0 \\ \vdots & \ddots & \vdots \\ 0 & \cdots & H_N^* \end{bmatrix} \right\}^T \\ &+ \begin{bmatrix} \mathbf{D}_{a_{11}} & \cdots & 0 \\ \vdots & \ddots & \vdots \\ 0 & \cdots & \mathbf{D}_{a_{NN}} \end{bmatrix} \begin{bmatrix} \mathbf{R}_1 & \cdots & 0 \\ \vdots & \ddots & \vdots \\ 0 & \cdots & \mathbf{R}_N \end{bmatrix} \left\{ \begin{bmatrix} \mathbf{D}_{a_{11}} & \cdots & 0 \\ \vdots & \ddots & \vdots \\ 0 & \cdots & \mathbf{D}_{a_{NN}} \end{bmatrix} \right\}^T \\ &+ \begin{bmatrix} \Gamma_1 & \cdots & 0 \\ \vdots & \ddots & \vdots \\ 0 & \cdots & G_N \end{bmatrix} \begin{bmatrix} \gamma_1 Q & \cdots & 0 \\ \vdots & \ddots & \vdots \\ 0 & \cdots & \gamma_N Q \end{bmatrix} \begin{bmatrix} G_1^T & \cdots & 0 \\ \vdots & \ddots & \vdots \\ 0 & \cdots & G_N^T \end{bmatrix} \end{aligned} \tag{5.60}$$

So, to summarize the time update equations for partition *i*:

$$\hat{x}_{i_{k+1}} = \left(\Phi_{ii} - \mathbf{D}_{a_{ii}} H_i^*\right)\hat{x}_{i_k} + \mathbf{D}_{a_{ii}} \zeta_{ik} \tag{5.61}$$

$$\begin{aligned} \mathbf{P}_{ii_{k+1}} = &\left(\Phi_{ii} - \mathbf{D}_{a_{ii}} H_i^*\right)\mathbf{P}_{ii_k}\left(\Phi_{ii} - \mathbf{D}_{a_{ii}} H_i^*\right)^T \\ &-\mathbf{D}_{a_{ii}}\left(H_i^T \Gamma_i \gamma_i \mathbf{Q} \Gamma_i^T H_i^T\right)\mathbf{D}_{a_{ii}}^T + \Gamma_i \gamma_i \mathbf{Q} \Gamma_i^T \end{aligned} \tag{5.62}$$

where

$$H_i^* \equiv H_i \Phi_i - \Psi_i H_i \tag{5.63}$$

$$\mathbf{D}_{a_{ii}} \equiv \Gamma_i \gamma_i \mathbf{Q} \Gamma_i^T H_i^T \left( H_i \Gamma_i \gamma_i \mathbf{Q} \Gamma_i^T H_i^T + \overline{\mathbf{Q}}_{ii} \right)^{-1} \tag{5.64}$$

Note that the choice for the initial covariance relies on the fact that

$$\begin{bmatrix} \mathbf{P} & \cdots & \mathbf{P} \\ \vdots & \ddots & \vdots \\ \mathbf{P} & \cdots & \mathbf{P} \end{bmatrix} \leq \begin{bmatrix} \gamma\mathbf{P} & \cdots & 0 \\ \vdots & \ddots & \vdots \\ 0 & \cdots & \gamma\mathbf{P} \end{bmatrix} \tag{5.65}$$

This is used to initialize the covariance matrices and to decouple the covariance matrix time updates. As pointed out in Carlson [1990], once the covariance matrices are decoupled, no cross coupling can be introduced due to the structure of equation (5.62). All the *a priori* values of the covariance matrix will be the same since no measurement information is used to arrive at the *a priori* state estimate.

Note that information sharing appears in the covariance time update and unshared process noise appears in both the state and covariance time update. Contrast this with the standard (Carlson) formulation where information sharing only occurs in one term of the covariance time update and no unshared process noise appears in the time updates. (Recall that this process noise was introduced as a result of defining **D** so that no cross-correlation between the global differenced process and measurement noises would appear.) Also note that the standard (Carlson)

formulation only requires $\gamma$ to appear linearly in the propagation equations. Here $\gamma$ appears nonlinearly.

**Measurement Update**

In this subsection, the global measurement update for the measurement differencing federated filter is formulated and it is shown that it can be partitioned.

The measurement update will be of the form:

$$\hat{x}^{+} = \hat{x}^{-} + \mathrm{K}\left(\zeta_i - H_i^{*}\hat{x}_i^{-}\right) \tag{5.66}$$

$$\mathbf{P}^{+} = \mathbf{P}^{-} - \mathrm{K}H^{*}\mathbf{P}^{-} \tag{5.67}$$

Expanding K into matrix form yields

$$K_k = \begin{bmatrix} P_{11} & \cdots & P_{1N} \\ \vdots & \ddots & \vdots \\ P_{N1} & \cdots & P_{NN} \end{bmatrix} \begin{bmatrix} H_1^{*} & \cdots & 0 \\ \vdots & \ddots & \vdots \\ 0 & \cdots & H_N^{*} \end{bmatrix} \left\{ \begin{bmatrix} H_1^{*} & \cdots & 0 \\ \vdots & \ddots & \vdots \\ 0 & \cdots & H_N^{*} \end{bmatrix} \begin{bmatrix} P_{11} & \cdots & P_{1N} \\ \vdots & \ddots & \vdots \\ P_{N1} & \cdots & P_{NN} \end{bmatrix} \begin{bmatrix} H_1^{*} & \cdots & 0 \\ \vdots & \ddots & \vdots \\ 0 & \cdots & H_N^{*} \end{bmatrix}^{T} + \begin{bmatrix} \left(H_1\Gamma_1\gamma_1\mathbf{Q}\Gamma_1^{T}H_1^{T} + \overline{\mathbf{Q}}_{11}\right) & \cdots & 0 \\ \vdots & \ddots & \vdots \\ 0 & \cdots & \left(H_N\Gamma_N\gamma_N\mathbf{Q}\Gamma_N^{T}H_N^{T} + \overline{\mathbf{Q}}_{NN}\right) \end{bmatrix} \right\}^{-1} \tag{5.68}$$

where the same conservative approximation for **R** from the propagation step has been used. Note that in overestimating **R**, **K** tends to be underestimated; therefore, the current measurement is slightly devalued.

Finally, keep in mind that the estimate given at time $k$ (in either the master filter or the local filters) is conditioned on the measurement at time $k$+1. To obtain the best estimate of the state at time $k$+1 conditioned on the measurement at time $k$+1, use the prediction equation

$$\hat{x}_{k+1|k+1} = \Phi\hat{x}_{k|k+1} + \mathbf{D}_{a_{ii}}\left(\zeta_i - H^*\hat{x}_{k|k+1}\right) \tag{5.69}$$

Expanding this into matrix form and using the choice for **D** given in equation (5.45) above gives the following result for the partition $i$ measurement update:

$$\hat{x}_{k+1|k+1} = \Phi\hat{x}_{k|k+1} + \mathbf{D}_{a_{ii}}\left(\zeta_i - H^*\hat{x}_{k|k+1}\right) \tag{5.70}$$

Note that unshared process noise appears in the measurement update via the procedure for ensuring the global process and measurement noise have zero cross correlation.

## 5.5 Estimate Fusion for the Quaternion Filter

The nonlinear combination properties of quaternions leads to a nonstandard implementation of the state estimate fusion (given by equation 5.2) for spacecraft attitude determination. The state estimate fusion method presented in this section applies to both the measurement differencing and conventional federated filters.

Recall that the state estimate covariance is defined as the noise covariance of the state estimation errors, *i.e.*,

$$P = \mathrm{E}\left[\Delta\tilde{x}\cdot\Delta\tilde{x}^{T}\right] = \mathrm{E}\left[\begin{bmatrix}\delta q\\ \Delta b\end{bmatrix}\cdot\begin{bmatrix}\delta q\\ \Delta b\end{bmatrix}^{T}\right] \tag{5.71}$$

which is not equivalent to $\mathrm{E}\left[\left(\tilde{x}-\hat{\tilde{x}}\right)\cdot\left(\tilde{x}-\hat{\tilde{x}}\right)^{T}\right]$.

The master filter fused covariance matrix for the JAWSAT attitude estimation scheme is given as

$$P_{M}^{-1} = P_{1}^{-1} + P_{2}^{-1} \tag{5.72}$$

where $P_1$ and $P_2$ are the covariance matrices from local filters 1 and 2.

Since the global covariance matrix describes the errors in the state estimate correction, $\Delta\tilde{x}$, and since this correction is nonlinearly related to the state (due to the quaternion composition relations), the master filter state vector correction is formed as

$$\Delta\tilde{x}_M = P_M\left(P_1^{-1}\Delta\tilde{x}_1 + P_2^{-1}\Delta\tilde{x}_2\right) \tag{5.73}$$

where

$$\Delta\tilde{x}_i = \begin{bmatrix}\delta q_i \\ \Delta b_i\end{bmatrix} \tag{5.74}$$

In this formulation $\delta q_i$ represents the small angle quaternion of dimension three expressing the rotation between the *a priori* master state estimate, $\bar{q}_M^{-}$, and the estimate from local filter number *i*. Using the quaternion composition relations,

$$\delta\bar{q}_i = \hat{\bar{q}}_i \otimes \hat{\bar{q}}_M^{-1} \tag{5.75}$$

Since the line bias terms combine linearly, this gives

$$\Delta b_i = \hat{b}_i - \hat{b}_M \tag{5.76}$$

and the master state correction computed in equation (5.73) is

$$\Delta\tilde{x}_M = \begin{bmatrix} \delta q_M \\ \Delta b_M \end{bmatrix} \tag{5.77}$$

The master fusion estimate of the full state is then computed using

$$\bar{q}_M{}^+ = \delta\bar{q}_M \otimes \hat{\bar{q}}_M{}^- \tag{5.78}$$

and

$$b_M{}^+ = \Delta b_M + \hat{b}_M{}^- \tag{5.79}$$

This estimate fusion method is used for the quaternion filter simulation results that are discussed in the next section.

## 5.6 Simulation Results and Discussion

Simulation results are presented for federated filter algorithms developed in this chapter. The standard federated filter algorithm is compared with the

measurement differencing federated filter using GPS multipath errors from ground tests and RADCAL flight tests. The simulations also use high quality gyros and digital sun sensors in the attitude determination system. Gyro measurements are taken every second, and GPS and sun sensor measurements are taken every 12 seconds. Sun visibility is modeled for a dawn-dusk orbit, so that sun sensor measurements are always available for the integrated filter. The **U-D** factorization method was not used in these simulations since the covariance matrix remains well conditioned due to the regular incorporation of GPS measurements.

**Ground Test Results**

Figures 5.2 and 5.3 compare attitude and bias estimation errors for the centralized and federated Kalman filter algorithms using GPS ground test data.

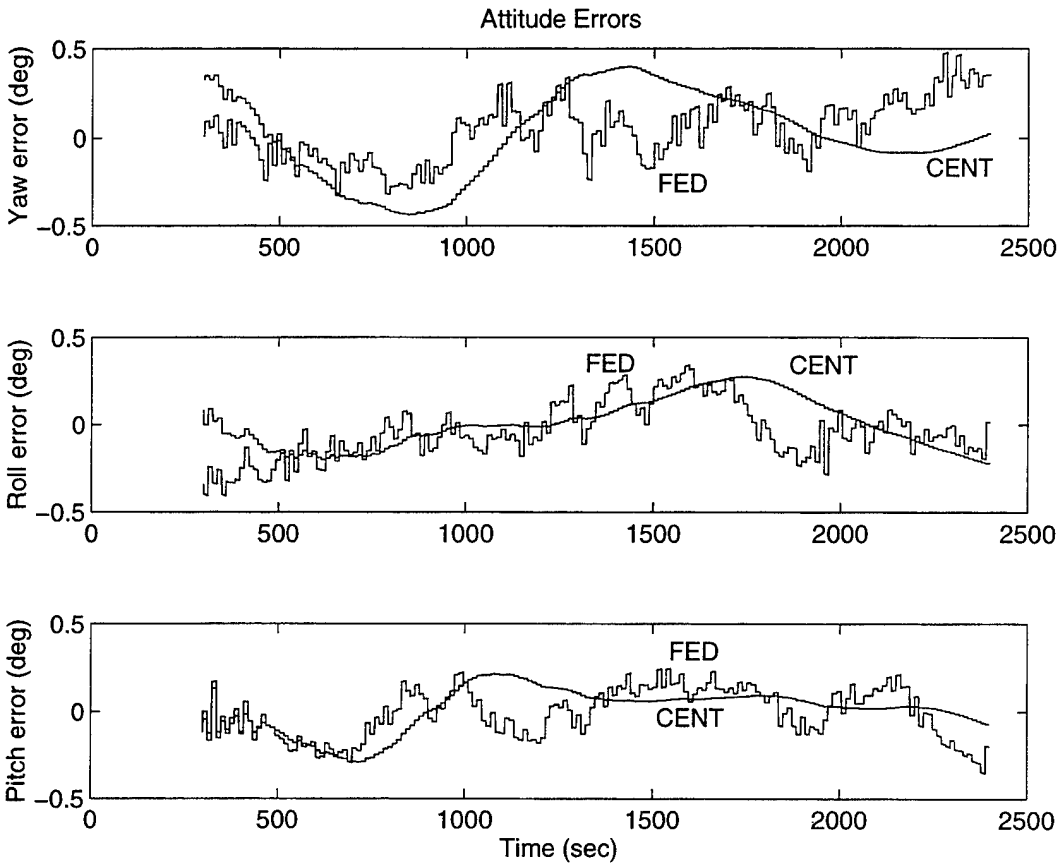


**Fig. 5.2.** Attitude Error Comparison: Centralized and Federated Kalman Filters with Measurement Differencing Using GPS Ground Data.

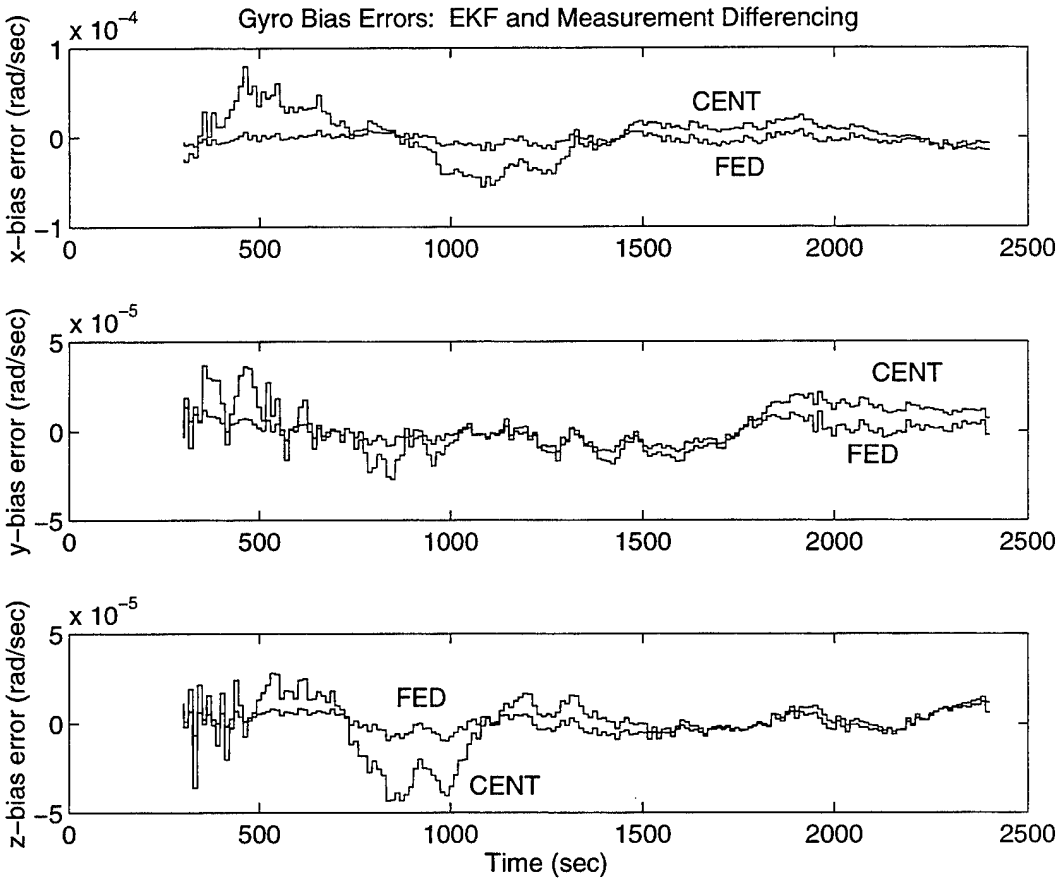


**Fig. 5.3.** Gyro Bias Error Comparison: Centralized and Federated Kalman Filters with Measurement Differencing Using GPS Ground Data.

Note that the measurement differencing algorithms for both the centralized and federated Kalman filters perform very similarly overall. The fact that no significant differences in accuracy exists for the two algorithms indicates that the approximations necessary to accommodate measurement differencing in the federated filter have no appreciable effect on filter accuracy. An evaluation of the fault tolerance and failure detection capabilities of the various federated filter implementations is a topic for future research.

## RADCAL Results

Figures 5.4 and 5.5 compare attitude and bias estimation errors for the centralized and federated Kalman filter algorithms using GPS data from RADCAL.

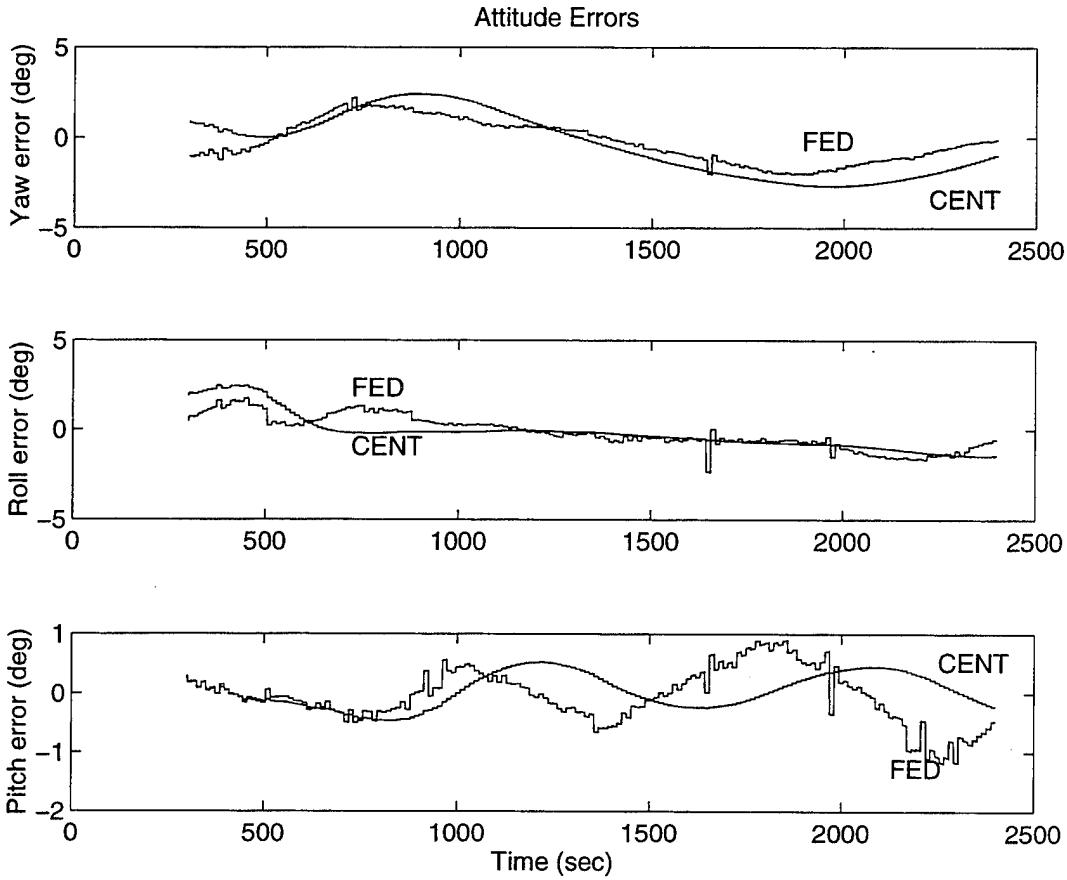


**Fig. 5.4.** Attitude Error Comparison: Centralized and Federated Kalman Filters with Measurement Differencing Using GPS Data from RADCAL.

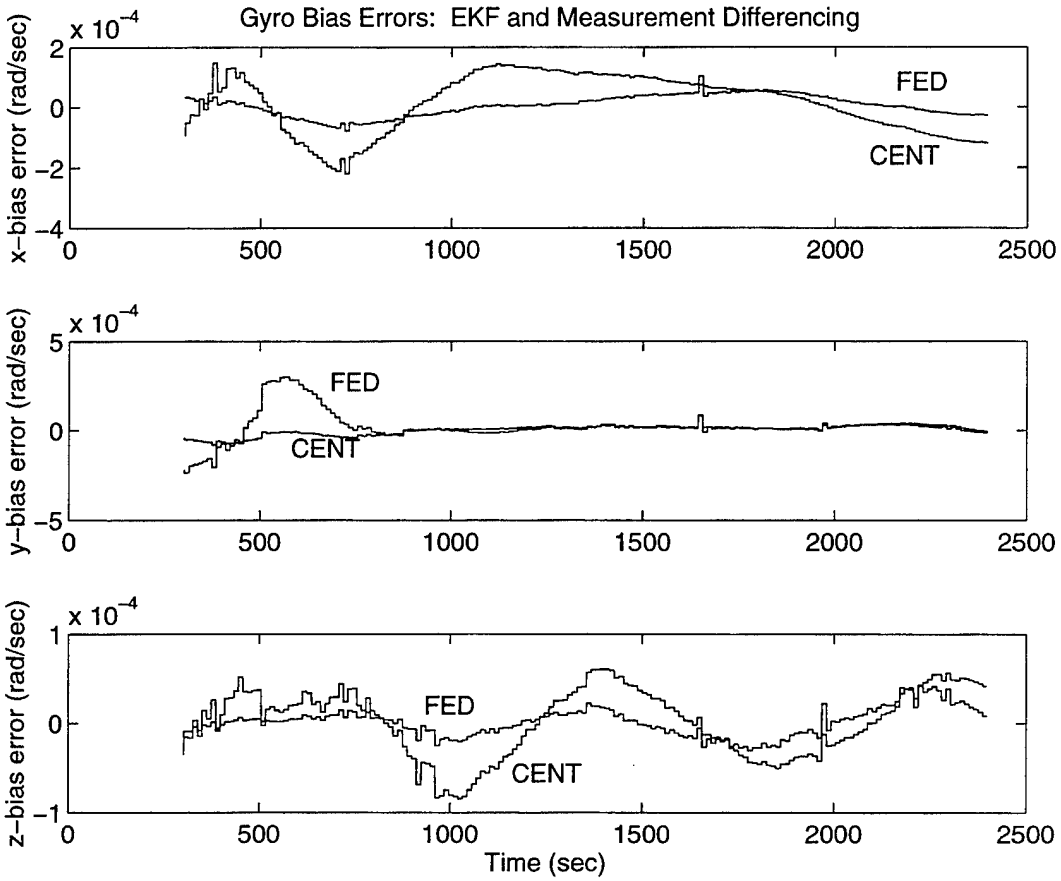


**Fig. 5.5.** Gyro Bias Error Comparison: Centralized and Federated Kalman Filters with Measurement Differencing Using GPS Data from RADCAL.

Note that the attitude errors in the centralized filter lag the federated filter errors for both the RADCAL and ground test data. The federated filter formulation introduces conservatively large process noise which causes it to de-weight the propagated estimate and follow the measurements more closely. Although the dynamics of the two estimation processes differ, the effects on the attitude control system are expected to be minor. Controller bandwidths are typically in the range of 0.1 - 0.001 Hz, and the bandwidth differences in the estimation algorithms are not large compared with the controller bandwidth.

Results from the federated filter consistently appear more jumpy than the centralized filter. This occurs because each GPS attitude measurement is included in two pseudomeasurement updates. This makes the federated filter more sensitive to outliers in the measurement data, since an erroneous data point will be incorporated in twice. The existence of outliers in the GPS measurement data suggests a non-Gaussian error distribution. These non-Gaussian errors will be considered further in the nonlinear filter discussed in Chapter 6.

## 5.7 Summary and Conclusion

An algorithm for federated Kalman filtering in the presence of time-correlated multipath errors has been developed in this chapter. The new algorithm employs measurement differencing to reduce the effects of multipath errors and uses conservative approximations of the process noise to allow the global state information to be partitioned into distinct local filters. An estimate fusion method for combining the local filter quaternion estimates to form the global estimate was also presented. Simulation results indicate that the federated filter with measurement differencing performs comparably to a centralized filter with measurement differencing, validating the conservative assumptions used in the derivation of the algorithm. Investigation of federated filter modes to enhance fault tolerance and failure detection is identified as a topic for future research.

*Chapter 6:*

# *NONLINEAR FILTERING OF GPS AND GYRO MEASUREMENTS*

Preliminary analysis of an alternative filtering technique based on a nonlinear gain function is presented in this chapter. The chapter begins with a summary of the Kalman filtering equations for a linear system subject to non-white measurement errors, such as multipath. Simulation results are presented for a spacecraft attitude estimation algorithm using a nonlinear Kalman gain function based on heuristics. The results of this simulation indicate that a nonlinear filtering technique is a promising area for future research.

## 6.1 Nonlinear Filtering of Spacecraft Attitude

Integrated measurements from GPS and gyros can be used for attitude determination on small satellites in a number of ways. For example, as an alternative to the measurement differencing approach for mitigating multipath errors, nonlinear filtering methods may yield promising results.

A nonlinear filtering approach for integrating GPS and FOG measurements begins with the same basic estimation strategy used throughout this dissertation.

That is, gyros measurements would be used to perform the time propagation of the state estimates with GPS measurements used to update the estimates. However, the non-Gaussian measurement errors due to GPS multipath would be accounted for using nonlinear estimation techniques. The particular nonlinear state estimation techniques for this case would be based on linear state equations with non-Gaussian measurement noise (represented by the GPS error covariance). Nonlinear state estimation for this case was first addressed by Masreliez [1975].

The gist of the filtering approach is to compute a statistically correct nonlinear gain function for the non-Gaussian measurement noise. The linear system equations are given by

$$\begin{aligned} x_{k+1} &= \Phi_k x_k + w_k \\ z_k &= H_k x_k + v_k \end{aligned} \tag{6.1}$$

where $w$ is Gaussian with covariance $Q$ and $v$ is non-Gaussian. The minimum variance estimate can be computed recursively using the score function [Masreliez, 1975]

$$\hat{x}_k^{+} = \hat{x}_k^{-} + P_k^{-} H_k^T g(z_k) \tag{6.2}$$

$$P_k^{+} = P_k^{-} - P_k^{-} H_k^T G(z_k) H_k P_k^{-T} \tag{6.3}$$

$$P_{k+1}^{-} = \Phi P_k^{+} \Phi^T + Q \tag{6.4}$$

where $g(\cdot)$ is the score function and $G(\cdot)$ is the derivative of the score function defined as

$$g(z_k) = -\left[\frac{\partial f(z_k|Z^{k-1})}{\partial(z_k)}\right]\left[f(z_k|Z^{k-1})\right]^{-1} \tag{6.5}$$

$$G(z_k) = \frac{\partial\{g(z_k)\}}{\partial(z_k)} \tag{6.6}$$

where $f$ is the moment generating function for the observation sequence and $Z^{k-1}$ is the set of observations $(z_1, z_2, \cdots, z_{k-1})$.

The score function approach has the intuitively appealing characteristic that it de-emphasizes large measurement residuals if the noise distribution is long tailed and tends to emphasize large residuals if the distribution is short tailed [Wu and Kundu, 1992]. Note that the score function reduces to the linear gain equations of the Kalman filter if $v$ is Gaussian. For a proof, see Wu and Kundu [1992] and Masreliez [1975].

The evaluation of the score function requires computation of the convolution of $f(H_k x_k|Z^{k-1})$ with $f(v_k)$ [Wu and Kundu, 1989]. Numerical convolution can itself be difficult to implement, and this problem is compounded when the moment

generating functions are unknown. Three basic approaches have been used to address this problem. The first approach uses a series expansion to approximate the score function [Wu, 1994; Wu and Kundu, 1989]. The second approach uses influence curves that have a desired functional form based on the expected noise characteristics [Hewer *et al.*, 1987]. In other words, the influence function is chosen to emphasize or de-emphasize measurement residuals that arise from the non-Gaussian measurement errors. The third approach attempts to approximate the non-Gaussian observation noise as a finite sum of Gaussian noises [Hilands and Thomopoulos, 1994]. The Gaussian sum approach proves to be computationally intensive, even for off-line analysis. The score function approximation method and the influence function method have been applied successfully to the case of radar glint, a phenomenon that leads to correlated measurement errors [Wu, 1994; Hewer *et al.*, 1987].

## 6.2 Simulation Results and Discussion

Applying the score function method and the influence function method to an integrated GPS and gyro attitude determination system could lead to alternative multipath mitigation methods. The fact that the GPS attitude errors are non-Gaussian suggests that multipath errors may be reduced using a nonlinear Kalman gain function. Preliminary numerical investigations using a nonlinear gain function

based on heuristics rather than evaluation of the score function have yielded promising results. The gain function used was based on the functional form of the "Huber psi" influence curve [see Hewer *et al.*, 1987], although other forms of the gain function could be evaluated. The form of the nonlinear gain function used in this preliminary analysis is shown in Fig. 6.1. Note that this gain function tends to de-weight large measurement residuals due to multipath errors.

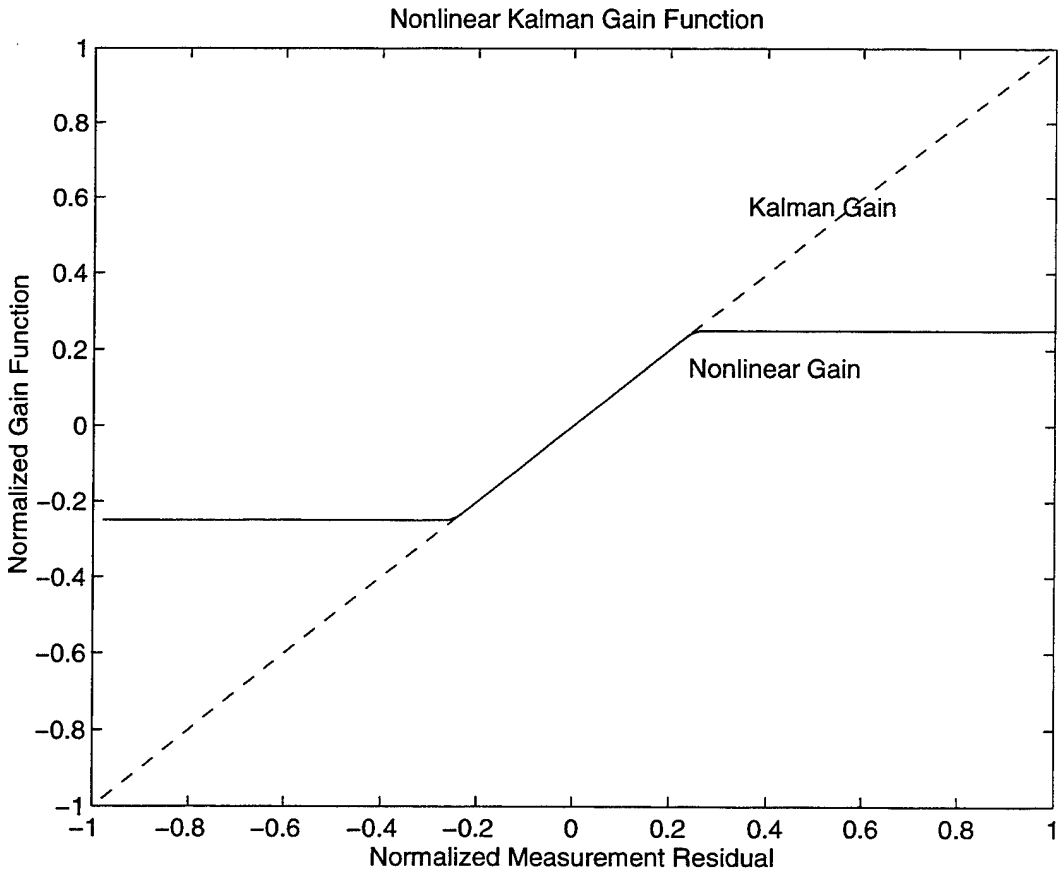


**Fig. 6.1.** Nonlinear Kalman Gain. *Figure shows a comparison of the linear Kalman gain function (dashed line) and the nonlinear gain function (solid line).*

A sample of attitude estimation errors using the nonlinear gain function is shown in Fig. 6.2, using RADCAL GPS data and high quality gyros (simulation two,

Table 3.1). The point where the nonlinear gain breaks from the Kalman gain was chosen heuristically, and no attempt has been made to characterize the best nonlinear gain function analytically. The fact that the nonlinear approach appears to outperform the measurement differencing approach in the case shown in Fig. 6.2 indicates that this may be a fruitful area of future study. The accuracy of the line bias estimates using the nonlinear and measurement differencing filters is compared in Fig. 6.3. Note that the two methods give gyro bias results that are indistinguishable for all practical purposes.

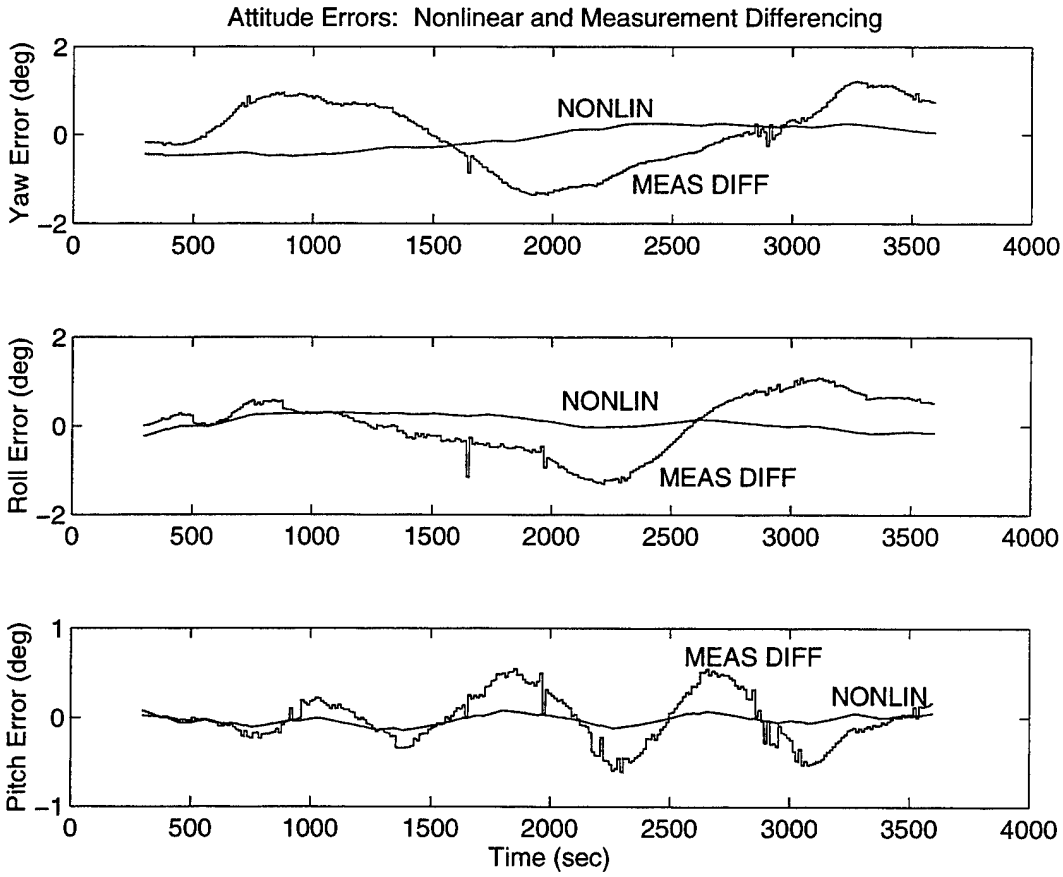


**Fig. 6.2.** Attitude Error Comparison for Nonlinear Filter. *Plots show attitude estimation errors for measurement differencing and nonlinear filter algorithms. GPS data from RADCAL is used with simulated inertial quality gyros.*

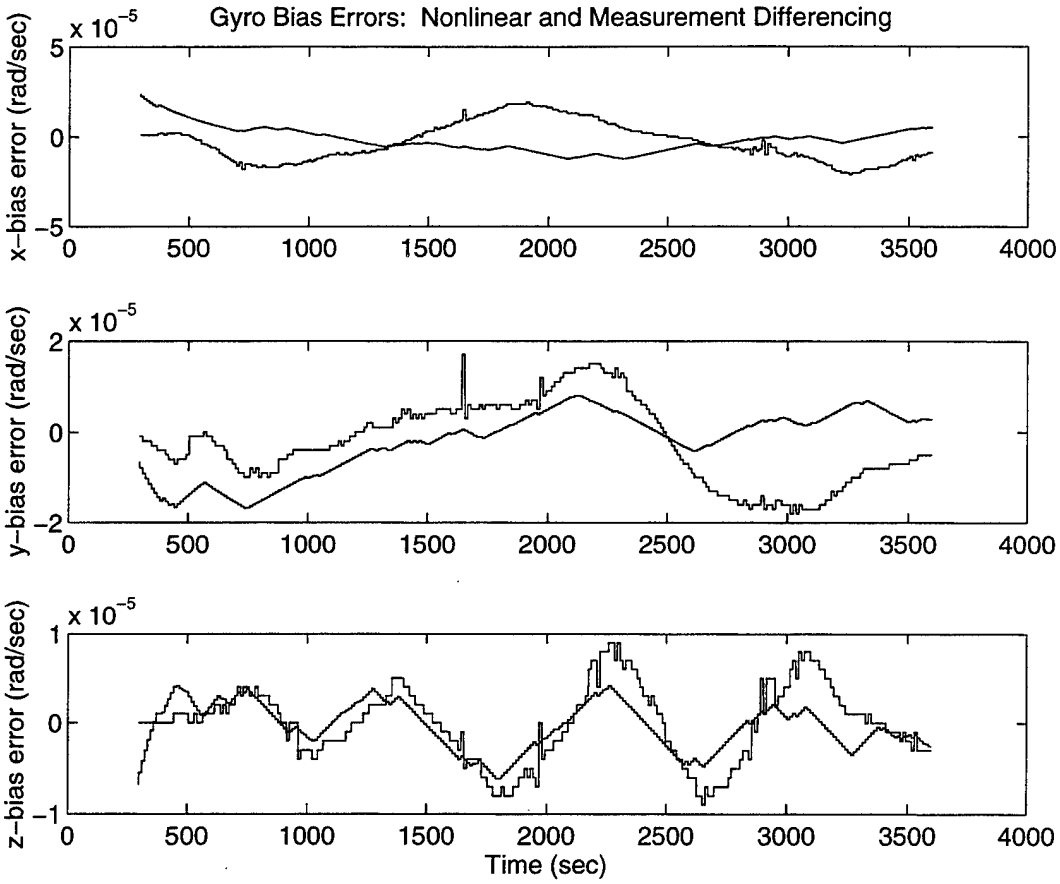


**Fig. 6.3.** Gyro Bias Error Comparison for Nonlinear Filter. *Plots show bias estimation errors for measurement differencing and nonlinear filter algorithms. GPS data from RADCAL is used with simulated inertial quality gyros.*

Table 6.1 compares the computed 1-$\sigma$ attitude errors for the nonlinear and measurement differencing algorithms. Note that the nonlinear filter algorithm produces error standard deviations at least a factor of two better than the measurement differencing approach.

**Table 6.1.** Computed error statistics for Nonlinear Kalman Filter and Measurement Differencing Kalman Filter Algorithms using GPS RADCAL Data.

| | YAW<br>std error | ROLL<br>std error | PITCH<br>std error |
|---|---|---|---|
| NONLINEAR FILTER | 0.29 deg | 0.18 deg | 0.06 deg |
| MEAS. DIFFERENCING | 0.73 deg | 0.61 deg | 0.26 deg |

The measurement differencing method accounts for the time correlated multipath errors as a first-order Markov process. This approach more closely models multipath errors than the nonlinear method which does not include a time constant in the measurement model. Inclusion of a simple dynamic model for multipath in the nonlinear filter could further improve estimation accuracy. A detailed analysis of the nonlinear filtering approach, including an analytical characterization of the non-Gaussian nature of the time-correlated measurements, is an interesting topic for future study that could lead to further advances in multipath mitigation for integrated GPS attitude determination systems.

## 6.3 Summary and Conclusions

Preliminary analysis of an attitude estimation algorithm for combining GPS and gyros using a nonlinear gain function was presented in this chapter. This analysis suggests that errors can be reduced by a factor of two over the measurement

differencing algorithm. I plan to pursue the development of these nonlinear methods for reducing GPS multipath errors in integrated attitude determination systems in my future research.

*Chapter 7:*

# *FUTURE WORK AND SUMMARY*

Applications and extensions of the integrated GPS attitude determination methods developed in this dissertation are considered in this chapter. The applications where combined use of GPS and gyros could lead to performance improvements over stand-alone systems include dynamic mode identification for large space structures and modeling of additional error states.

The chapter is organized as follows. First, two levels of integration for GPS and gyro measurements, loosely and tightly coupled, are presented. Second, applications where the state vector is augmented in a tightly coupled configuration are discussed as promising methods to characterize dynamic structural modes or GPS error states such as line biases. Third, future work for JAWSAT is discussed. Finally, the research contributions of this dissertation are summarized.

## 7.1 Levels of Sensor Integration

There are two main design approaches for integrating gyroscope angular velocity measurements with GPS, a loosely coupled and a tightly coupled configuration. Some integrated applications may require raw GPS differential phase

*Chapter 7:*

# *FUTURE WORK AND SUMMARY*

Applications and extensions of the integrated GPS attitude determination methods developed in this dissertation are considered in this chapter. The applications where combined use of GPS and gyros could lead to performance improvements over stand-alone systems include dynamic mode identification for large space structures and modeling of additional error states.

The chapter is organized as follows. First, two levels of integration for GPS and gyro measurements, loosely and tightly coupled, are presented. Second, applications where the state vector is augmented in a tightly coupled configuration are discussed as promising methods to characterize dynamic structural modes or GPS error states such as line biases. Third, future work for JAWSAT is discussed. Finally, the research contributions of this dissertation are summarized.

## 7.1 Levels of Sensor Integration

There are two main design approaches for integrating gyroscope angular velocity measurements with GPS, a loosely coupled and a tightly coupled configuration. Some integrated applications may require raw GPS differential phase

measurements rather than processed attitude solutions. The loosely coupled approach uses computed GPS attitude point solutions combined with gyro measurements. The advantage of the loosely coupled formulation is that existing receiver hardware and software can be used without modification or additional cost. The loosely coupled configuration is depicted in Fig. 7.1. Note that the JAWSAT attitude estimation system will be configured in this loosely coupled mode consistent with a low cost design philosophy.

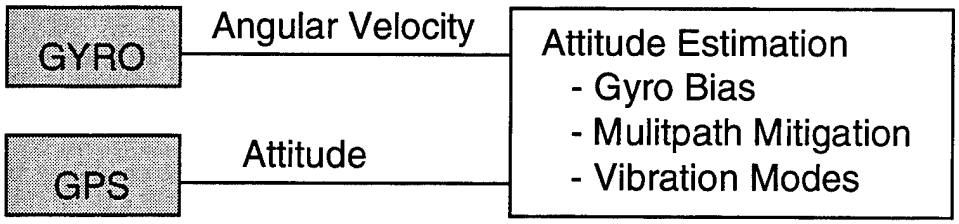


**Fig. 7.1.** Loosely Coupled Attitude Estimation Algorithm.

The tightly coupled formulation requires GPS differential phase measurements to be incorporated with gyro measurements as shown in Fig. 7.2. Observability of certain states may be improved due to the relative abundance of differential phase measurements in the tightly coupled formulation. This improved observability may outweigh the additional complexity in hardware and software required to implement this approach for certain applications. Assessing the performance of the loosely coupled and tightly coupled algorithms for the application areas discussed below is an open area for future research.

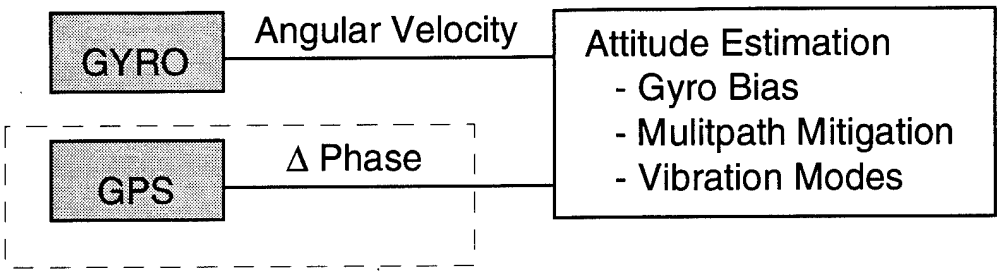


**Fig. 7.2.** Tightly Coupled Estimation Algorithm.

## 7.2 Augmenting the State Vector

In addition to spacecraft attitude, it may be possible to estimate several other key quantities using GPS and gyro measurements. Three examples are presented that previously have been addressed using only GPS differential phase measurements. The addition of gyro measurements could enhance and extend these existing methods. The additional applications include system identification for flexible space structures, estimation of GPS antenna baselines, and calibration of GPS hardware biases.

**Large Space Structure System Identification**

Although structural flexure is typically a negligible problem for small, low-cost spacecraft, large space structures may be able to exploit the combination of GPS and gyro measurements for system identification. The combination of precision gyros and a multi-antenna GPS attitude determination receiver is planned for NASA's Space Station Alpha [Saunders and Barton, 1995].

Because of its large size and the difficulty of characterizing vibration modes in the presence of gravity prior to launch, on-orbit characterization of the Space Station structure may be required [Saunders and Barton, 1995, p. 635]. The differential measurements over relatively long baselines inherent in a GPS attitude system make it attractive for characterizing structural vibration in addition to attitude. Combining gyro and GPS measurements may be ideally suited to sensing changes in the length and orientation of the antenna baselines due to structural vibration.

In the absence of gyro measurements, GPS carrier phase interferometry has already been proposed for structural mode identification. Teague and Parkinson [1993] describe a system identification experiment for a vibrating beam using a GPS pseudolite. Their preliminary results showed very close agreement between predicted behavior and measured response using what they call "self-differential

GPS." These promising results could be extended to include the gyroscope measurements available on Space Station to characterize the vibrations of the structural members on which the GPS antennas are located.

Two previous studies aimed at integrating GPS and gyro measurements for attitude and antenna baseline estimation have been reported. Sullivan [1995, 1994] has described a combined GPS/INS system that integrates GPS differential phase measurements and gyroscope angular velocity measurements in an Euler angle attitude formulation. Litton Guidance and Control Systems, a leading manufacturer of fiber optic gyros, has proposed a similar configuration using a single GPS antenna baseline in an azimuth alignment system using GPS and FOGs [Tazartes *et al.*, 1995]. Neither of these studies has explicitly considered structural modes as states to be estimated. These studies, combined with the attitude estimation algorithms presented in Chapters 3 and 5, could be extended to large structures such as Space Station based on the method outlined by Teague and Parkinson [1993].

The accurate angular velocity measurements available directly from the gyros may allow structural vibration to be distinguished from rigid body attitude dynamics. Multipath errors, on the other hand, may be indistinguishable from slow vibration modes. Developing and testing algorithms to estimate structural modes in addition to attitude has the potential to advance the development of integrated INS/GPS attitude determination systems.

## GPS Error State Modeling

*Antenna Baseline Estimation*

One of the key factors affecting performance of a GPS attitude determination system is accurate knowledge of the antenna baselines. A baseline error of only 1 cm over a baseline length of 1 m can lead to attitude errors on the order of 0.5 deg. For terrestrial applications, a static baseline self-survey lasting over eight hours is performed [Trimble, 1994]. Such a survey is generally not possible for a fully integrated spacecraft. A critical step in spacecraft attitude determination has been the development of algorithms to compute and refine antenna baseline estimates on orbit [Ward and Axelrad, 1995; Axelrad and Ward, 1994].

Note that neither the static self-survey nor the on-orbit baseline estimation algorithm allows simultaneous attitude and baseline estimates to be computed due to a lack of observability. Cohen and Parkinson [1992] presented an algorithm for estimating aircraft attitude and wing flexure constrained to a single axis together in real time. The addition of gyro measurements allows full three-dimensional antenna baseline estimates to be considered along with attitude as reported by Sullivan [1994].

*Line Bias Calibration*

Using gyro measurements in an integrated line bias estimation algorithm may improve our ability to isolate line bias variations from other effects, such as errors due to baseline flexure. The variations in the bias values may be better tracked over time and possibly correlated with environmental effects such as magnetic field changes or thermal variations. The possibility that line biases might change over time due to environmental effects is an important facet of GPS attitude determination that has not yet received adequate attention. The inclusion of gyro measurements in a line bias estimation scheme could lead to a more comprehensive method for modeling and predicting changes in the line bias parameters, particularly in the harsh tehrmal and electromagnetic environment environment experienced in spacecraft applications.

*Cross-Correlation of GPS Attitude Solutions*

Since the attitude point solution computed by the Vector receiver represents a composite of the multipath-contaminated phase measurements at each antenna, the GPS attitude output does not report three statistically independent quantities. Further characterization of the error correlation present in the GPS attitude receiver output could provide an extension of the nonlinear estimation methods discussed in the previous subsection. In other words, if the time varying off-diagonal terms in the measurement error covariance matrix can be computed, then the cross-correlation information can be used by the integrated attitude filter with GPS and gyro measurements.

An analytical formulation of the cross-correlation could be carried out by tracing the effect of errors in the differential phase measurements through the GPS attitude solution equations. This analytical formulation could then be compared with experimentally determined cross-correlations for validation. These cross-covariance terms could then be used in integrated algorithms to improve the fidelity of filtered attitude solutions.

## 7.3 Future Work for JAWSAT

As design, fabrication and testing of JAWSAT subsystems continues, several important issues are being addressed for the attitude determination system. The final design and fabrication of the sun sensors has not been completed, and the gyro hardware has not been selected. Once this hardware configuration is finalized, system integration and flight software need to be addressed.

Currently, electromagnetic interference testing is underway at the NASA Lewis Research Center to characterize the effects of the PPTs on other critical systems including the GPS attitude receiver. The results of these tests have important implications for spacecraft operations as discussed in Section 3.7. Namely, the extent to which the GPS receiver and other on-board systems will be hindered by the PPTs will determine many of the operational constraints of the

spacecraft. These constraints will be used to finalize the mission profile, the orbit maneuvering experiments, and consequently the flight software for many of the on-board systems.

Several open issues also remain in the software architecture for the real-time, on-board implementation of the Vector receiver. These issues include definition of input/output data, finite word length, computer speed and operating system, and failure modes.

## 7.4 Summary of Research Contributions

An integrated GPS attitude determination system has been developed to meet JAWSAT operational requirements. In addition, this dissertation focused on attitude estimation algorithms to improve the accuracy and redundancy of an integrated system composed of a GPS attitude receiver, FOGs, and digital sun sensors.

Estimation algorithms using GPS and gyros were developed using a measurement differencing approach to reduce the effects of multipath errors in the attitude solution. Measurement differencing accounts for time-correlated measurement errors by modeling them as a first-order Markov process with a known

time constant. Applying this measurement differencing technique to GPS multipath errors reduces attitude estimation errors from standard Kalman filtering approaches.

A decentralized attitude estimation algorithm based on the federated filter was used in a framework that enhances redundancy and fault tolerance. The global state estimate update process was extended to account for the nonlinear combination of quaternions components, and a measurement differencing approach was derived to account for time-correlated multipath errors in the GPS attitude receiver. Simulation results show that the federated filter with measurement differencing reduces multipath errors in the integrated attitude determination system.

Sun sensor measurements were combined with gyro measurements using a dead zone algorithm. This algorithm was developed to overcome filter errors introduced by the large quantization errors in the digital sun sensor. The dead zone algorithm allows the attitude determination system to meet JAWSAT mission requirements during extended intervals when GPS measurements are not available.

Finally, preliminary results of a nonlinear filtering method to reduce multipath errors were also introduced. This method used a nonlinear gain function to de-emphasize the influence multipath errors that result in large measurement residuals. Further characterization of the statistical distribution of GPS attitude errors, and the evaluation of the associated nonlinear gain function, is identified as a potentially

fruitful area of future research in the development of improved attitude estimation methods.

## 7.5 Conclusion

This dissertation focused on the integration of GPS measurements into an attitude determination system for small satellites. The use of GPS in combination with other sensors has been identified as a fruitful area for achieving improved performance at a lower cost and weight [NRC, 1994]. Algorithms have been developed for combining measurements from a GPS attitude receiver with other sensors that improve the accuracy of attitude estimates in the presence of multipath. The developments presented in this dissertation advance the state of the art in combined attitude determination systems for small satellites using GPS and other sensors.

## *REFERENCES*


Albertine, J.R. "An Azimuth Determination System Utilizing the Navy Navigation Satellites," *Navigation,* Vol. 21, No. 1, Spring 1974, pp. 54-60.

Arditty, H.J. and Lefèvre, H.C. "Sagnac Effect in Fiber Gyroscopes," *Optics Letters*, Vol. 6, No. 8, August 1981, pp. 401-403.

Axelrad, P., and Chelsey, B.C. "Performance Testing of a GPS Based Attitude Determination System," AIAA-93-3787, *Proceedings of the AIAA Guidance, Navigation, and Control Conference*, Monterey, California, August 9-11, 1993, pp. 809-819.

Axelrad, P., Chesley, B.C., and Ward, L.M. "GPS Based Spacecraft Attitude Determination," Final Report for October 1992 - September 1993 to the Naval Research Laboratory, Colorado Center for Astrodynamics Research, Boulder, Colorado, September, 1993.

Axelrad, P., Comp, C.J., and MacDoran, P.F. "Use of Signal-to-Noise Ratio for Multipath Error Correction in GPS Differential Phase Measurements: Methodology and Experimental Results," *Proceedings of the ION GPS-94 Conference*, Salt Lake City, Utah, September 20-23, 1994, pp. 655-666. Also in *IEEE Transactions on Aerospace Electronic Systems* (to appear).

Axelrad, P. and Ward, L.M. "On-Orbit GPS Based Attitude and Antenna Baseline Estimation," *Proceedings of the ION National Technical Meeting*, San Diego, California, January 24-26, 1994, pp. 441-450.

Bailey, Mark A. and Sims, Craig S. "Decentralized Reduced-Order Filters," *IEEE Transactions on Aerospace and Electronic Systems*, Vol. AES-26, No. 2, March 1990, pp. 254-262.

Bar-Itzhack, I.Y. and Idan, M. "Recursive Attitude Determination form Vector Observations: Euler Angle Estimation," *Journal of Guidance, Control and Dynamics,* Vol. 10, No. 2, March-April 1987, pp. 152-157.

Bar-Itzhack, I.Y. and Oshman, Y. "Attitude Determination from Vector Observations: Quaternion Estimation," *IEEE Transactions on Aerospace and Electronic Systems,* Vol. 35, No. 1, January 1985, pp. 128-135.

Bar-Itzhack, I.Y. and Reiner, J. "Recursive Attitude Determination form Vector Observations: Direction Cosine Matrix Identification," *Journal of Guidance, Control and Dynamics,* Vol. 7, No. 1, January-February 1984, pp. 51-56.

Bass, C.A., Karmokolias, C. and Khatri, A. "Attitude Error Estimation with a General GPS Observation Matrix," ION 48th Annual Meeting, Washington, DC, 29 June - 1 July 1992.

Battin, Richard H. *An Introduction to the Mathematics and Methods of Astrodynamics*. American Institute of Aeronautics and Astronautics, Inc., New York, 1987.

Bauer, F.H., Lightsey, E.G., McCullough, J., O'Donnell, J., and Schnurr, R. "Pre-Flight Testing of the SPARTAN GADACS Experiment," *Proceedings of the ION GPS-94 Conference*, Salt Lake City, Utah, September 20-23, 1994, pp. 1233-1241.

Belaforte, G., Bona, B., and Cerone, V. "Identification, Structure Selection and Validation of Uncertain Models with Set-Membership Error Description," *Mathematics and Computers in Simulation,* Vol. 32, No. 5&6, December 1990, pp. 561-569.

Berg, T.M. and Durrant-White, H.F. "On Distributed and Decentralized Estimation," *Proceedings of the 1992 Automatic Control Conference*, Chicago, Illinois, June 24-26, 1992, pp. 3304-3305.

Bierman, Gerald J. and Thornton, Catherine L. "Numerical Comparison of Kalman Filter Algorithms: Orbit Determination Case Study," *Automatica*, Vol. 13, No. 1, January 1977, pp. 23-35.

Bierman, G.J. and Belzer, M.R. "A Decentralized Square Root Information Filter/Smoother," *Proceedings of the 24th IEEE Conference on Decision and Control*, Ft. Lauderdale, Florida, December 1985.

Blanco, Joe and Geen, John "Micromachined Inertial Sensor Development at Northrop," *Proceedings of the ION 49th Annual Meeting,* Cambridge, Massachusetts, June 21-23, 1993, pp. 577-585.

Broatch, S.A. and Henley, A.J. "An Integrated Navigation System Manager Using Federated Kalman Filtering," *Proceedings of the IEEE NAECON '92*, Dayton, Ohio, May 1992, pp. 422-426.

Brown, R.A. "Instantaneous GPS Attitude Determination," *Proceedings of the IEEE Position Location and Navigation Symposium*, Monterey, California, March 1992, pp. 113-120.

Brown, R.G. and Hwang, P.Y.C. *Introduction to Random Signals and Applied Kalman Filtering*, 2nd ed., Wiley and Sons, New York, 1992.

Brown, R.A. and Ward, P. "A GPS Receiver with Built-in Precision Pointing Capability," *Proceedings of the IEEE Position Location and Navigation Symposium*, Las Vegas, Nevada, March 1990, pp. 83-93.

Bryson, A.E. and Henrickson, L.J. "Estimation Using Sampled Data Containing Sequentially Correlated Noise," *Journal of Spacecraft and Rockets*, Vol. 5, No. 6, June 1968, pp. 662-665.

Bryson, Arthur E. and Ho, Yu-Chi *Applied Optimal Control.* Hemisphere Publishing, New York, 1975.

Carlson, Neal A. "Federated Filter for Fault-Tolerant Integrated Navigation Systems," *Proceedings of the IEEE Position Location and Navigation Symposium*, Orlando, Florida, November 1988, pp. 110-119.

Carlson, Neal A. "Federated Square Root Filter for Decentralized Parallel Processes," *IEEE Transactions on Aerospace and Electronic Systems*, Vol. AES-26, No. 3, May 1990, pp. 517-525.

Carlson, Neal A. and Berarducci, Michael P. "Federated Kalman Filter Simulation Results," *Navigation*, Vol. 41., No. 3, pp. 297-321. Also in *Proceedings of the Institute of Navigation 49th Annual Meeting*, Cambridge, Massachusetts, June 1993, pp. 421-435.

Carpenter, J. Russell and Bishop, Robert H. "Target State Estimation for Suboptimal Rendezvous Navigation via Fusion of Inertial and Rendezvous Filter Estimates," AAS-95-214, AAS/AIAA Spaceflight Mechanics Meeting, Albuquerque, New Mexico, February 13-16, 1995.

Carpenter, J. Russell and Bishop, Robert H. "General Methods of Estimate Fusion Applied to Spacecraft Rendezvous," AIAA-94-3548-CP, *Proceedings of the AIAA Guidance, Navigation, and Control Conference*, Scottsdale, Arizona, August 1-3, 1994, pp. 71-81.

Carpenter, J. Russell and Bishop, Robert H. "Estimate Fusion for Lunar Rendezvous," AIAA-93-3700-CP, *Proceedings of the AIAA Guidance, Navigation, and Control Conference*, Monterey, California, August 9-11, 1993, pp. 1-10.

Castañon, D.A. and Teneketzis, D. "Distributed Estimation Algorithms for Nonlinear Systems," *IEEE Transacations on Automatic Control*, Vol. AC-30, No. 5, May 1985, pp. 418-425.

Cayley, Arthur "On the Motion of Rotation of a Solid Body," *Cambridge Mathematical Journal,* Vol. III, No. XVII, February 1843, pp. 224-232.

Cerone, V. "Feasible Parameter Set for Linear Models with Bounded Errors in All Variables," *Automatica*, Vol. 29, No. 6, 1993, pp. 1551-1555.

Chang, Tsi-Shuan, "Comments on 'Computation and Transmission Requirements for a Decentralized Linear-Quadratic-Gaussian Control,'" *IEEE Transacations on Automatic Control*, Vol. AC-25, No. 3, June 1980, pp. 609-610.

Chesley, B.C. and Axelrad P. "Mitigating Measurement Errors in a Low Cost Satellite Attitude Determination System," *Proceedings of the 1995 ION National Technical Meeting,* Anaheim, California, January 18-20, 1995, pp. 763-774.

Cohen, C.E. *Attitude Determination Using GPS*, Ph.D. Dissertation, Stanford University, December 1992.

Cohen, C.E., Cobb, H.S., and Parkinson, B.W. "Generalizing Wahba's Problem for High Output Rates and Evaluation of Static Accuracy Using a Theodolite," *Proceedings of the ION GPS-'92 Conference*, Albuquerque, New Mexico, Sept. 16-18, 1992.

Cohen, C.E. and Parkinson, B.W. "Aircraft Applications of a GPS-Based Attitude Determination," *Proceedings of the ION GPS-'92 Conference*, Albuquerque, New Mexico, Sept. 16-18, 1992.

Cohen, C.E. and Parkinson, B.W. "Mitigating Multipath in GPS-Based Attitude Determination," *Advances in the Astronautical Sciences,* AAS Guidance and Control Conference, Keystone, Colorado, Vol. 74, Univelt, San Diego, 1991.

Combettes, Patrick L. "The Foundations of Set Theoretic Estimation," *Proceedings of the IEEE*, Vol. 81, No. 2, February 1993, pp. 182-208.

Curry, Renwick E. *Estimation and Control with Quantized Measurements,* M.I.T. Press, Cambridge, Massachusetts, 1970.

Evans, R.J., Zhang, C., and Soh, Y.C. "Bounded-Error Estimation Using Dead Zone and Bounding Ellipsoid," *International Journal of Adaptive Control and Signal Processing*, Vol. 8, No. 1, January 1994, pp. 31-42.

Farrell, J.L. "Attitude Determination by Kalman Filtering," *Automatica*, Vol. 6, No. 3, May 1970, pp. 419-430.

Farrenkopf, R.L. "Analytic Steady-State Accuracy for Two Common Spacecraft Attitude Estimators, *Journal of Guidance, Conrol, and Dynamics*, Vol. 1, No. 4, July-August 1978, pp. 282-284.

Felter, Stephen C. "A Covariance Analysis Technique for the Federated Kalman Filter," *Proceedings of the IEEE NAECON '92*, Dayton, Ohio, May 1992, pp. 399-406.

Fisher, H.L., Shuster, M.D., and Strikwerda, T.E. "Attitude Determination for the Star Tracker Mission," *Advances in the Astronautical Sciences*, Vol. 71, Part I, Astrodynamics 1989, Paper No. AAS 89-365, pp. 139-150.

Fogel, Eli and Huang, Y.F. "On the Value of Information in System Identification—Bounded Noise Case," *Automatica*, Vol. 18, No. 2, 1982, pp. 229-238.

Gao, Y. Krakiwsky, E.J., and Abousalem, M.A. "Comparison and Analysis of Centralized, Decentralized, and Federated Filters," *Navigation*, Vol. 40, No. 1, Spring 1993, pp. 69-86.

Gao, Y., Krakiwsky, E.J., and McLellan, J.F. "Experience with the Application of Federated Filter Design to Kinematic GPS Positioning," *Proceedings of the IEEE Position Location and Navigation Symposium*, 1992, pp. 314-320.

Gelb, Arthur (ed.) *Applied Optimal Estimation.* MIT Press, Cambridge, Massachusetts, 1974.

Georgiadou, Y. and Kleusberg, A. "On Carrier Signal Multipath Effects in Relative GPS Positioning," *Manuscripta Geodaetica,* Vol. 13, No. 1, 1988, pp. 1-8.

Gold, K., Born, G., Irish, K., Reichart, A., Markin, R., Binning, P., Axelrad, P., Mitchell, S., Frazier, W., Bertiger, W., and Hajj, G. "Precision Orbit Determination in the Geosat Orbit," *Proceedings of the 1995 ION National Technical Meeting,* Anaheim, California, January 18-20, 1995, pp. 579-591.

Gomez, S., Carpenter, J., and Semar, C. "GPS Attitude Determination Performance Evaluation Using Ground Test Data," *Proceedings of the 1995 ION National Technical Meeting,* Anaheim, California, January 18-20, 1995, pp. 793-802.

Gray, Robert M. "Quantization Noise Spectra," *IEEE Transactions on Information Theory,* Vol. 36, No. 6, November, 1990, pp. 1220-1244.

Hansen, V.W., Summers, R.A., and Clapp, W.G., "Eyes in the Sky—Building Satellites for Education," SPIE Vol. 1495, *Small Satellite Technology and Applications 1991*, pp. 115-122.

Hashemipour, H.R., Roy, S., and Laub, A.J. "Decentralized Structures for Parallel Kalman Filtering," *IEEE Transacations on Automatic Control*, Vol. AC-33, No. 1, January 1988, pp. 88-94.

Hewer, G.A., Martin, R.D., and Zeh, J.E. "Robust Preprocessing for Kalman Filtering of Glint Noise," *IEEE Transactions on Aerospace and Electronic Systems*, Vol. AES-23, No. 1, January 1987, pp. 120-128.

Hilands, Thomas W. and Thomopoulos, Stelios C.A. "High-Order Filters for Estimation in Non-Gaussian Noise," *Information Sciences*, Vol. 80 (1994), pp. 149-179.

Hong, Lang "Distributed Filtering Using Set Model for Systems with Non-Gaussian Noise," *Approximate Kalman Filtering*, Guanrong Chen (editor), World Scientific Publishing, 1993, pp. 161-176.

Kaminski, P.G., Bryson, A.E., and Schmidt, S.F. "Discrete Square Root Filtering: A Survey of Current Techniques," *IEEE Transactions on Automatic Control*, Vol. AC-16, December 1971, pp. 727-735.

Kerr, Thomas "Decentralized Filtering and Redundancy Management for Multisensor Navigation," *IEEE Transactions on Aerospace and Electronic Systems*, Vol. AES-23, No. 1, January 1987, pp. 83-119.

Kudva, P. and Throckmorton, A. "Attitude Determination Studies for EOS-AM1," AIAA-94-3561-CP, *Proceedings of the AIAA Guidance, Navigation, and Control Conference*, Scottsdale, Arizona, August 1-3, 1994, pp. 188-196.

LASP, "Student Nitric Oxide Explorer: Investigation and Technical Plan—Abridged," Laboratory for Atmospheric and Space Physics, University of Colorado (C.A. Barth, Principal Investigator), 1994.

Lawrence, Paul J. and Berarducci, Michael P. "Comparison of Federated and Centralized Kalman Filters with Fault Detection Considerations," *Proceedings of the IEEE Position Location and Navigation Symposium*, Las Vegas, Nevada, April 11-15, 1994, pp. 703-710.

Lefèvre, H.C. *The Fiber Optic Gyroscope.* Artech House, Boston, Mass., 1993.

Lefèvre, H.C., Bergh, R.A., and Shaw, H.J. "An Overview of Fiber-Optic Gyroscopes," *Journal of Lightwave Technology*, Vol. LT-2, No. 2, April 1984, pp. 91-107.

Lefferts, E.J., Markley, F.L., and Shuster, M.D. "Kalman Filtering for Spacecraft Attitude Estimation," *Journal of Guidance, Control and Dynamics,* Vol. 5, No. 5, September-October 1982, pp. 417-429.

Lightsey, E.G, Cohen, C.E., and Parkinson, B.W. "Application of GPS Attitude Determination to Gravity Gradient Stabilized Spacecraft," AIAA-93-3788-CP,

*Proceedings of the AIAA Guidance, Navigation, and Control Conference*, Monterey, California, August 9-11, 1993, pp. 820-826.

Lightsey, E.G., Cohen, C.E., Feess, W.A., and Parkinson, B.W. "Analysis of Spacecraft Attitude Measurements Using Onboard GPS," AAS Guidance and Control Conference, Keystone, Colorado, Februrary, 1994.

Litton Systems, Inc. "Technical Description of the LN-200 Family," Guidance and Control Systems Division, Document No. 20896C, Woodland Hills, California, September, 1994.

Lu, Gang *Development of a GPS Multi-Antenna System for Attitude Determination*, Ph.D. Dissertation, University of Calgary, December 1994.

Lu G., Cannon, M.E., Lachapelle, G. and Kielland, P. "Attitude Determination in a Survey Launch Using Multi-Antenna GPS Technologies," *Proceedings of the ION National Technical Meeting*, San Francisco, California, 20-22 January 1993.

Maher, Robert C. "On the Nature of Granulation Noise in Uniform Quantization Systems," *Journal of the Audio Engineering Society,* Vol. 40, No. 1/2, January/February 1992, pp. 12-20.

Mark, J., Tazartes, D., Fidric, B., and Cordova, A. "A Rate Integrating Fiber Optic Gyro," *Navigation*, Vol. 38, No. 4, Winter 1991-92, pp. 341-353.

Markley, F. Landis "Attitude Determination and Parameter Estimation Using Vector Observations: Theory," *Journal of the Astronautical Sciences,* Vol. 37, No. 1, January-March, 1989, pp. 41-58.

Markley, F. Landis "Attitude Determination and Parameter Estimation Using Vector Observations: Application," *Journal of the Astronautical Sciences,* Vol. 39, No. 3, July-September, 1991, pp. 367-381.

Markley, F. Landis "Attitude Determination Using Vector Observations and the Singular Value Decomposition," *Journal of the Astronautical Sciences,* Vol. 36, No. 3, July-September, 1988, pp. 245-258.

Markley, F.L. "Attitude Determination Using Vector Observations: A Fast Optimal Matrix Algorithm," *Journal of the Astronautical Sciences,* Vol. 41, No. 2, April-June 1993, pp. 261-280.

Markley, F.L., Berman, N., and Shaked, U. "$H_\infty$-Type Filter for Spacecraft Attitude Estimation," *Advances in the Astronautical Sciences*, Vol. 84, Part I, Spaceflight Dynamics 1993, Paper No. 93-298, pp. 697-711.

Maseeh, F. "Inexpensive Miniature Gyroscope for Intelligent Control Systems," *Proceedings of the ION 49th Annual Meeting,* Cambridge, Massachusetts, June 21-23, 1993, pp. 617-621.

Masreliez, C.J. "Approximate Non-Gaussian Filtering with Linear State and Observation Relations," *IEEE Transactions on Automatic Control*, Vol. AC-20, No. 2, February 1975, pp. 107-110.

Mathews, A. "Utilization of Fiber Optic Gyros in Inertial Measurement Units," *Navigation*, Vol. 37, No. 1, Spring 1990, pp. 17-38.

Maybeck, Peter S. *Stochastic Models, Estimation, and Control, Vol. I and II.* Academic Press, Orlando, Florida, 1979, 1982.

Moorman, Martin J. and Bullock, Thomas E. "A Federated Kalman Filter with Appliction to Passive Target Tracking," *Proceedings of the IEEE NAECON '93*, Dayton, Ohio, May 1993, pp. 399-405.

NRC. *Technology for Small Spacecraft.* Panel on Small Spacecraft Technology, Aeronautics and Space Engineering Board, National Research Council, National Academy Press, Washington, D.C., 1994.

Nuttall, J. "Optical-fibre Gyroscopes," *Electronics World and Wireless World*, July 1990, pp. 608-611.

Oppenheim, Alan V. and Schafer, Ronald W. *Discrete-Time Signal Processing,* Prentice Hall, Englewood Cliffs, New Jersey, 1989.

Page, Jerry and Sugarbaker, Daniel "Central Inertial Guidance Test Facility (CIGTF) Testing of a Depolarized Fiber Optic Gyro Inertial Sensor Assembly," *Proceedings of the 1995 ION National Technical Meeting,* Anaheim, California, January 18-20, 1995, pp. 651-656.

Pandit, S.M. and Zhang, W. "Modeling Random Gyro Drift Rate by Data Dependent Systems," *IEEE Transactions on Aerospace Electronic Systems*, Vol. AES-22, No. 4, July 1986, pp. 455-459.

Pao, Lucy Y. "Distributed Multisensor Fusion," AIAA-94-3549-CP, *Proceedings of the AIAA Guidance, Navigation, and Control Conference*, Scottsdale, Arizona, August 1-3, 1994, pp. 82-91.

Post, E.J. "Sagnac Effect," *Reviews of Modern Physics*, Vol. 39, April 1967, pp. 475-493.

Rao, A.K. and Huang, Y.F. "Analysis of Finite Precision Effects on a Recursive Set Membership Parameter Estimation Algorithm," *IEEE Transactions on Signal Processing*, Vol. 40, No. 12, December 1992, pp. 3081-3085.

Rath, J. and Ward, P. "Attitude Estimation Using GPS," *Proceedings of the ION National Technical Meeting*, San Mateo, California, January 1989.

Reeves, Emery I. U.S. Air Force Academy, Department of Astronautics. Personal communication, 1994.

Roy, S. and Iltes, R.A. "Decentralized Linear Estimation in Correlated Measurement Noise," *IEEE Transactions on Aerospace and Electronic Systems*, Vol. AES-27, No. 6, November, 1991, pp. 939-941.

Satz, H.S., Cox, D.B., Beard, R.L. and Landis, G.P. "GPS Inertial Attitude Estimation via Carrier Accumulated-Phase Measurements," *Navigation,* Vol. 38, No. 3, Fall 1991, pp. 273-285.

Saunders, Penny and Barton, Gregory "GPS on the International Space Station Alpha," *Proceedings of the 1995 ION National Technical Meeting,* Anaheim, California, January 18-20, 1995, pp. 631-639.

Schwarz, K.P., El-Mowafy, A., and Wei, M. "Testing a GPS Attitude System in Kinematic Mode," *Proceedings of the ION GPS-'92 Conference*, Albuquerque, New Mexico, September 16-18, 1992.

Schweppe, Fred C. "Recursive Estimation: Unknown but Bounded Errors and System Inputs," *IEEE Transactions on Automatic Control*, Vol. 13, No. 1, February 1968, pp. 22-28.

Schweppe, Fred C. *Uncertain Dynamic Systems.* Prentice Hall, Englewood Cliffs, New Jersey, 1973.

Sedlak, J. and Chu, D. "Kalman Filter Estimation of Attitude and Gyro Bias with the QUEST Observation Model," *Advances in the Astronautical Sciences*, Vol. 84, Part I, Spaceflight Dynamics 1993, Paper No. 93-297, pp. 683-696.

Shuster, M.D. "A Survey of Attitude Representations," *Journal of the Astronautical Sciences*, Vol. 41, No. 4, October-December 1993, pp. 439-518.

Shuster, M.D. "Kalman Filtering of Spacecraft Attitude and the QUEST Model," *Journal of the Astronautical Sciences,* Vol. 38, No. 3, July-September 1990, pp. 377-393.

Shuster, M.D. "Maximum Likelihood Estimation of Spacecraft Attitude," *Journal of the Astronautical Sciences,* Vol. 37, No. 1, January-March 1989, pp. 79-88.

Shuster, M.D. and Natanson, G.A. "Quaternion Computation from a Geometric Point of View," *Journal of the Astronautical Sciences*, Vol. 41, No. 4, October-December 1993, pp. 545-556.

Shuster, M.D. and Oh, S.D. "Three-Axis Attitude Determination from Vector Observations," *Journal of Guidance and Control,* Vol. 4, No. 1, January-February 1981, pp. 70-77.

Shuster, Malcolm D. "A Simple Kalman Filter and Smoother for Spacecraft Attitude," *Journal of the Astronautical Sciences,* Vol. 37, No. 1, January-March, 1989, pp. 89-106.

Shuster, Malcolm D. "A Comment on Fast Three-Axis Attitude Determination," *Journal of the Astronautical Sciences,* Vol. 31, No. 4, October-December 1983, pp. 579-584.

Siouris, G.M. *Aerospace Avionics Systems: A Modern Synthesis,* Academic Press, San Diego, 1993.

Sitomer, J., Connelly, J., and Martin, J. "Silicon Micromachined IMU Integrated Electronics Development," *Proceedings of the ION 49th Annual Meeting,* Cambridge, Massachusetts, June 21-23, 1993, pp. 623-628.

Sorensen, J.A., Schmidt, S.F., and Goka, T. "Application of Square Root Filtering for Spacecraft Attitude Contol," *Journal of Guidance, Control and Dynamics*, Vol. 2, No. 5, September-October 1979, pp. 426-433.

Smith, Jay L. and Liefer, Randall "Exploring Space with a Microsat...Where No Microsat has Gone Before," *SPIE Small-Satellite Technology and Applications III* (1993), Vol. 1940, pp. 12-18.

Speyer, Jason L. "Computation and Transmission Requirements for a Decentralized Linear-Quadratic-Gaussian Control Problem," *IEEE Transactions on Automatic Control*, Vol. AC-24, No. 2, April 1979, pp. 266-269.

Sullivan, W.I. "Performance Analysis of an Integrated GPS/Inertial Attitude Determination System," *Proceedings of the 1995 ION National Technical Meeting,* Anaheim, California, January 18-20, 1995, pp. 783-791.

Sullivan, W.I. "Performance Analysis of an Integrated GPS/Inertial Attitude Determination System," M.S. Thesis, Massachusetts Institute of Technology, CSDL-T-1227, May, 1994.

Tazartes, D., Buchler, R., Tipton, H., and Grethel, R. "Synergistic Interferometric GPS-INS," *Proceedings of the 1995 ION National Technical Meeting,* Anaheim, California, January 18-20, 1995, pp. 657-671.

Teague, H. and Parkinson, B.W. "Translation, Rotation, and Vibration Control of Large Space Structures Using Self-Differential GPS (SDGPS)," AAS 93-011, AAS Guidance and Control Conference, Keystone, Colorado, February, 1993.

Trimble Navigation, Ltd. "TANS Vector Specification and User's Manual," May 1994.

Twiggs, R.J., and Reister, K.W., "WEBERSAT: A Low-Cost Imaging Satellite," SPIE Vol. 1495, *Proceedings of the Small Satellite Technology and Applications Conference 1991*, pp. 12-18.

Udd, E. (editor) *Fiber Optic Sensors: An Introduction for Engineers and Scientist*s, John Wiley and Sons, New York, 1991.

Van Graas, F. and Braasch, M. "GPS Interferometric Attitude and Heading Determination: Initial Flight Test Results," *Navigation,* Vol. 38, No. 4, Winter 1991-92, pp. 297-317.

Vathsal, S. "Spacecraft Attitude Determination Using a Second-Order Nonlinear Filter," *Journal of Guidance, Control and Dynamics,* Vol. 10, No. 6, November-December, 1987, pp. 559-566

Wahba, Grace "Problem 65-1: A Least Squares Estimate of Spacecraft Attitude," *SIAM Review*, Vol. 7, No. 3, July 1965, p. 409.

Wahba, Grace, *et al.* "Problem 65-1 (Solutions), A Least Squares Estimate of Spacecraft Attitude," *SIAM Review*, Vol. 8, 1966, pp. 384-386.

Walter, Eric and Piet-Lahanier, Hélène "Estimation of Parameter Bounds from Bounded-Error Data: A Survey," *Mathematics and Computers in Simulation,* Vol. 32, No. 5&6, December 1990, pp. 449-468.

Ward, Lisa M. and Axelrad, P. "Spacecraft Attitude Estimation Using GPS: Methodology and Results for RADCAL," *Proceedings of the 1995 ION National Technical Meeting,* Anaheim, California, January 18-20, 1995, pp. 813-825.

Weinberg, M., Bernstein, J., Cho, S., King, A.T., Kourepenis, A., and Maciel, P. "A Micromachined Comb-Drive Tuning Fork Rate Gyroscope," *Proceedings of the ION 49th Annual Meeting,* Cambridge, Massachusetts, June 21-23, 1993, pp. 595-601.

Weinberg, M., Bernstein, J., Cho, S., King, A.T., Kourepenis, A., and Ward, P. "Micromechanical Tuning Fork Gyroscope Test Results," AIAA-94-3687-CP, *Proceedings of the AIAA Guidance, Navigation, and Control Conference*, Scottsdale, Arizona, August 1-3, 1994, pp. 1298-1303.

Wertz, J.R. (editor) *Spacecraft Attitude Determination and Control*, Kluwer Academic Publishers, Dordrecht, The Netherlands, 1978.

Wu, Weng-Rong "Target Tracking with Glint Noise," *IEEE Transactions on Aerospace and Electronic Systems*, Vol. AES-29, No. 1, January 1993, pp. 174-185.

Wu, Weng-Rong and Kundu, Amlan "Image Estimation Using Fast Modified Reduced Update Kalman Filter," *IEEE Transactions on Signal Processing*, Vol. 40, No. 4, April 1992, pp. 915-926.

Wu, Weng-Rong and Kundu, Amlan "Kalman Filtering in Non-Gaussian Environment Using Efficient Score Function Approximation," *Proceedings of the 1989 IEEE International Symposium on Circuits and Systems*, Vol. I, Portland, Oregon, May 8-11, 1989, pp. 413-416.